REMOVAL OF CIPROFLOXACIN AND CARBAMAZEPINE BY GRAPHENE OXIDE MODIFIED BI-FUNCTIONAL GROUP MESOPOROUS SILICA

Miss Jitsupa Suthkota

A Thesis Submitted in Partial Fulfillment of the Requirements
for the Degree of Master of Science Program in Hazardous Substance and Environmental Management
(Interdisciplinary Program)
Graduate School
Chulalongkorn University
Academic Year 2015

การกำจัดซิโพรฟลอกซาซินและคาร์บาเมซพินโดยเมโซพอรัสซิลิกาที่ติดต่อหมู่ฟังก์ชันสองชนิดและกราฟีนออกไซด์

นางสาวจิตสุภา สุดโกทา

วิทยานิพนธ์นี้เป็นส่วนหนึ่งของการศึกษาตามหลักสูตรปริญญาวิทยาศาสตรมหาบัณฑิต
สาขาวิชาการจัดการสารอันตรายและสิ่งแวดล้อม (สหสาขาวิชา)
บัณฑิตวิทยาลัย จุฬาลงกรณ์มหาวิทยาลัย
ปีการศึกษา 2558

Thesis Title	REMOVAL OF CIPROFLOXACIN AND CARBAMAZEPINE BY GRAPHENE OXIDE MODIFIED BI-FUNCTIONAL GROUP MESOPOROUS SILICA
By	Miss Jitsupa Suthkota
Field of Study	Hazardous Substance and Environmental Management
Thesis Advisor	Associate Professor Patiparn Punyapalakul, Ph.D.

Accepted by the Graduate School, Chulalongkorn University in Partial Fulfillment of the Requirements for the Master's Degree

.....Dean of the Graduate School
(Associate Professor Sunait Chutintaranond, Ph.D.)

THESIS COMMITTEE

.....Chairman
(Assistant Professor Chantra Tongcumpou, Ph.D.)

.....Thesis Advisor
(Associate Professor Patiparn Punyapalakul, Ph.D.)

.....Examiner
(Doungkamon Phihusut, Ph.D.)

.....Examiner
(Pummarin Khamdahsag, Ph.D.)

.....External Examiner
(Panida Prarat, Ph.D.)

จิตสุภา สุดโกทา : การกำจัดซิโพรฟลอกซาซินและคาร์บาเมซพินโดยเมโซพอรัสซิลิกาที่ติดต่อหมู่ฟังก์ชันสองชนิดและกราฟีนออกไซด์ (REMOVAL OF CIPROFLOXACIN AND CARBAMAZEPINE BY GRAPHENE OXIDE MODIFIED BI-FUNCTIONAL GROUP MESOPOROUS SILICA) อ.ที่ปรึกษาวิทยานิพนธ์หลัก: รศ. ดร.ปฏิภาณ ปัญญาพลกุล, 110 หน้า.

งานวิจัยนี้มีวัตถุประสงค์เพื่อศึกษากลไกการดูดซับซิโพรฟลอกซาซิน (CIP) และคาร์บาเมซพิน (CBZ) โดยเมโซพอรัสซิลิกาที่ติดต่อหมู่ฟังก์ชันสองชนิดที่ต่อติดด้วยกราฟีนออกไซด์ (GO) โดยทำการสังเคราะห์ตัวกลางดูดซับเมโซพอรัสซิลิกาที่ติดต่อหมู่ฟังก์ชัน 2 ชนิด ได้แก่ หมู่อะมิโนและหมู่เมอร์แคปโต รวมถึงต่อติดร่วมกันทั้ง 2 หมู่ (A-HMS M-HMS และ A5M5, ตามลำดับ) จากนั้นทำการติดต่อกับกราฟีนออกไซด์ ได้เป็น (GO-A-HMS และ GO-A5M5) เพื่อเพิ่มความสามารถในการดูดซับด้วยการถ่ายโอนอิเลคตรอนภายในวงแหวนอะโรมาติกและคุณสมบัติความไม่ชอบน้ำ คุณสมบัติทางกายภาพของตัวกลางดูดซับได้ถูกตรวจสอบด้วยวิธีการต่าง ๆ จากนั้นทำการศึกษากลไกการดูดซับโดยศึกษาจลนพลศาสตร์และไอโซเทอมการดูดซับในการทดลองแบบทีละเท จากผลการทดลองจลพลศาสตร์การดูดซับพบว่าสมการอันดับสองเสมือนสอดคล้องกับผลการทดลองมากที่สุดสำหรับตัวกลางดูดซับทุกประเภท และกระบวนการแพร่ภายในอนุภาคเป็นตัวกำหนดอัตราการเร็วในการดูดซับของ CIP และ CBZ การต่อติด GO บนพื้นผิวของ A-HMS สามารถเพิ่มประสิทธิภาพการดูดซับ CIP ในขณะที่หมู่เมอร์แคปโตบน GO-A5M5 มีบทบาทในการดูดซับมากกว่า ไอโซเทอมการดูดซับที่ได้จากการทดลองสอดคล้องกับสมการฟรุนดิชซึ่งอาจเกี่ยวข้องกับการดูดซับแบบหลายชั้น แรงดึงดูดทางประจุไฟฟ้ามีผลต่อการดูซับของ CIP และ CBZ โดยการดูดซับจะลดลงเมื่อค่าพีเอสสูงขึ้น

การดูดซับของ CIP และ CBZ บน GO-A-HMS และ GO-A5M5 ในสายละลายผสมต่างมีค่าลดลงเมื่อเทียบกับในสารละลายแบบเดี่ยว การแย่งพื้นที่การดูดซับของ CIP น่าจะเกี่ยวข้องกับการถ่ายโอนอิเลคตรอนภายในวงแหวนอะโรมาติกและแรงทางประจุไฟฟ้า ส่วน CBZ ได้แก่คุณสมบัติความไม่ชอบน้ำของพื้นผิว

สาขาวิชา การจัดการสารอันตรายและสิ่งแวดล้อม ลายมือชื่อนิสิต .....

ลายมือชื่อ อ.ที่ปรึกษาหลัก .....

ปีการศึกษา 2558

5787509620 : MAJOR HAZARDOUS SUBSTANCE AND ENVIRONMENTAL MANAGEMENT
KEYWORDS: ADSORPTION / CIPROFLOXACIN / CARBAMAZEPINE / GRAPHENE OXIDE / HEXAGONAL MESOPOROUS SILICA

JITSUPA SUTHKOTA: REMOVAL OF CIPROFLOXACIN AND CARBAMAZEPINE BY GRAPHENE OXIDE MODIFIED BI-FUNCTIONAL GROUP MESOPOROUS SILICA. ADVISOR: ASSOC. PROF. PATIPARN PUNYAPALAKUL, Ph.D., 110 pp.

The purpose of this study was to investigate the adsorption mechanism of ciprofloxacin (CIP) and carbamazepine (CBZ) on graphene oxide modified bi-functional mesoporous silica. Hexagonal Mesoporous silica (HMS) was synthesized and modified surface functional group with two different types of organosilanes, i.e. amino-, mercapto- and amino- + mercapto- functional groups (A-HMS, M-HMS, A5M5, respectively). Then synthesized adsorbents were modified by graphene oxide (GO) as GO-A-HMS and GO-A5M5 in order to enhance the adsorption capacity by **π-π** interaction and hydrophobicity. The physicochemical properties of the synthesized adsorbents were characterized by various techniques. The adsorption kinetic and adsorption isotherm were performed to investigate the mechanism in batch experiment. According to the kinetic study, the pseudo-second-order kinetic model gave the best correlation with experimental results for all adsorbents and intraparticle diffusion were suggested to be the rate limiting step for both CIP and CBZ. The presence of GO on A-HMS can enhance CIP adsorption capacity, on the other hand, mercapto functional group on GO-A5M5 are supposed to be the key functional group for CBZ adsorption. The adsorption isotherms were well-fitted with Freundlich isotherm model as multilayer adsorption. Electrostatic interaction was proved by the decrease of CIP and CBZ adsorption capacity with the increasing of pH.

The lower adsorption capacities of CIP and CBZ on GO modified HMS (GO-A-HMS and GO-A5M5) in binary-solute solution than single-solute solution were observed. The competitive adsorption of CIP was supposed to relate with **π-π** interaction and electrostatic interaction. In contrast, the hydrophobic interaction might play the key role for CBZ adsorption mechanism.

Field of Study: Hazardous Substance and Environmental Management Student's Signature .....
Advisor's Signature .....
Academic Year: 2015

ACKNOWLEDGEMENTS

First of all, I would like to express my sincere gratitude to my advisor Assoc. Prof. Patiparn Punyapalakul for his advice, suggestion, and support. Moreover, I would like to be thankful to my committee members, Assist. Prof. Chantra Tongcumpou the chairman of the committee, and all the committee members; Dr. Doungkamon Phihusut, Dr. Pummarin Khamdahsag and Dr. Panida Prarat for their comments and suggestions.

I would like to acknowledge the financial support from The Thailand Research Fund, Thailand under grant no. RSA5880018. This work was carried out as part of the research cluster "Hazardous Substance Management in Agricultural Industry" granted by the Center of Excellence for Hazardous Substance Management (HSM) and Research unit Control of Emerging Micropollutants in Environment from Chulalongkorn University. This research has been supported by the Ratchadaphiseksomphot Endowment Fund (2015) Chulalongkorn University (CU-58-060-CC). The authors would like to thank the support from research grant of Kurita Water and Environment Foundation (2014). This research was also supported by 2013 Overseas Research Grants from the Asahi Glass Foundation.

Finally, I would like to express my appreciation to my family for their support. Furthermore, I am extremely grateful for the encouragement from my friends and help me during these two years. However, I would like to thanks Miss Wanchalach Sathienthammanee for her assistance in the laboratory as lab-mate.

CONTENTS

Page

Page

Page

Page

Page

LISTS OF FIGURE

Page

LISTS OF TABLE

Page

LISTS OF ABBREVIATION

A5M5	=	Amino and mercapto-grafted hexagonal mesoporous silica
A-HMS	=	Amino-grafted hexagonal mesoporous silica
APTES	=	3-aminopropyltriethoxysilane
BET	=	Brunner-Eller-Teller
BF-HMS	=	Bi-functional hexagonal mesoporous silica
BJH	=	Barret-Joyner-Halenda
CIP	=	Ciprofloxacin
CBZ	=	Carbamazepine
DCC	=	N-N_0-dicyclohexylcarbodiimide
DMF	=	Dimethylformamide
FT-IR	=	Fourier transform infrared
GO	=	Graphene oxide
GO-A-HMS	=	Graphene oxide modified amino-grafted hexagonal mesoporous silica
GO-A5M5	=	Graphene oxide modified amino and mercapto-grafted hexagonal mesoporous silica
HPLC	=	High performance liquid chromatography
HMS	=	Hexagonal mesoporous silica
IS	=	Ionic strength
M-HMS	=	Mercapto-grafted hexagonal mesoporous silicate
MPTMS	=	3-mercaptopropyltrimethoxysilane
PAC	=	Powdered Activated Carbon

SEM	=	Scanning electron microscope
SF-HMS	=	Single-functional hexagonal mesoporous silica
TEM	=	Transmission electron microscope
TEOS	=	Tetraethylorthosilicate or tetraethoxysilane
XPS	=	X-ray photoelectron spectroscopy
XRD	=	X-ray diffraction

LISTS OF NOMENCLATURE

$1/n$	=	Freundlich constant related to sorption intensity of the adsorbent
C_0	=	Initial concentration (μg L^{-1} or mg L^{-1})
C_e	=	Concentration at equilibrium (μg L^{-1} or mg L^{-1})
h	=	Initial adsorption rate (mg g^{-1} h^{-1})
k_2	=	Pseudo-second-order rate constant (g mg^{-1} min^{-1})
k_R	=	Ritchie's-second-order rate constant (g mg^{-1} min^{-1})
K_{ip1}	=	Film diffusion rate constant (mg g^{-1} $min^{-0.5}$)
K_{ip2}	=	Intraparticle diffusionrate constant (mg g^{-1} $min^{-0.5}$)
K_F	=	Freundlich constant (mg g^{-1})
K_L	=	Langmuir constant (L mg^{-1})
M	=	Mass (gram)
q_e	=	Adsorption capacity at equilibrium (mg g^{-1})
q_m	=	Maximum adsorption capacity (mg g^{-1})
q_t	=	Adsorption capacity at time (mg g^{-1})
R^2	=	The correlation coefficient
S_{BET}	=	Specific surface area (m^2 g^{-1})
t	=	Time (min)
$t^{0.5}$	=	Half-life (min)
V	=	Volume (Liter)
V_p	=	Pore volume (mm^3 g^{-1})

CHAPTER 1
INTRODUCTION

1.1 STATE OF PROBLEM

During the last several decades, pharmaceutical residues became an emerging concern in the water resources worldwide due to the large amounts of usage and their persistence in the environment. Ciprofloxacin (CIP) and carbamazepine (CBZ) are two pharmaceuticals which were frequently detected from several sources such as wastewater from municipal, drug manufacture treatment plant, hospital wastewater, etc. CIP is one of the fluoroquinolone group which used for infectious treatment. CBZ is an antiepileptical drug used for remediation for treatment of nervous system disorder. Due to their poor metabolism and slow degradation, the persistence of CIP and CBZ in the environment has been a great concern. The adverse effects of the pharmaceutical residues can be impact aquatic ecosystem and human health.

In order to remove the pharmaceutical residues from wastewater, various treatment processes including biotic, physical and chemical treatment can be applied to remove the contamination in several method such as biodegradation, membrane filtration, ozonation, ultraviolet irradiation, adsorption, etc. Adsorption is one of the most popular physicochemical process for the removal of pharmaceuticals in the environment. Mesoporous silica (such as HMS) is an effective adsorbent in adsorption process due to its uniform structure, high pore volume and high surface area. Moreover, the functionalized HMS provided higher adsorption capacity than HMS depend on hydrophobicity/hydrophilicity and hydrogen bonding.

Graphene oxide (GO) has been recently used as a high-performance adsorbent for remove pharmaceuticals in wastewater. Nevertheless, GO is difficult to completely separate from the aqueous solution, due to the highly solubility of GO in water. Accordingly, the modification of GO-based adsorbents for prohibit aggregation as GO modified HMS will be studied for higher efficiency.

The overall purpose of this study were to determine the comparative removal of pharmaceutical residues by adsorption on various types of adsorbent such as HMS, functionalized-HMS, GO and GO modified HMS. The physicochemical properties of synthesized adsorbents were characterized using many instruments and methods. Adsorption kinetic and adsorption isotherm were conducted under batch experiments by controlling ionic strength. The results were interpreted as kinetic parameters and adsorption isotherm model to understand the effect of surface functional group and the adsorption mechanism including hydrophobic interaction, electrostatic interaction and hydrogen bonding. Moreover, selective adsorption in binary-solute solution of pharmaceuticals on the synthesized adsorbents were studied.

1.2 HYPOTHESIS

Modification of graphene oxide as mesoporous silica-grafted graphene oxide increase its adsorption capacity comparing with mesoporous silicas via **π-π** interaction and hydrophobicity.

1.3 OBJECTIVES

The main objectives of this research is to study the ability of mesoporous silicas and GO modified HMS for removal of pharmaceutical residues by adsorption process. The objectives can be concluded as following:

1.3.1 To synthesize and characterize GO modified HMS.

1.3.2 To determine adsorption capacities of ciprofloxacin (CIP) and carbamazepine (CBZ) on GO modified HMS comparing with pristine HMS in aqueous phase.

1.3.3 To determine the effects of surface functional groups on ciprofloxacin (CIP) and carbamazepine (CBZ) adsorption capacity.

1.3.4 To determine the selectivity of ciprofloxacin (CIP) and carbamazepine (CBZ) onto GO modified HMS in binary-solute solution.

1.4 SCOPE OF THE STUDY

The scope of this study can be divided into four step as followed and the experiment framework is shown in Figure 1.

1.4.1 Synthesis of adsorbents

Synthesized adsorbents were hexagonal mesoporous silica (HMS) which were modified surface by co-condensation method with two types of surface functional group; amino- and mercapto-functional group as A-HMS, M-HMS and A5M5, respectively. Graphene oxide was also synthesized and the modification of GO was performed as GO modified HMS (GO-A-HMS and GO-A5M5). In conclusion, seven adsorbents will be synthesized and used in this study (as followed):

- Hexagonal mesoporous silica (HMS)
- Amino grafted HMS (A-HMS)
- Mercapto grafted HMS (M-HMS)
- Amino and mercapto grafted HMS (A5M5)
- Graphene oxide (GO)
- GO modified A-HMS (GO-A-HMS)
- GO modified A5M5 (GO-A5M5)

1.4.2 Characterization of synthesized adsorbents

The physicochemical properties of synthesized adsorbents by various techniques such as XRD, FT-IR, SEM, TEM, nitrogen adsorption isotherm (BET), CHNS/O elemental analysis, XPS etc.

1.4.3 Adsorption study of ciprofloxacin (CIP) and carbamazepine (CBZ) on adsorbents

Adsorption study was performed under batch experiments in concentration range of CIP and CBZ were 1 - 10 $mg \cdot L^{-1}$ and pH 7.0 controlled ionic strength using 0.01 M phosphate buffer at 25°C.

1.4.4 Selective adsorption study

Selective adsorption study was performed by comparing the adsorption capacity of the synthesized adsorbents in single-solute solution and binary-solute solution.

1.4.5 Low concentration adsorption study

Low concentration adsorption study was performed under batch experiments in concentration range of CIP and CBZ were 10-200 $\mu g \cdot L^{-1}$ and pH 7.0 controlled ionic strength using 0.01 M phosphate buffer at 25°C.

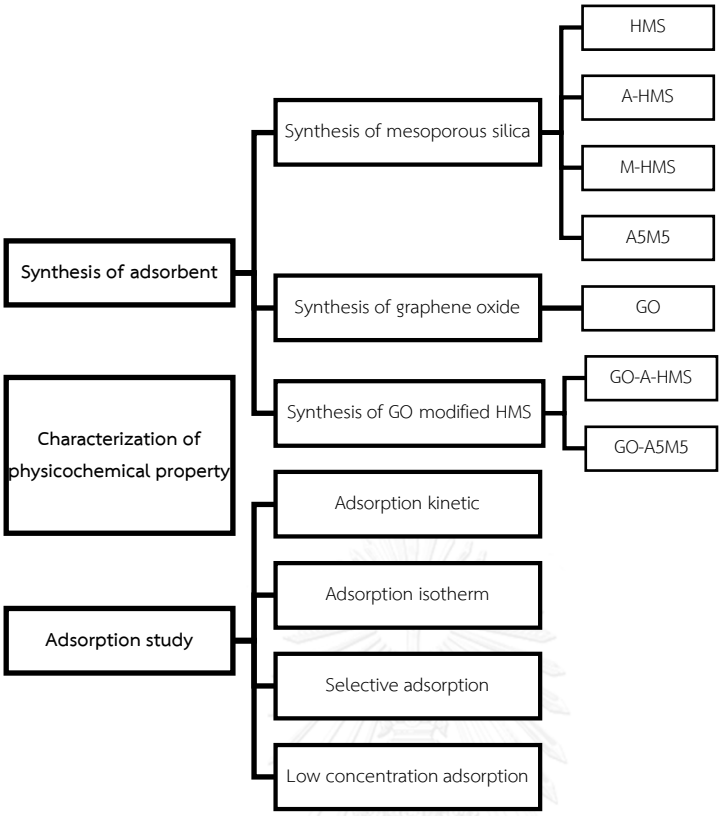

Figure 1 Experimental framework of this study

CHAPTER 2
THEORETICAL BACKGROUND AND LITERATURE REVIEWS

2.1 PHARMACEUTICAL RESIDUES IN THE ENVIRONMENT

In the last several decades, pharmaceutical residues became an emerging concern in the water resources worldwide due to the large amounts of usage and their persistence in the environment. The contamination of pharmaceutical residues were detected in several sources such as in wastewater from households, livestock farms, hospitals and pharmaceutical manufactures. The adverse effects of the pharmaceutical residues can be impact aquatic ecosystem and human health (Sim, Lee et al. 2011).

Pharmaceuticals are widely use in human medicine and veterinary medicine for preventing or treating microbial infections (Kümmerer 2009). Moreover, in some countries were used in fruit growing and growth promoter of animal farming. Pharmaceuticals can be divided into several groups due to their chemical structures and chemical mechanism such as quinolones, sulphonamides and others. Most of these compounds could not reach completed metabolism and had less biodegradable, and then the large quantities of residue were remain in several aquatic environment. In general, concentrations were in the higher μg/L range in hospital effluent, in the lower μg/L range in municipal wastewater, and in the higher and lower μg/L range in different surface waters, groundwater and seawater in a harbor (Xu, Zhang et al. 2007, Xu, Bai et al. 2008).

Sources of pharmaceutical residues in the environment were discharged from the use of human and veterinary medicine (Homem and Santos 2011). Human pharmaceuticals were released into the environment via excretion through sewer network to wastewater treatment plants (WWTPs) and sludge. They can be transported to surface and groundwater due to incomplete removal of pharmaceuticals in WWTPs. Moreover, the contaminated surface water can reach the drinking water treatment plants (DWTPs). Another disposal of human pharmaceuticals is unused or expired drugs from manufacturing via directly discharged in the sewage network and landfills. In case

of veterinary pharmaceuticals, the contamination were released via excretion in livestock wastewater and aquaculture. They can be contaminated in manure, soil, food chain and groundwater. The origin and contamination routes of human and veterinary pharmaceuticals can be summarized as Figure 2.

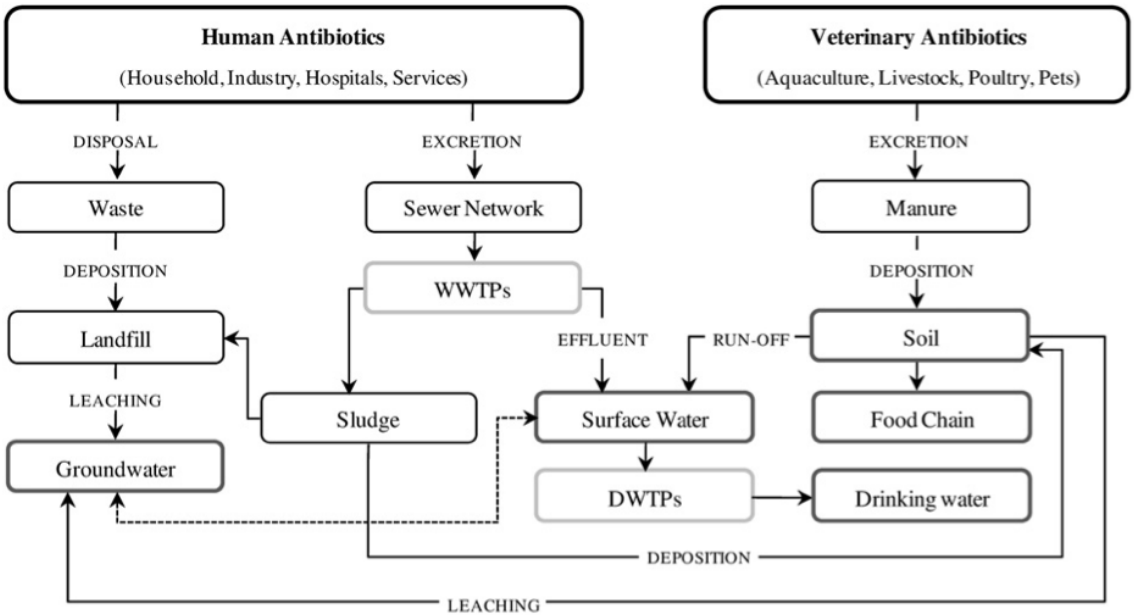

Figure 2 The origin and contamination routes of human and veterinary antibiotics (Homem and Santos 2011)

2.2 CIPROFLOXACIN (CIP)

Ciprofloxacin (CIP) is one of the pharmaceuticals in fluoroquinolone group which was actived against several diseases caused by both Gram-positive and Gram-negative bacteria including tract infection, respiratory tract infection, alimentary infection, etc (Nakata, Kannan et al. 2005). Moreover, ciprofloxacin can inhibit enzyme activity for DNA gyrase and an important enzyme in DNA replication(Bryan, Bedard et al. 1989). The molecular structure and physicochemical properties of ciprofloxacin can be displayed in Figure 3 and Table 1, respectively.

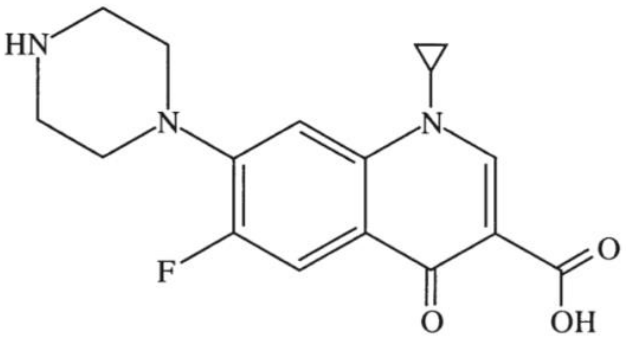

Figure 3 The molecular structure of ciprofloxacin (CIP)
(Halling-Sørensen, Lützhøft et al. 2000)

Table 1 Physicochemical properties of ciprofloxacin (CIP)

Parameter	Description
Appearance	Powder, crystalline powder
Color	Yellowish, light yellow
Molecular formula	$C_{17}H_{18}FN_3O_3$
Molecular weight	331.341523 g/mol
Water solubility	30000 mg/L (at 20°C)
$\log K_{ow}$	0.28
pK_a	6.09 and 8.74
Melting point	255-257 °C

Ciprofloxacin is one of the most frequently detected pharmaceutical residue with the wide range of concentration (0.4 ppb - 160 ppm) from several sources; effluent from municipal wastewater (Renew and Huang 2004), drug manufacture treatment plant (Larsson, de Pedro et al. 2007), hospital wastewater (Duong, Pham et al. 2008), etc. Furthermore, it can be measured as aqueous phase in sludge solid containing 2.2 mg/L and 0.427 µg/L in sewage-filtered effluent (Cordova-Kreylos and Scow 2007). The effects of ciprofloxacin on the microbial community were investigated that exposure of 0.02-200 µg/L of ciprofloxacin can affect sulfate-reducer bacteria and also harm to bacteria in activated sludge (Halling-Sørensen, Lützhøft et al. 2000).

2.3 CARBAMAZEPINE (CBZ)

Carbamazepine (CBZ) is an antiepileptical drug used worldwide. The usages of this drug are for the treatment of psychomotor and temporal lobe epilepsy and also for relieving of diseases such as alcoholism, opiate withdrawal, depressant and epileptic (Punyapalakul and Sitthisorn 2010). The molecular structure and physicochemical properties of ciprofloxacin can be displayed in Figure 4 and Table 2, respectively.

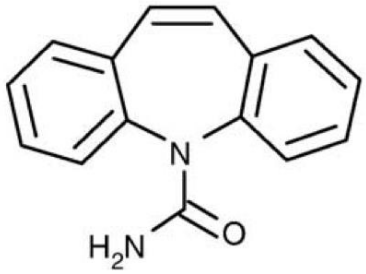

Figure 4 The molecular structure of carbamazepine (CBZ)
(Scheytt, Mersmann et al. 2006)

Table 2 Physicochemical properties of carbamazepine (CBZ)

Parameter	Description
Appearance	Powder
Color	White - slight yellow
Molecular formula	$C_{15}H_{12}N_2O$
Molecular weight	236.26858 g/mol
Water solubility	17.7 mg/L
$\log K_{ow}$	2.45
pK_a	13.90
Melting point	189-193°C

Carbamazepine was frequently detected in the environment with the concentration below 1 ppb from several sources; effluent from sewage treatment plant, ground water, drinking water, etc. (Heberer, Reddersen et al. 2002). The acute toxicity of carbamazepine was affected marine bacteria, a freshwater invertebrate and Japanese medaka fish were reported (Kim, Choi et al. 2007).

2.4 HEXAGONAL MESOPOROUS SILICA (HMS)

Hexagonal mesoporous silicates (HMS) is one kind of mesoporous silicates conformed by the neutral synthesis pathway (S^0I^0) (Tanev and Pinnavaia 1996). HMS was synthesized from neutral inorganic precursor (I^0) and neutral primary amine micelles (S^0) based on hydrogen bonding. The S^0I^0 templating mechanism of formation of HMS mesoporous molecular sieves was represented as Figure 5. The organic template that was formed hexagonal material can be removed by solvent extraction.

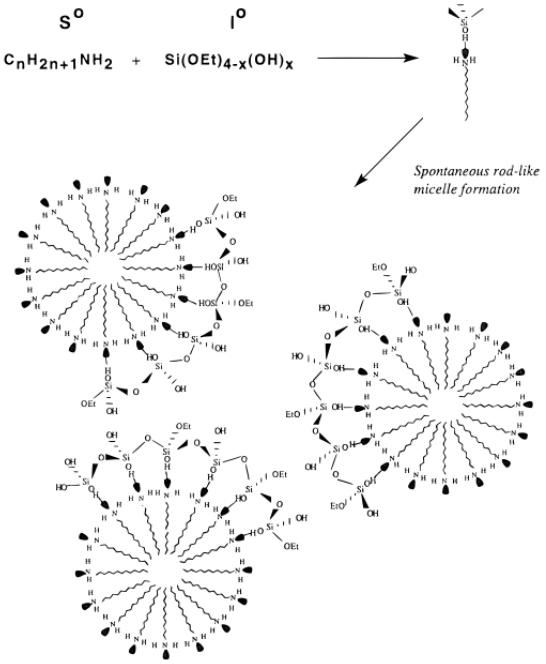

Figure 5 Schematic representation of the S^0I^0 templating mechanism of formation of HMS mesoporous molecular sieves
(Tanev and Pinnavaia 1996)

2.5 ADSORBENT SURFACE MODIFICATION

The modification of functional group on the surface of mesoporous silicates can be synthesized using two methods; post synthetic functionalization of silicas or grafting and co-condensation or direct synthesis (Hoffmann, Cornelius et al. 2006).

2.5.1 Post synthetic functionalization of silicas or post grafting

Grafting refer to the modification with organic functional group on the inner surfaces of mesoporous silicates. The functionalized adsorbents using this method can be provided the good preservation of the structure after post grafting. However, the main drawback is limited in quantity of functional groups can be grafted. This process is performed by reaction of organosilanes of the type $(R'O)_3SiR$, or chlorosilanes $ClSiR_3$ or silazanes $HN(SiR_3)_3$, with the free silanol groups of the pore surfaces as Figure 6.

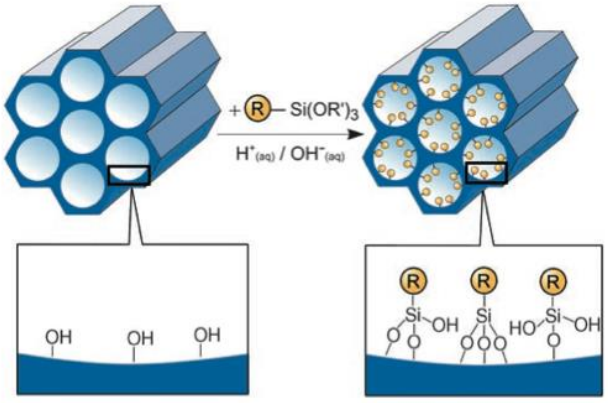

Figure 6 Grafting (postsynthetic functionalization) for organic modification of mesoporous pure silica phases with terminal organosilanes of the type $(R'O)_3SiR$. R = organic functional group. (Hoffmann, Cornelius et al. 2006)

2.5.2 Co-condensation or direct synthesis

Co-condensation method can be produced higher and more uniform surface coverage of functionalization than post grafting method. This method involves the preparation of mesostructured silica phases by the co-condensation of tetraalkoxysilanes [$(RO)_4Si$ (TEOS or TMOS)] with terminal trialkoxyorganosilanes of the organic residues anchored covalently to the pore walls as Figure 7. By using structure-directing agents known from the synthesis of pure mesoporous silica phases (e.g. MCM or SBA silica phases), organically modified silicas can be prepared in such a way that the organic functionalities present into the pores.

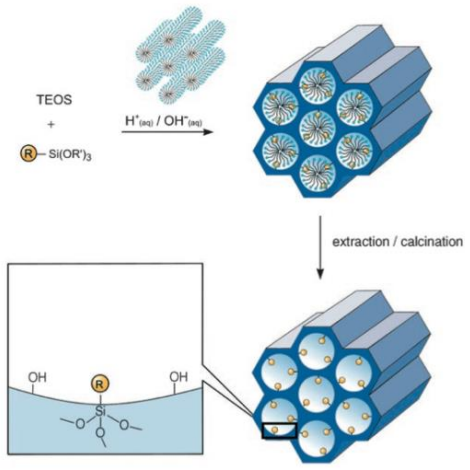

Figure 7 Co-condensation method (direct synthesis) for the organic modification of mesoporous pure silica phases, R= organic functional group
(Hoffmann, Cornelius et al. 2006)

2.6 GRAPHENE OXIDE (GO)

Graphene has become very popular as a nanomaterial using in environmental remediation. Graphene oxide (GO) is an oxidized form of graphene consisting of various functional groups such as hydroxyl, carboxyl, and epoxy group (Figure 8) which serve as sorption sites for many aqueous contaminants in water(Chen, Gao et al. 2015). Moreover, GO possessed layered structure and negatively charged surface that can be efficiently bind metal ions and positively charged organic compounds(Li, Wang et al. 2015). The interactions between contaminants and GO can be controlled by several mechanisms, including electrostatic attraction, hydrogen bonding, Lewis acid-base interaction, **π- π** stacking.

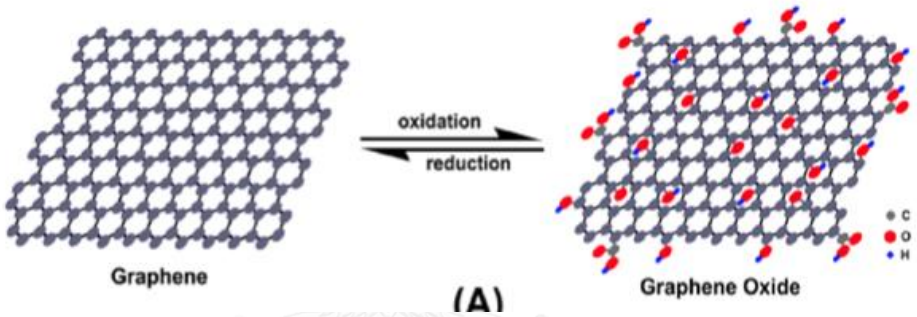

Figure 8 Scheme of structural model of graphene and graphene oxide (GO). (Li, Wang et al. 2015)

2.7 MESOPOROUS SILICA-GRAFTED GRAPHENE OXIDE

Graphene oxide has been used as a high-performance adsorbent for many application. Nevertheless, GO is difficult to completely separate from the aqueous solution, due to the highly solubility of GO in water. Furthermore, the adsorption capacity of GO can be decreased by high interplanar interaction and irreversible aggregation may occur in the adsorption process. Accordingly, the modification of GO-based adsorbents for prohibit aggregation of GO and develop the efficiency was evaluated (Li, Wang et al. 2015). Preparation of SBA-15-grafted GO (GO–SBA-15) was performed amino groups were grafted onto SBA-15 (NH_2– SBA-15) and GO carboxyl groups as active site to bind the amino groups of NH_2–SBA-15 as shown in Figure 9.

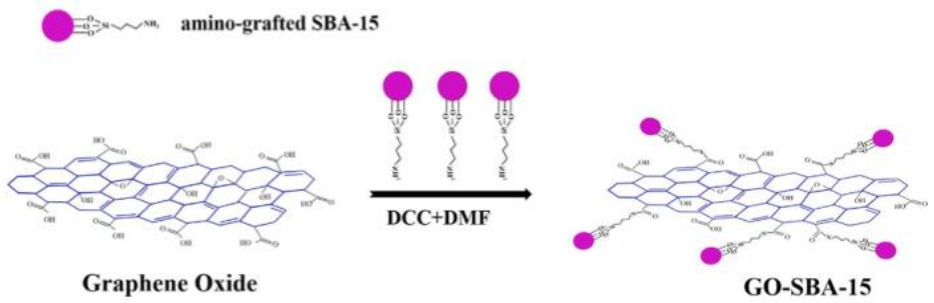

Figure 9 Schematic depiction of the formation of GO–SBA-15 (Li, Wang et al. 2015)

2.8 ADSORPTION THEORY

2.8.1 Adsorption Mechanism

Adsorption is a surface phenomena of solid substances being contact with surface molecules of solutions. Solid that are used to adsorb substances are called adsorbents and the adsorbed molecules are called adsorbate. The adsorption mechanism could be separated via basic forces to two types; chemisorption and physisorption. The basic force causing chemisorption (or chemical adsorption) is electron transfer between adsorbate and surface of adsorbent, while physisorption (or physical adsorption) is intermolecular or van der Waals force. For a solid-liquid adsorption process was commonly included of three step as following:

1. Film diffusion, which involves the movement of adsorbate molecules from the bulk of the solution towards the external surface of the adsorbent.
2. Particle diffusion, where the adsorbate molecules move in the interior of the adsorbent particles.
3. Adsorption of the adsorbate molecules onto active sites interior of adsorbent particles.

2.8.2 Adsorption Kinetic

The adsorption kinetic study is represented the adsorption rate for performing and modeling process. Adsorption kinetic mechanisms can be depended on chemical reaction kinetics or diffusion mass transfer processes. There are many kinetic models were used to analyze the experimental data. The pseudo-first-order model and pseudo-second-order model are commonly used to evaluate the adsorption kinetic.

2.8.2.1 Pseudo-first-order Model

The pseudo-first-order model is one of the most widely used procedures for the adsorption of a solute from aqueous solution. The pseudo-first-order model can be defined as in the Equation (2.1):

$$\frac{dq_t}{dt} = k_t(q_e - q_t) \quad (2.1)$$

Where k_1 is the pseudo-first-order rate constant (min^{-1}), q_e and q_t is the adsorption capacity ($mg \cdot g^{-1}$) at equilibrium and time t (min), respectively. Equation (2.1) can be derived as in the Equation (2.2):

$$ln(q_e - q_t) = ln(q_e) - k_1 t \quad (2.2)$$

The values of q_e and k_1 were determined from the slope of linear plot between $ln(q_e - q_t)$ and t.

2.8.2.2 Pseudo-second-order Model

The pseudo-second-order model is based on a chemisorption. The pseudo-second-order equation can be defined as in the Equation (2.3):

$$\frac{dq_t}{d_t} = k_2(q_e - q_t)^2 \quad (2.3)$$

Where k_2 is the pseudo-second-order rate constant ($g \cdot mg^{-1} \cdot min^{-1}$). Equation (2.3) can be rearranged as in the Equation (2.4):

$$\frac{t}{q_t} = \frac{1}{k_2 {q_e}^2} + \frac{t}{q_e} \quad (2.4)$$

The values of q_e and k_2 were determined from the slope of linear plot between t/qt and t. Moreover, the initial adsorption rate can be calculated as in the Equation (5):

$$h = k_2 {q_e}^2 \quad (2.5)$$

Where h is the initial sorption rate $(mg \cdot (g \cdot min)^{-1})$

2.8.3 Adsorption Isotherm

The adsorption isotherm study is described the relationship between the amount of pollutant on the adsorbent at constant temperature and its equilibrium concentration. The adsorption capacity (q_e) can be calculated as Equation (2.6):

$$q = \frac{(C_0 - C_e)V}{M} \quad (2.6)$$

Where q_e is the adsorption capacity ($mg \cdot g^{-1}$), C_0 and C_e are the initial and equilibrium concentration ($mg \cdot L^{-1}$), respectively. V is the volume of the solution (L) and M is the mass of adsorbent (g).

There are many isotherm models were used to analyze the experimental data. The linear, Langmuir, and Freundlich isotherm models are commonly used for interpretation of the adsorption isotherm.

2.8.3.1 Linear Model

Linear model is the simplest isotherm that can be described the relationship between the adsorption capacity and concentration of pollutant at the equilibrium. Linear model can be written as Equation (2.7):

$$q_e = K_p C_e \quad (2.7)$$

Where q_e is the adsorption capacity ($mg \cdot g^{-1}$) at the equilibrium, k_p is linear constant and C_e is the equilibrium concentration ($mg \cdot L^{-1}$).

2.8.3.2 Langmuir Model

The Langmuir model is widely used to describe the adsorption of a solute in aqueous solution and can be applied to many adsorption processes. The Langmuir model can be written as Equation (2.8):

$$q_e = \frac{K_L q_m C_e}{1 + K_L C_e} \quad (2.8)$$

The linear form of the Langmuir isotherm can be described as Equation (2.9):

$$\frac{1}{q_e} = \frac{1}{q_m} + \frac{1}{K_L q_m C_e} \quad (2.9)$$

Where q_m is the maximum adsorption capacity ($mg \cdot g^{-1}$) and k_L is the Langmuir constant.

2.8.3.3 Freundlich Model

The Freundlich model is used in case of multilayer adsorption process. This model does not determine the saturation of the concentration of pollutant adsorbed on adsorbent. The Freundlich model can be written as Equation (2.10):

$$q_e = K_F C_e^{\frac{1}{n}} \quad (2.10)$$

The linear form of the Freundlich isotherm can be described as Equation (2.11):

$$ln(q_e) = ln(K_F) + \frac{1}{n} ln(C_e) \quad (2.11)$$

Where k_F is the Freundlich constant and n is the adsorption intensity (dimensionless).

2.9 LITERATURE REVIEWS

2.9.1 Removal of pharmaceutical residues in the environment

The removal of pharmaceutical residues in wastewater effluent and water resources has become the important consideration. The various treatment processes including biotic, physical and chemical treatment can be applied to remove the contamination in several methods such as biodegradation, membrane filtration, ozonation, ultraviolet irradiation, adsorption, etc. Biodegradation during water treatment have been studied such as effect of oxido-reduction properties of soil, specific microorganisms from biosolids, metabolization by microbial flora, metabolic pathway of phenazone in sand filters, etc. Actually, biodegradation may be limited by the adsorption of pharmaceutical products in water sediments, the complexation with dissolved organic matter (DOM), sorption into the shallow layer of soil, or during bank filtration (Mompelat, Le Bot et al. 2009).The removal of pharmaceuticals by the membrain filtration (reverse osmosis and nanofiltration) is one of the effective treatment has been reported (Li, Li et al. 2004). RO treatment can reduce more than 92% in high concentration of oxytetracycline in wastewater. However, the fouling by the precipitation of chemicals may occur in membranes that can change the physicochemical properties of its surface. Chemical and photochemical oxidation processes, chlorination and ozonation of the pharmaceuticals including sulfonamide, tetracycline and fluoroquinolone has been reported as an effectively removal method (Gibs, Stackelberg et al. 2007). Nonetheless, the formation of by-products via chloronation and ozonation may have more toxic than the parent compounds. Polychromatic ultraviolet irradiation combines pH modification can increase degradation of sulfamethoxazole, oxytetracycline and ciprofloxacin are over 90% removal efficiency (Lester, Avisar et al. 2010). The organic matter can be reduced the quantity of pharmaceuticals leading the lower degradation of pharmaceutical in the water system.

Adsorption is one of the most popular process for the removal of pharmaceutical in the environment. The pharmaceutical removal by the adsorption process from water and wastewater by activated carbon has been reported (Adams,

Wang et al. 2002). The concentration of many pharmaceuticals have been decreased by 49-90% with only 10-20 mg/L of powder activated carbon (PAC). The great efficiency of activated carbon has been obtained, while the disadvantages is low selectivity. Therefore, the surface of the adsorbent should be modified for the higher selectivity.

Mesoporous silica such as HMS, MCM-41, and SBA-15 is an effective adsorbent in adsorption process due to its uniform structure, high pore volume and high surface area. The removal efficiency of pharmaceuticals including carbamazepine, diclofenac, ibrupofen, ketoprofen by SBA-15 are over 80% removal efficiency and 49% for clofibric acid (Bui and Choi 2009). Removal of ciprofloxacin and carbamazepine by adsorption on functionalized mesoporous silicates has been reported (Punyapalakul and Sitthisorn 2010). The functionalized HMS provided higher adsorption capacity than HMS depend on hydrophobicity/hydrophilicity and hydrogen bonding.

The effect of surface functional groups amino-, nitrile-, mercapto, phenyl-, and n-octyl-dimethoxychloro- grafted superparamagnetic particles coated with HMS (HMS-SPs) on the adsorption of ciprofloxacin (CIP) was reported (Hongsawat, Prarat et al. 2014). Adsorption capacity of hydrophobic adsorbents had higher than hydrophilic adsorbents due to the interaction of **π-π** electron-donor acceptors and electrostatic force. In case of low concentration of CIP, tannic acid (TA) could enhance the adsorption capacity by multilayer adsorption on adsorbent surfaces.

Graphene oxide (GO) is recently applied in adsorption process for remove pharmaceuticals in wastewater. The adsorption process of sulfamethoxazole and carbamazepine on graphene oxide and graphite has been investigated as the competition between two antibiotics (Wang, Li et al. 2013). The selectivity of surface functional group of GO has been expected from the negatively charged interaction which carbamazepine had higher adsorption. GO can be a very suitable adsorbent for the removal of ciprofloxacin and sulfamethoxasole from aqueous solutions (Chen, Gao et al. 2015).

Nevertheless, GO is difficult to completely separate from the aqueous solution, due to the highly solubility of GO in water. Accordingly, the modification of GO-based

adsorbents for prohibit aggregation of GO and develop the higher efficiency for lead adsorption was evaluated (Li, Wang et al. 2015). Praparation of SBA-15-grafted GO (GO–SBA-15) was performed amino groups were grafted onto SBA-15 (NH_2– SBA-15) and GO carboxyl groups as active site to bind the amino groups of NH_2–SBA-15. Owing to the similar chemical linking of NH_2–SBA-15 and NH_2–HMS (A-HMS), this method can be applied to the synthesized mesoporous silica-grafted graphene oxide material.

According to many studies, adsorption of ciprofloxacin and carbamazepine by graphene oxide (GO) modified mesoporous silica (HMS) has not been studied yet. GO modified HMS was bound between amino groups on HMS and carboxylic groups on GO, then the adsorbents were performed as amino grafted HMS (A-HMS) to bind GO, denoted as GO-A-HMS. Moreover, mercapto grafted HMS (M-HMS) which is the hydrophobic adsorbent could be provided higher adsorption capacity of selected pharmaceuticals than HMS and A-HMS. Therefore, amino and mercapto functionalized HMS (A5M5) was synthesized to bind GO with amino group and develop mercapto group for enhance the adsorption capacity, denoted as (GO-A5M5). Adsorption mechanism has been considered and proposed by various interaction mechanisms such as electrostatic interaction, hydrophobic force, hydrogen bonding, **π-π** interaction, etc.

CHAPTER 3
METHODOLOGY

3.1 MATERIALS

3.1.1 Chemical reagents

- Acetone	HPLC	LAB SCAN
- Acetonitrile	HPLC	LAB SCAN
- Carbamazepine	97%	SIGMA ALDRICH
- Ciprofloxacin	97%	Wako pure Co. Ltd
- Dimethylformamide	AR	LAB SCAN
- Dipotassium hydrogenphosphate	>97%	Ajax Finechem
- Dodecylamine	98%	ACROSS ORGANICS
- Ethyl alcohol absolute	RPE-ACS	CARLO ERBA
- Graphite poder		SIGMA ALDRICH
- Hydrochloric acid	37%	CARLO ERBA
- Hydrogenperoxide	30%	MERCK
- Methanol	HPLC	LAB SCAN
- Nitric acid	65%	CARLO ERBA
- N-N_0-dicyclohexylcarbodiimide	99%	SIGMA ALDRICH
- Potassium dihydrogenphosphate	AR grade	Riedel-de-Haen
- Potassiumpermanganate		SIGMA ALDRICH
- Sodium hydroxide	99%	MERCK
- Sulfuric acid	96%	CARLO ERBA

- Tetraeethylorthosilicate	98%	Fluka
- Toluene	98%	LAB SCAN
- 3-aminopropyltriethoxysilane	>98%	Fluka
- 3-mercaptopropyltrimethoxysilane	>98%	Fluka

3.1.2 Analytical Instruments

- High Performance Liquid Chromatography (HPLC-DAD)
- Column C18 Hypersil ODS 4 mm x 250 mm, 5 µm, Agilent, USA
- UV-Visible spectroscopy
- Syringe filter (Nylon Syringe Filter, 0.45 µm, 25 mm)
- Filter paper (Quantitative 5, 70 mm)
- Magnetic stirrer
- Vacuum filtration apparatus
- Vacuum pump
- Oven
- Thermometer
- Hot plate
- Shaker
- pH meter

3.2 PREPARATION OF ADSORBENT

3.2.1 Synthesis of hexagonal mesoporous silica (HMS)

Hexagonal mesoporous silica (HMS) was synthesized via hydrolysis of tetraethyl orthosilicate (TEOS) in dodecylamine, water and ethanol (Tanev and Pinnavaia 1996). In a typical synthesis, 0.27 mol of dodecylamine, 9.09 mol of ethanol and 29.6 mol of deionized water were mixed under vigorous stirring for 10 min to form organic template. Then, 1.0 mol of TEOS was added to a vigorously stirred solution. The reaction mixture was aged at ambient temperature for 18 h. The aged product was filtrated and washed with deionized water, and air-dried for 24 h. 1 g of the air-dried product was removed organic template by solvent extraction for 24 h with 150 mL of boiling ethanol. The final product was dried at 80°C for 1 h.

3.2.2 Synthesis of Single-funcional HMS (SF-HMS: A-HMS and M-HMS)

Single-functional HMS was synthesized via co-condensation (Lee, Kim et al. 2001). In a typical synthesis, 0.25 mol of dodecylamine, 10.25 mol of ethanol and 50 mol of deionized water were mixed under vigorous stirring for 10 min to form organic template. Then, 1.0 mol of TEOS was added to a vigorously stirred solution for 30 min. The reaction mixture was added with 0.25 mol of 3- aminopropyltriethoxysilane (APES) or 3- mercaptopropyltrimethoxysilane (MPTMS) and was vigorously stirred for 20 h at ambient temperature. The product was filtrated and washed with deionized water, and air-dried for 24 h. 1 g of the air-dried product was removed organic template by solvent extraction for 24 h with 150 mL of boiling ethanol. The final product was dried at 80°C for 1 h.

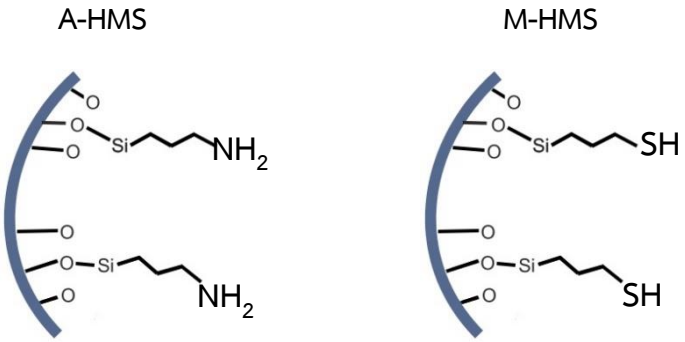

Figure 10 Surface functional group on A-HMS and M-HMS

3.2.3 Synthesis of Bi-funcional HMS (BF-HMS: A5M5)

Bi-funcional HMS was synthesized via co-condensation (Lee, Kim et al. 2001). In a typical synthesis, 0.25 mol of dodecylamine, 10.25 mol of ethanol and 50 mol of deionized water were mixed under vigorous stirring for 10 min to form organic template. Then, 1.0 mol of TEOS was added to a vigorously stirred solution for 30 min. The reaction mixture was added with 0.125 mol of APES and 0.125 mol of MPTMS and was vigorously stirred for 20 h at ambient temperature. The product was filtrated and washed with deionized water, and air-dried for 24 h. 1 g of the air-dried product was removed organic template by solvent extraction for 24 h with 150 mL of boiling ethanol. The final product was dried at 80°C for 1 h.

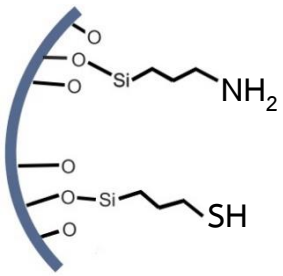

Figure 11 Surface functional group on A5M5

3.2.4 Synthesis of graphene oxide (GO)

Graphene oxide (GO) was synthesized via Hummers' method (Xu, Bai et al. 2008). In typical synthesis, 2 g of graphite powder was added to 120 mL of cold concentrated H_2SO_4 at 0°C under vigorous stirring in the ice bath. Then, 15 g of $KMnO_4$ was slowly added to vigorously stirred solution and the mixture was stirred at 35°C in water bath for 2h. Then, 250 mL of DI water was slowly added to the mixture in the ice bath which the temperature was kept below 20°C and the mixture was stirred at room temperature for 2h. After that, 700 mL of DI water was added under stirring and stir for 5 min, then additional of 20 mL of 30% H_2O_2 was added. The mixture was filtered and washed with 1 L of 5% HCl solution to remove metal ions followed by 1 L of DI water to remove the acid. The final product was dried at 60°C overnight.

3.2.5 Synthesis of mesoporous silica-grafted graphene oxide (GO-A-HMS and GO-A5M5)

Mesoporous silica-grafted graphene oxide (GO-A-HMS) was synthesized (Li, Wang et al. 2015). In a typical synthesis, 0.04 g of GO was added to 100 mL of dimethylformamide (DMF) into homogeneous dispersion via sonication for 30 min. Then, 0.2 g of A-HMS and 0.04 g of N-N_0-dicyclohexylcarbodiimide (DCC) were added. In case of GO-A5M5, 0.4 g of A5MS was used and others are the same as above. The reaction mixture was stored in a water bath at 60°C for 24 h. The final product was filtrated and washed with DMF followed by ethanol, and dried at 50°C for 24 h.

3.3 CHARACTERIZATION OF ADSORBENTS

Determination of the physicochemical characteristics of adsorbents were analyzed using instruments and analysis method as shown in Table 3.

Table 3 Analysis method of the physicochemical characteristics of adsorbents

Parameter	Instrument/Analysis method
Surface area	N_2 adsorption isotherm using BET theory
Pore size and pore volume	N_2 adsorption isotherm using BJH theory
Porous structure	X-Ray Diffraction (XRD)
Surface charge	Acid-Base Titration
Functional group	Fourier Transform Infrared Spectrometer (FT-IR)
Sulfur/Nitrogen contents	Elemental analyzer (CHNS/O)
Surface appearance	Scanning Electron Microscopy (SEM) and Transmission Electron Microscopy (TEM)
Elemental composition	X-ray Photoelectron Spectroscopy (XPS)
Graphene oxide content	Furnace

3.3.1 Surface area and pore size

Pore size, pore volume, and specific surface area were detrmined by nitrogen adsorption-desorption isotherm using Model Autosorb 1 MP Quantachrome automatic volumetric sorption analyzer at 77 K. The specific surface are (S_{BET}) was calculated using Brunner-Eller-Teller (BET) equation. Pore size and pore volume were calculated using Barrett-Joyner-Halenda (BJH) equation.

3.3.2 Porous structure

XRD pattern and crystal structure were measured by low and high angle X-ray diffraction (XRD) using fixed monochromator with Cu, 40 kV, 20 mA, and scanning rate 1,000 θ/min between 0.7° – 5° (2θ) for low angle and 5° - 40° (2θ) for high angle.

3.3.3 Surface charge measurement

The point of zero charge of the synthesized adsorbents were performed under batch equilibrium method. 0.005 g of the synthesized adsorbent was mixed with 10 mL of DI water by varying pH from 3.0 – 12.0 using a nitric acid and sodium hydroxide solution. The mixture was shaken at 200 rpm for 24 hours. The initial and final pH was measured by pH meter. The obtained data was plotted and the point of zero charge was evaluated by the common plateau of the graph (Babić, Milonjić et al. 1999).

3.3.4 Surface functional group

The organic surface functional group on the synthesized adsorbents were identified by Fourier Transform Infrared spectrometer (FT-IR). The FT-IR spectra recorded in the transmittance mode between 4000-400 cm^{-1}.

3.3.5 Elemental analysis

Nitrogen and sulfur contents were measured by elemental analyzer (CHNS/O).

3.3.6 Morphology

The morphology were observed using Scanning electron microscope (SEM) and Transmission electron microscopy (TEM) to inspect the surface appearance.

3.3.7 Elemental composition

Elemental composition of the synthesized adsorbents were investigated by X-ray photoelectron spectroscopy (XPS). The obtained data were analyzed using fitting program.

3.3.8 Graphene oxide content

The amount of graphene oxide was measured by burning via the weight lost for confirm the presence of GO on the surface of the adsorbents. The furnace was used high temperature over 550°C for 10 hours to investigate the remaining material.

3.4 ADSORPTION EXPERIMENTS

The adsorption experiment was studied under batch experiment. The stock solutions of CIP and CBZ were prepared in DI water and methanol, respectively.

Batch adsorption experiment of pristine HMS and GO modified HMS were performed using 125-mL Erlenmeyer flask with glass stopper containing 1 g·L^{-1} of HMS, A-HMS, M-HMS and A5M5 or 250 mg·L^{-1} of GO-A-HMS and GO-A5M5 in 20 mL of solution. The ionic strength and pH was controlled using 0.01 M phosphate buffer, and then the sample was shaken at 25°C (200 rpm). The adsorbent was separated by filtration through nylon filter. The remaining pharmaceutical concentration was analyzed by UV-visible spectrophotometer and/or HPLC-DAD.

The stock solution of GO was prepared in DI water via sonication and stored at 4°C in darkness. Batch adsorption experiment of GO was conducted using 15-mL polytetrafluoroethylene centrifuge tubes containing 20 mg·L^{-1} of GO in 10 mL of solution. The ionic strength and pH was controlled using 0.01 M phosphate buffer, and then the sample was shaken at 25°C (200 rpm). The solution was centrifuged at 4500 rpm for 30 min and filtered through nylon filter. The remaining pharmaceutical concentration was analyzed by UV-visible spectrophotometer and/or HPLC-DAD.

The adsorption capacity was calculated as Equation (3.1):

$$q = \frac{(C_0 - C_e)V}{M} \quad (3.1)$$

Where q_e is the adsorption capacity (mg·g^{-1}), C_0 and C_e are the initial and equilibrium concentration (mg·L^{-1}), respectively. V is the volume of the solution (L) and M is the mass of adsorbent (g).

3.4.1 Adsorption kinetic study

The parameters in kinetic adsorption can be summarized in Table 4.

Table 4 The considered parameters in adsorption kinetic study

Parameters	Values of each adsorbents		
	HMS, A-HMS, M-HMS, A5M5	GO	GO-A-HMS, GO-A5M5
Adsorbent dose	1 g·L^{-1}	20 mg·L^{-1}	250 mg·L^{-1}
Initial pharmaceuticals concentration	5 mg·L^{-1}	5 mg·L^{-1}	5 mg·L^{-1}
Equilibrium time	0 - 3 h	0 - 48 h	0 - 24 h
Ionic strength	0.01 M phosphate buffer at pH 7.0		
Temperature	25°C		
Stirring speed	200 rpm		

Adsorption kinetic study was performed by varying equilibrate time from 0 - 48 h. The initial pharmaceutical concentration were 5 mg·L^{-1} for 1 g·L^{-1} of HMS, A-HMS, M-HMS, A5M5, 20 mg·L^{-1} of GO and 250 mg·L^{-1} of GO-A-HMS, GO-A5M5 in 0.01 M phosphate buffer pH 7.0. The sample was shaken at 25°C (200 rpm), and then the adsorbent was separated by filtration through nylon syringe filter, 0.45 μm 25 mm at time intervals. The remaining pharmaceutical concentration was analyzed by UV-visible spectrophotometer and/or HPLC-DAD as described in the analytical method. The obtained data were calculated and plotted between time interval and adsorption capacity as shown in Figure 12.

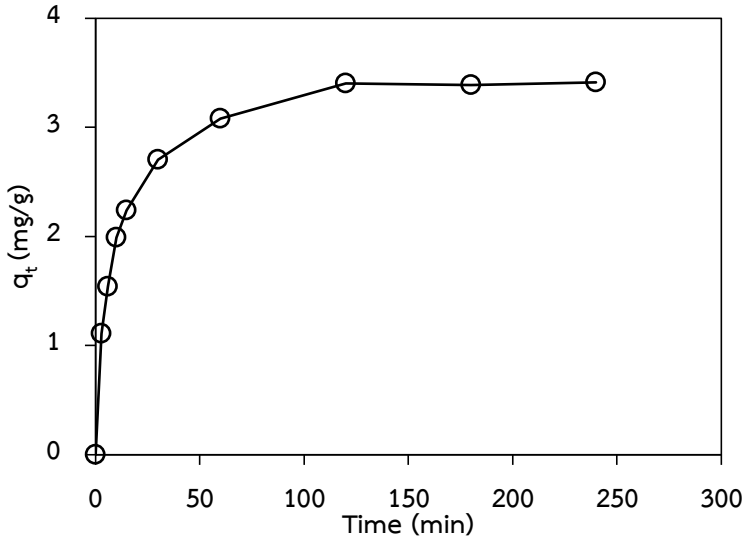

Figure 12 Adsorption kinetic is plotted between time (min) and adsorption capacity (q_t)

3.4.2 Adsorption isotherm study

The parameters in isotherm adsorption can be concluded in Table 5.

Table 5 The considered parameters in adsorption isotherm study

Parameters	Values of each adsorbents		
	HMS, A-HMS, M-HMS, A5M5	GO	GO-A-HMS, GO-A5M5
Adsorbent dose	1 g•L^{-1}	20 mg•L^{-1}	250 mg•L^{-1}
Initial pharmaceuticals concentration	0.1 - 10 mg•L^{-1}	0.1 - 10 mg•L^{-1}	0.1 - 10 mg•L^{-1}
Equilibrium time	3 h	48 h	24 h
Ionic strength	0.01 M phosphate buffer at pH 7.0		
Temperature	25°C		
Stirring speed	200 rpm		

Adsorption isotherm study was performed with the initial pharmaceutical concentration range between 0 - 10 mg•L^{-1} for 1 g•L^{-1} of HMS, A-HMS, M-HMS, A5M5, 20 mg•L^{-1} of GO and 250 mg•L^{-1} of GO-A-HMS, GO-A5M5 in 0.01 M phosphate buffer pH 7.0. The sample was shaken at 25°C (200 rpm), and then the adsorbent was separated by filtration through nylon syringe filter, 0.45 µm 25 mm at equilibrium time. The remaining pharmaceutical concentration was analyzed by UV-visible spectrophotometer and/or HPLC-DAD as described in the analytical method. The obtained data were calculated and plotted between equilibrium concentration and equilibrium adsorption capacity as shown in Figure 13.

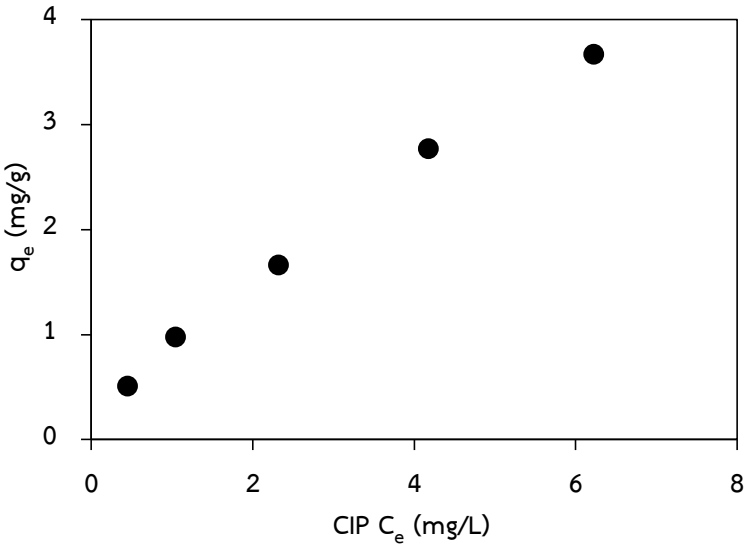

Figure 13 Adsorption isotherm is plotted between equilibrium concentration (C_e) and equilibrium adsorption capacity (q_e)

3.4.3 Selective adsorption study

Selective adsorption in binary-solute solution was determined by a mixture of CIP and CBZ on the synthesized adsorbents. The experiment was performed in the same condition as the single solute solution at pH 7.0. The remaining pharmaceutical concentration was analyzed by HPLC-DAD as described in the analytical method.

3.4.4 Low concentration adsorption study

Adsorption isotherm study was performed with the initial pharmaceutical concentration range between 10 - 200 mg•L^{-1} for 250 mg•L^{-1} of GO-A-HMS, GO-A5M5 in 0.01 M phosphate buffer pH 7.0. The sample was shaken at 25°C (200 rpm), and then the adsorbent was separated by filtration through nylon syringe filter, 0.45 µm 25 mm at equilibrium time. The remaining pharmaceutical concentration was analyzed by HPLC-DAD as described in the analytical method.

3.5 ANALYTICAL METHODS

3.5.1 Determination of pharmaceuticals in single solute solution

The concentration of CIP and CBZ at initial and equilibrium time in single solute solution was determined by UV-visible spectrophotometer at 271 and 286 nm, respectively.

3.5.2 Determination of pharmaceuticals in mixed solute solution

The concentration of CIP and CBZ at initial and equilibrium time in mixed solute solution and in low concentration adsorption were determined by HPLC-DAD. The remaining concentration of pharmaceuticals were analyzed by a reverse phase high performance liquid chromatography (HPLC) equipped with a photodiode array detector (260-280 nm). The condition to determine CIP and CBZ was performed at 25°C on a normal-phase HPLC column (4 mm x 250 mm, 5 µm; Hypersil ODS C18, Agilent, USA). The condition was performed using acetonitrile and KH_2PO_4 mixture (60:40 % v/v) as the mobile phase within 9 min. The flow rate was 1 mL•min^{-1} and injection volume was 40 µL.

CHAPTER 4
RESULTS AND DISCUSSION

4.1 PHYSICOCHEMICAL CHARACTERIZATION

In this study, hexagonal mesoporous silica (HMS) was synthesized and modified surface functional group by co-condensation method onto pristine HMS, with two different types of organosilanes, i.e. amino-, mercapto- and amino- + mercapto-functional groups (A-HMS, M-HMS, A5M5, respectively) to investigated the effect of hydrophilicity and hydrophobicity of each adsorbents on the adsorption capacities of CIP and CBZ. Furthermore, graphene oxide (GO) was also synthesized and modified with grafted mesoporous silicas as GO-A-HMS and GO-A5M5 to investigated the effect of **π-π** interaction and hydrophobicity on CIP and CBZ adsorption capacities compared to pristine HMS. The physico-chemical characteristics of the synthesized adsorbents (i.e. pore structure, morphology, surface area, surface charge, etc.) were studied together with the results of adsorption experiment. Summary of synthesized adsorbents used in this study are shown in Table 6.

Table 6 List of the synthesized adsorbents used in this study

Adsorbents	Surface functional group
Mesoporous silica	
HMS	Silanol (-OH)
A-HMS	Amino (-NH_2)
M-HMS	Mercapto (-SH)
A5M5	Amino and mercapto (-NH_2 and -SH)
Graphene oxide	
GO	Epoxides, hydroxyl, and ketones
GO modified HMS	
GO-A-HMS	Epoxides, hydroxyl, ketones, and silanol (-OH)
GO-A5M5	Epoxides, hydroxyl, ketones, and mercapto (-SH)

4.1.1 Morphology of adsorbents

The morphologies of HMS and grafted HMS were observed using a scanning electron microscope (SEM) to inspect their surface appearance. As shown in Figure 14, SEM images of pristine HMS, A-HMS, M-HMS, and A5M5 show their spherical particles, but A-HMS was slightly smaller (Hongsawat, Prarat et al. 2014).

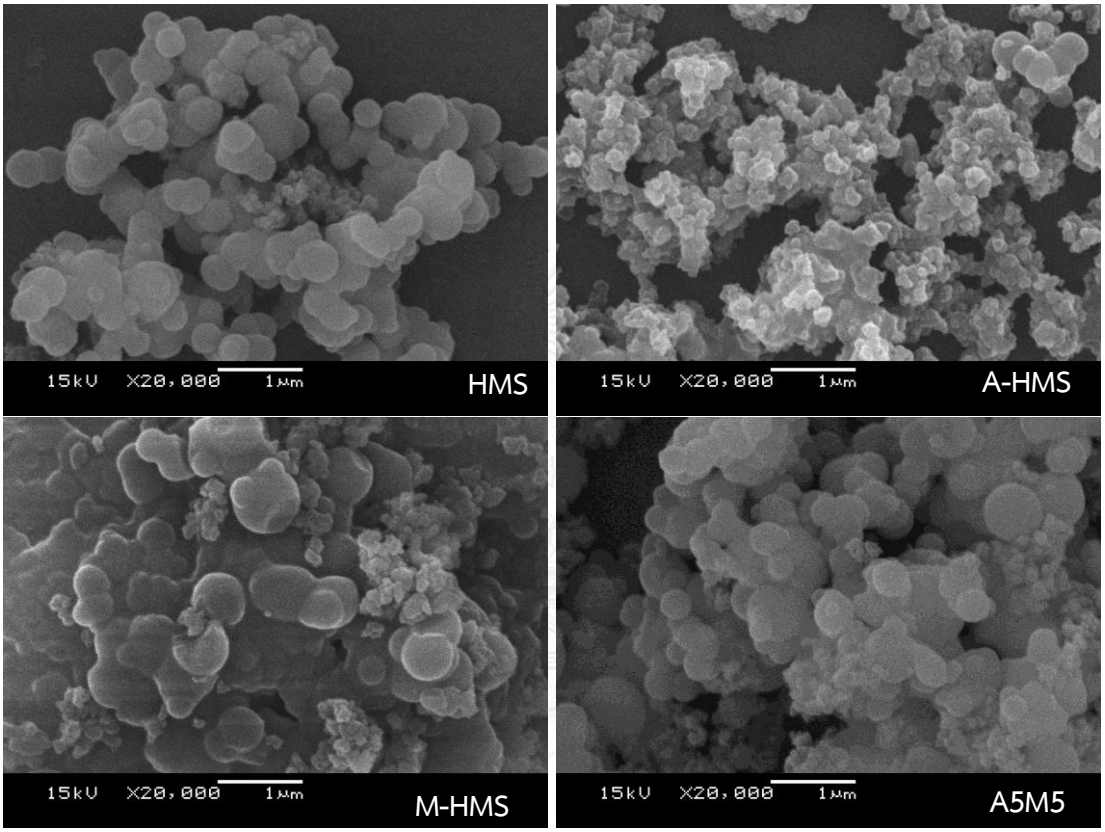

Figure 14 Representative SEM images of HMS, A-HMS, M-HMS, and A5M5 (x20000)

Figure 15 displays SEM and TEM images of GO and GO modified HMS. SEM and TEM images of GO shows the layer of GO nanosheets and the agglomeration on the surface. After combination, A-HMS and A5M5 particles were attached on the GO layer, as can be seen in the Figure 13. The surface of GO is quite more transparent than individual GO sheets due to the dispersion during the synthesis process and the particle of A-HMS and A5M5 were wrapped up on GO flakes as quite the same porous structure.

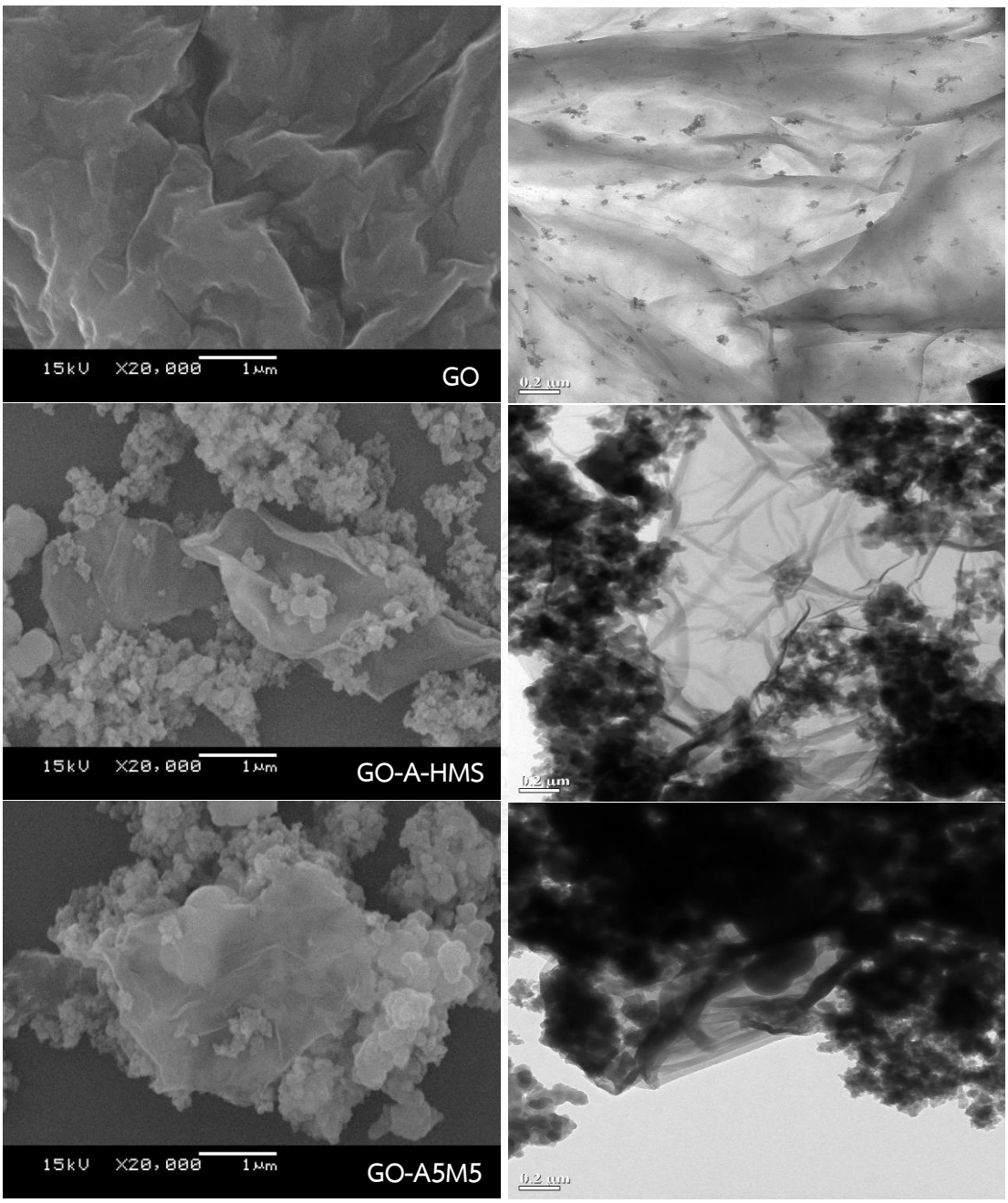

Figure 15 Representative SEM and TEM images of the GO, GO-A-HMS, and GO-A5M5 (x20000)

4.1.2 Hexagonal structure confirmation by powder XRD technique

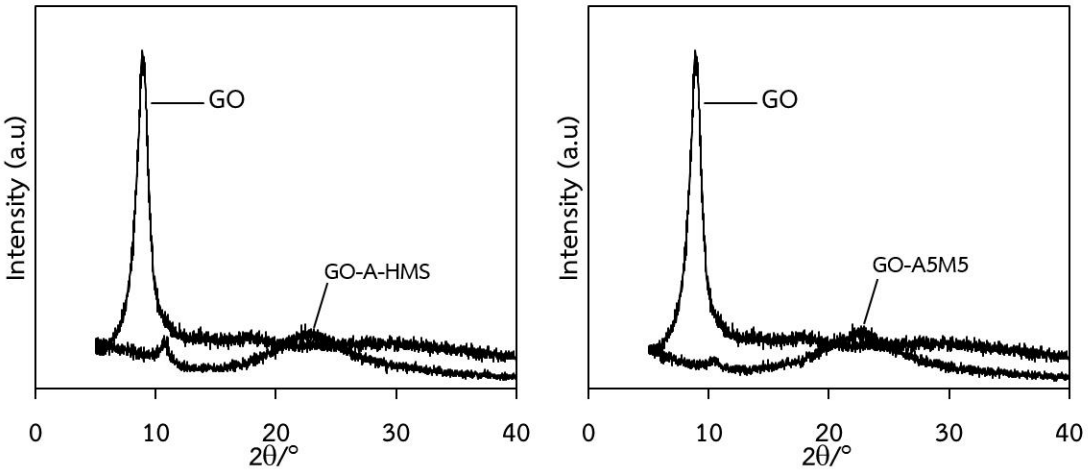

Figure 16 Representative X-ray powder diffraction patterns of GO comparing with GO-A-HMS, and GO-A5M5

Figure 16 shows the XRD patterns of GO comparing with GO-A-HMS and GO-A5M5. The intense GO diffraction peak at 2θ = 8.88° is characteristic of the interplanar d-spacing of plane (200) corresponding to confirm the successful of GO synthesis (Li, Wang et al. 2015). Following modification with A-HMS, the intense diffraction peak of GO-A-HMS was shifted to 2θ = 23.10°, implied that the oxygen-containing functional groups on GO were partially changed via the chemical interaction with A-HMS. As same as GO-A-HMS, the intense diffraction peak of GO-A5M5 was at 2θ = 22.74°.

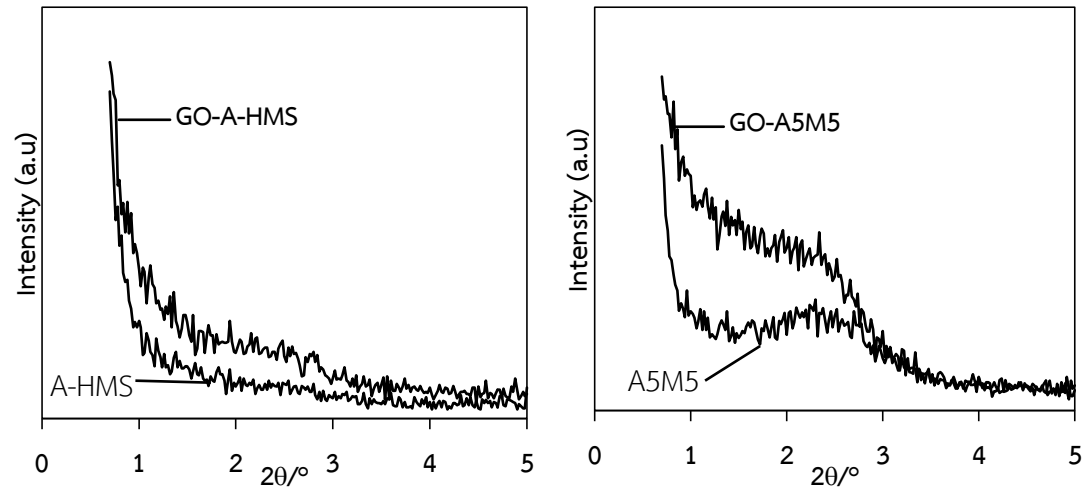

Figure 17 Representative small-angle X-ray powder diffraction patterns of A-HMS and GO-A-HMS, and A5M5 and GO-A5M5

Figure 17 shows the small-angle XRD patterns of A-HMS and GO-A-HMS. The peaks at 2θ = 0.5-2.5° corresponding to (100), (110), and (200) diffraction peaks of hexagonal symmetry XRD pattern (Li, Wang et al. 2015). The peaks of the small-angle GO-A-HMS diffraction pattern were observed by the position of the peaks were almost same as A-HMS. It can be concluded that the mesoporous structure was conserved during GO encapsulation. Similar to GO-A-HMS, the peaks of the small-angle GO-A5M5 diffraction pattern were almost identical to A5M5.

4.1.3 Surface area and pore structure characteristics

Figure 18 shows the N_2 adsorption-desorption isotherms of pristine HMS, grafted HMS, and GO modified HMS, which was typical of materials containing mesopores. The results show the BET surface area of HMS and grafted HMS followed the order: M-HMS HMS > GO-A5M5 > A5M5 > A-HMS > GO-A-HMS whereas the decrease of pore volume and surface area of A-HMS could be detected. It can be concluded that hydrophilic functional group could be more grafting onto HMS surface. The pore size distribution results are calculated from the Barett-Joyner-Halenda (BJH) method as shown in Figure 19. The pore size, pore volume, and BET surface area were summarized in Table 7.

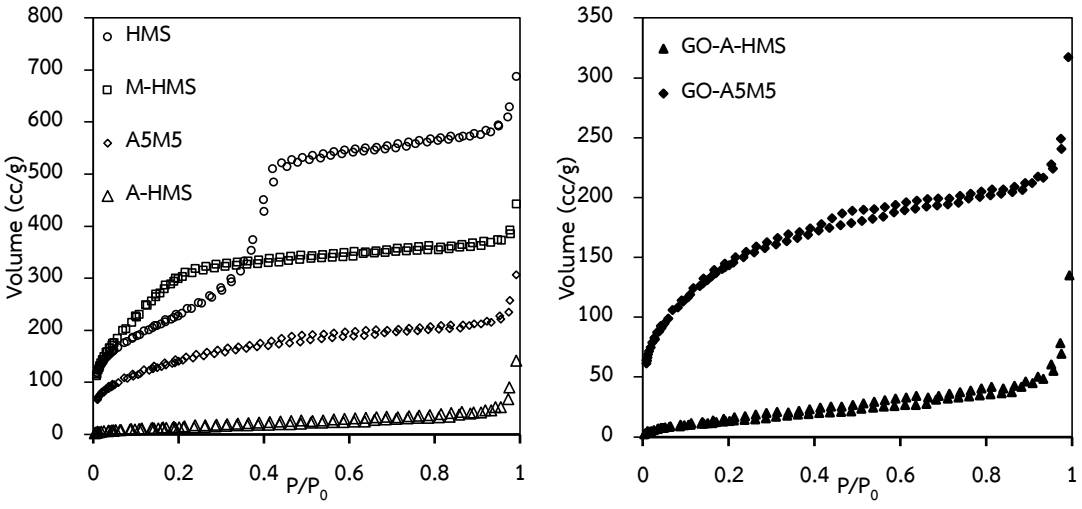

Figure 18 N_2 adsorption-desorption isotherms of the synthesized adsorbents

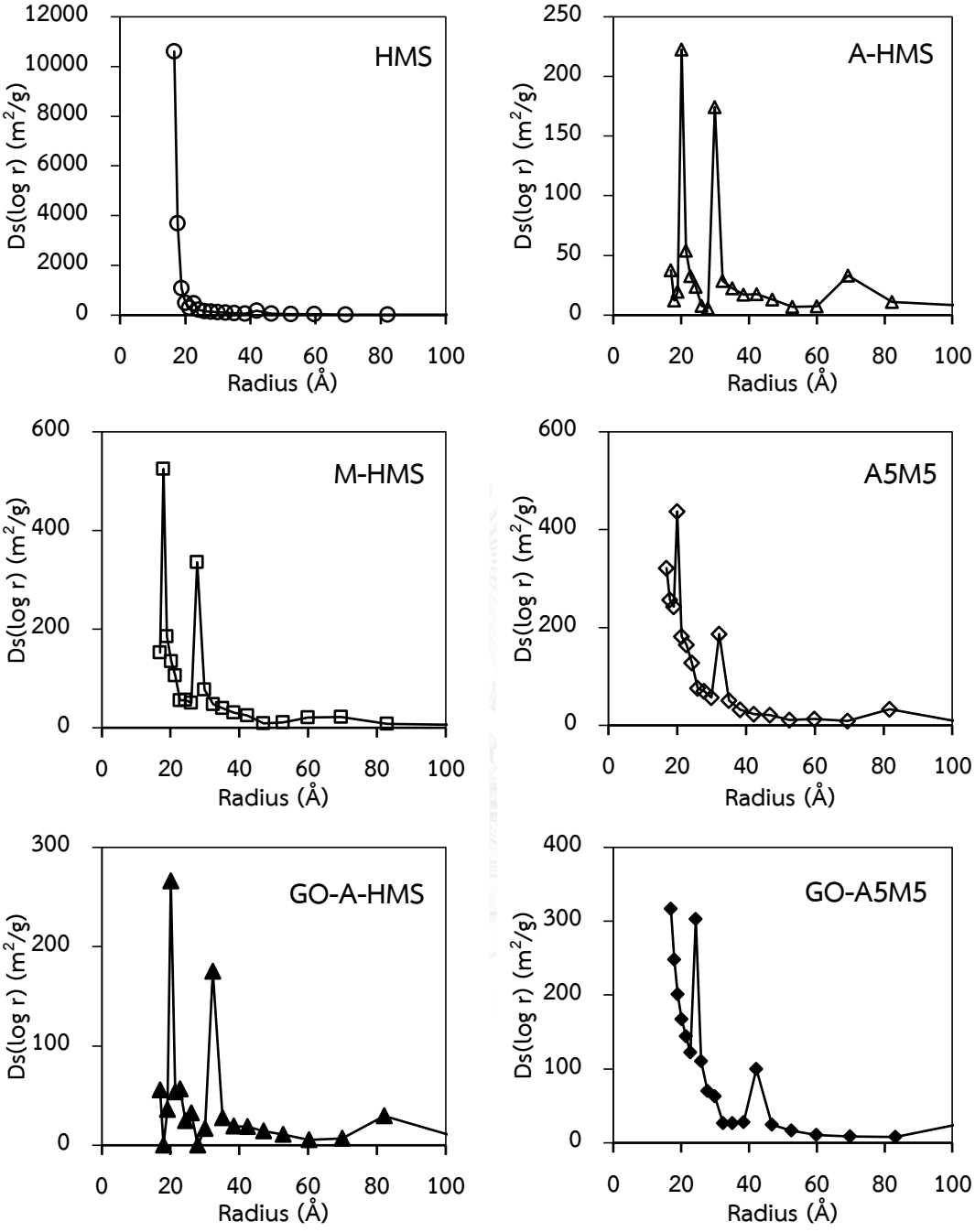

Figure 19 Pore size distribution of the synthesized adsorbents

Table 7 Mean pore diameter, BET surface area, and pore volume of HMS and grafted HMS

Adsorbents	Pore diameter (Å)	Pore volume (mm^3/g)	BET surface area (m^2/g)
HMS	41.94	1.0620	873.49
A-HMS	32.28	0.2183	52.32
M-HMS	27.76	0.6828	1233.12
A5M5	32.24	0.4743	518.98
GO	105.60	1.6580	3143.99
GO-A-HMS	32.32	0.2085	49.85
GO-A5M5	24.26	0.4903	546.59

4.1.4 Surface functional group characterization of organic-functionalized HMS by FT-IR spectroscopy

The functional group presenting on the surface of the adsorbents were identified by using Fourier Transform Infrared (FT-IR). The FT-IR spectra of pristine HMS and grafted HMS were displayed in Figure 20. Pristine HMS performed the O-H stretching at 3742 cm^{-1} of silanol group on the surface. The spectra of all mesoporous silica contained Si-O stretching and ring structure of SiO4 at 1092 and 804-814 cm^{-1}, respectively. Moreover, the broad peak around 3480-3300 cm^{-1} that implied the hydrogen bonded Si-OH (non-grafted silanol) onto the surface of all mesoporous silica (Hongsawat, Prarat et al. 2014).

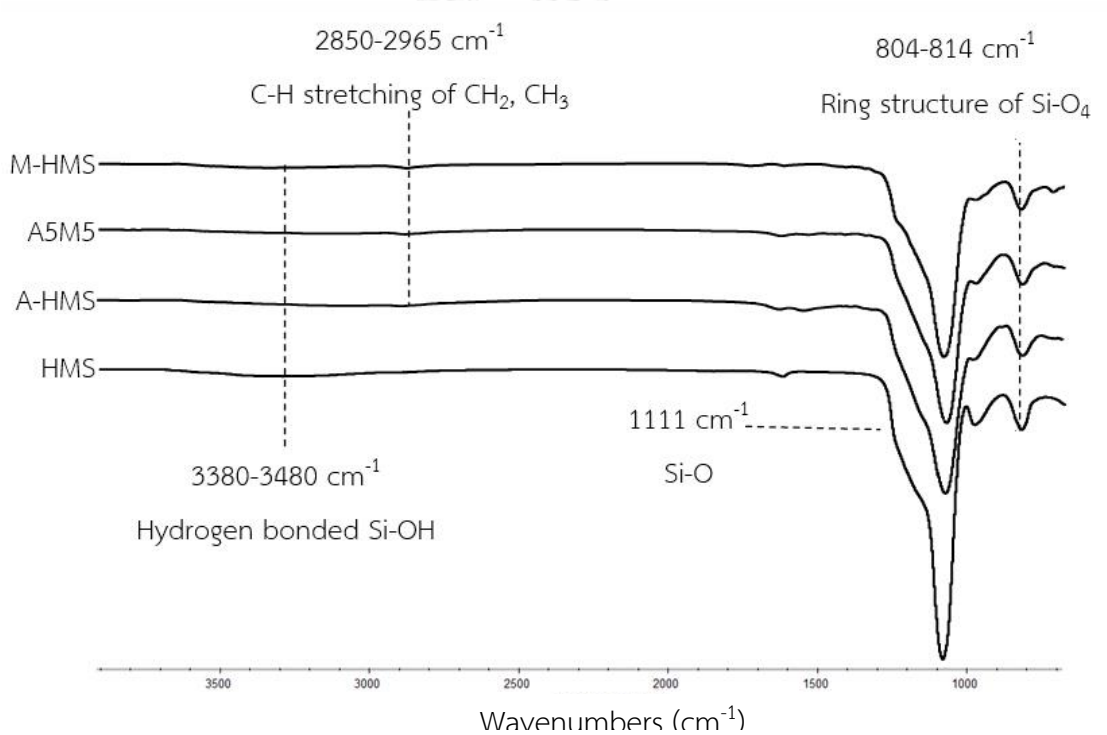

Figure 20 Representative FT-IR spectra of pristine HMS and grafted HMS

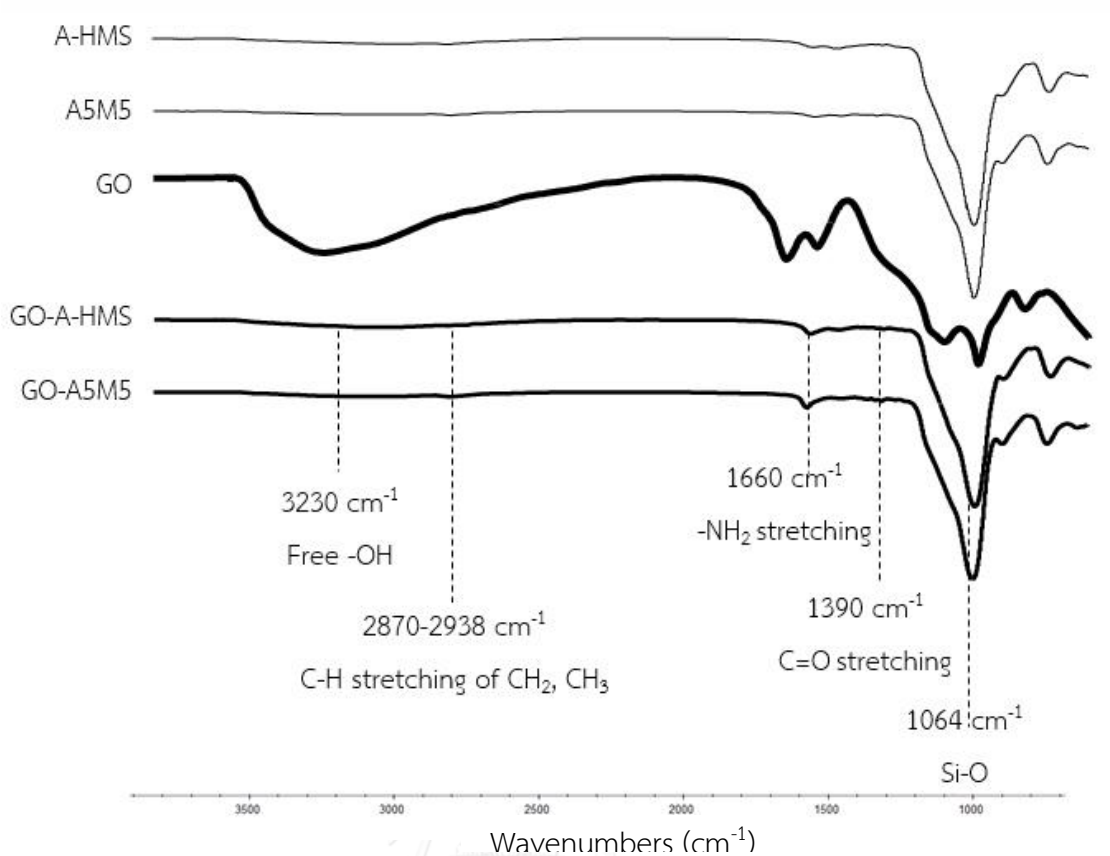

Figure 21 Representative FT-IR spectra of A-HMS, A5M5, GO, GO-A-HMS, and GO-A5M5

Figure 21 shows the FT-IR spectra of A-HMS, A5M5, GO, GO-A-HMS, and GO-A5M5. The peaks at 3230 cm^{-1} are indicated free hydroxyl group of GO (Li, Wang et al. 2015). The peaks 1064 cm^{-1} are exhibited the Si-O stretching vibrations. The bands at 1660 and 1390 cm^{-1} are indicated –NH2 and C=O stretching vibrations, respectively. It can be proved that A-HMS was chemically bonded to the GO sheet.

4.1.5 Nitrogen and sulfur contents of adsorbents

The quantification of nitrogen and sulfur in the synthesized adsorbents were evaluated by elemental analysis for confirming the presence of amino- and mercapto-functional group on the surface of A-HMS, M-HMS, A5M5, GO-AHMS, and GO-A5M5. From Table 8, N content of A-HMS was detected for indicating the amino group, and S content for confirming the presence of mercapto group on the surface of adsorbents.

Table 8 Nitrogen and sulfur content of the synthesized adsorbents

Adsorbents	Percent (% w/w)		Density of functional group (μmol/m^2)	
	S	N	S	N
HMS	-	-	-	
A-HMS	-	3.27		4.46
M-HMS	7.98	-	0.20	
A5M5	3.80	1.77	0.23	0.24
GO	-	-	-	-
GO-A-HMS	-	3.33	-	4.77
GO-A5M5	3.40	1.76	0.23	0.19

4.1.6 GO content on GO modified HMS

The quantification of GO were evaluated by burning using furnace. The weight lost was confirmed the presence of GO on the surface of GO-AHMS and GO-A5M5 as shown in Table 9. The furnace was used high temperature over 550°C for 10 hours to investigate the remaining material. Generally, the decomposition temperature of GO and mesoporous silica are 280-300°C and 500°C, respectively. Then, the weight lost at 550°C mean the quantification of GO and the remaining material is HMS.

Table 9 Quantity of GO on the synthesized adsorbents

Adsorbents	Percent (% w/w)
GO-A-HMS	22.85
GO-A5M5	18.39

4.1.7 Surface charge of adsorbents

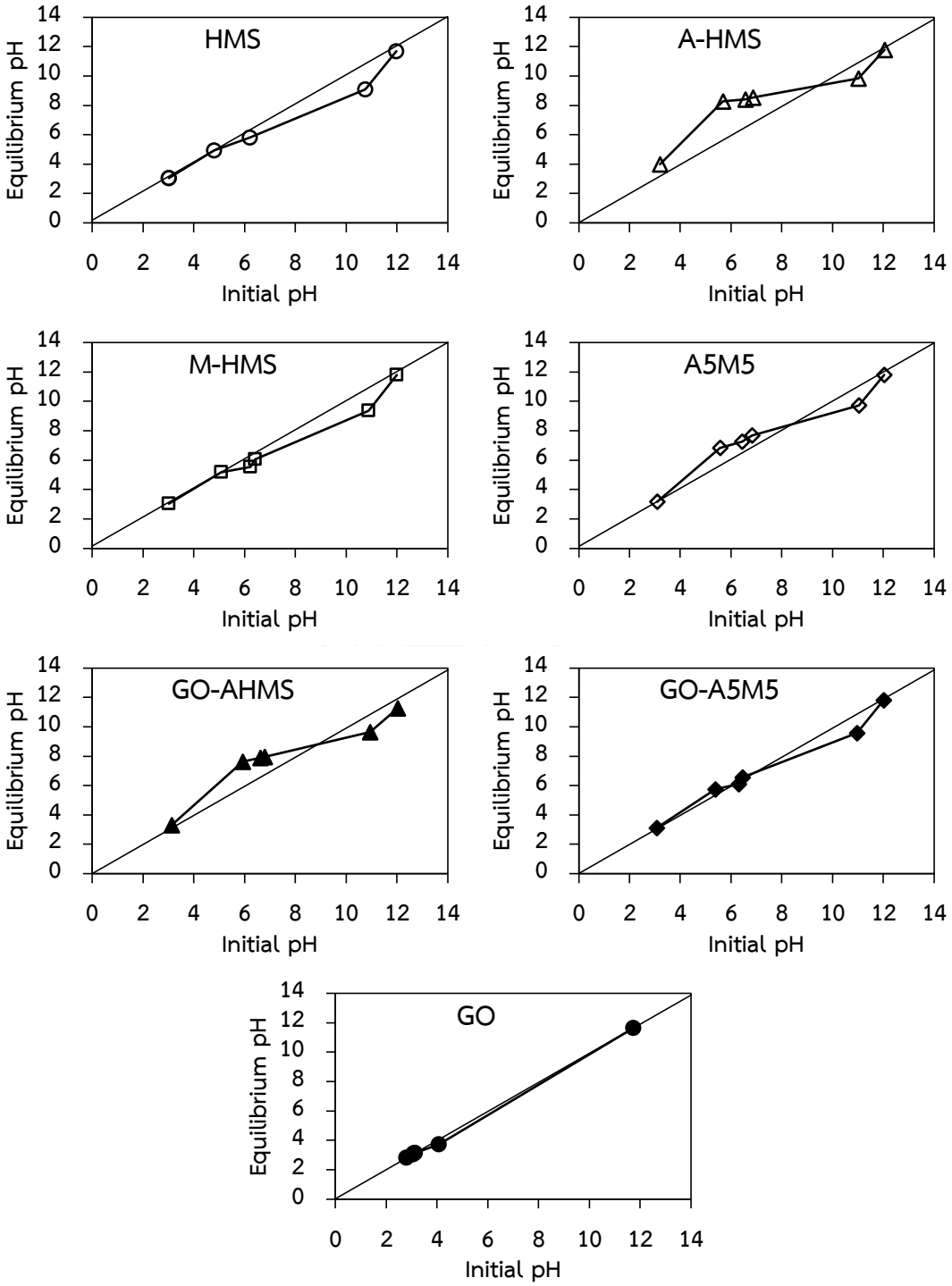

Figure 22 Surface charge of the synthesized adsorbents

The surface charge of the synthesized adsorbents were investigated by acid/base titration technique. The surface charge at initial and equilibrium pH in each pH range 3.0 – 12.0 were plotted as shown in Figure 22. The surface charge of the adsorbents were summarized as the zero point of charge (pH_{pzc}) in Table 10.

Table 10 pH_{pzc} of the synthesized adsorbents

Adsorbents	pH_{pzc}
HMS	5.3
A-HMS	9.3
M-HMS	5.6
A5M5	8.5
GO	3.3
GO-A-HMS	8.8
GO-A5M5	7.3

4.1.8 Hydrophobicity of adsorbents

In order to investigate the hydrophobicity of the synthesized adsorbents' surface, the contact angle (θ) of the adsorbent was summarized from previous reports. The contact angle of each adsorbent was obtained in the following order: M-HMS > HMS > A-HMS as shown in Table 11. A higher θ value shows a better hydrophobic characteristic of the adsorbent's surface. According to contact angle value, the adsorbents can be classified into two groups: hydrophobic adsorbent surface (M-HMS) and hydrophilic adsorbent surface (HMS and A-HMS).

Table 11 The contact angle of the synthesized adsorbents

Adsorbents	Contact angle (θ)
HMS	45.06 [a]
A-HMS	40.18 [a]
M-HMS	89.65 [a]
A5M5	-
GO	-
GO-A-HMS	-
GO-A5M5	-

[a] Reference: (Hongsawat, Prarat et al. 2014)

4.1.9 X-ray photoelectron spectroscopy (XPS)

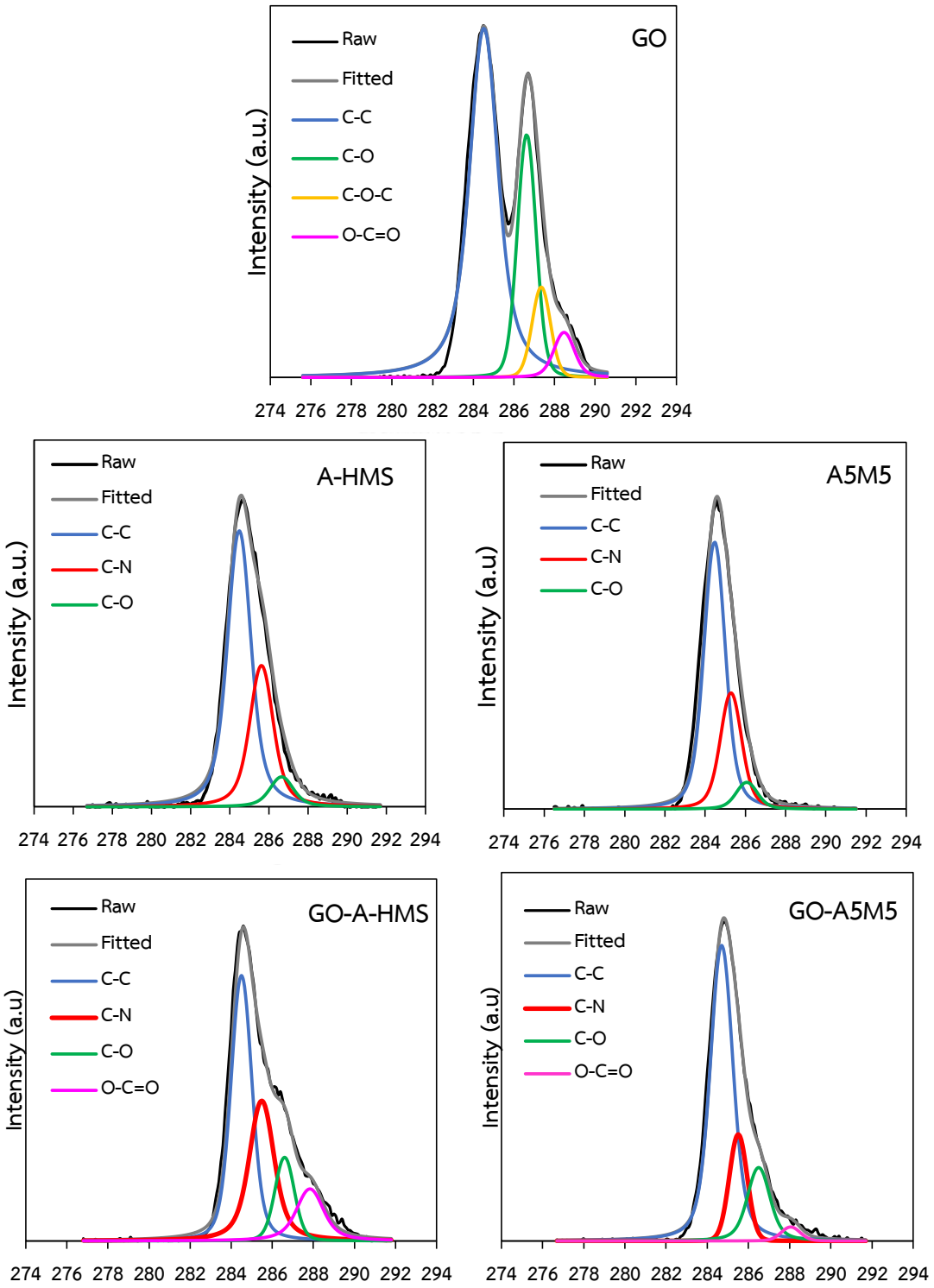

Figure 23 Representative XPS spectra C 1s of GO, A-HMS, A5M5, GO-A-HMS, and GO-A5M5

Figure 23 shows XPS spectra of GO, A-HMS, A5M5, GO-A-HMS, and GO-A5M5 in term of C 1s using X-ray photoelectron spectroscopy. In case of GO, the components included C-C (284.6 eV), C-O (286.7 eV), C-O-C (287.5 eV), and O-C=O (288.6 eV), respectively. It can be seen A-HMS and A5M5 contained C-C (284.6 eV), C-N (285.7 eV), and C-O (286.8 eV), respectively. For GO-A-HMS, the components of C-C (284.6 eV), C-N (285.6 eV), C-O (286.7 eV), and O-C=O (287.9 eV), respectively, were observed. It can be conclude that GO was chemical bonded with HMS due to C-N bond (Yang, Li et al. 2015).

4.2 ADSORPTION KINETICS

The adsorption kinetic study is represented the pharmaceuticals uptake rate on the adsorbent and the rate limiting step for performing and modeling adsorption process. The adsorption rate and equilibrium time can be used to describe the adsorption mechanism via film diffusion and intraparticle diffusion. The data are calculated and fitted with adsorption kinetic models i.e. pseudo-first-order model, pseudo-second-order model and intraparticle diffusion model to determine the adsorption order, rate constant, and the adsorption mechanism.

The adsorption kinetic of selected pharmaceuticals including ciprofloxacin (CIP) and carbamazepine (CBZ) on pristine HMS, grafted HMS, GO, and GO modified HMS were conducted to investigate the effects of surface functional group. The batch experiment were performed at pH around 7 with ionic strength of 0.01 M controlled by phosphate buffer. The experimental data were calculated and fitted with kinetic models to analyze the possible adsorption mechanism.

4.2.1 Effect of surface functional group

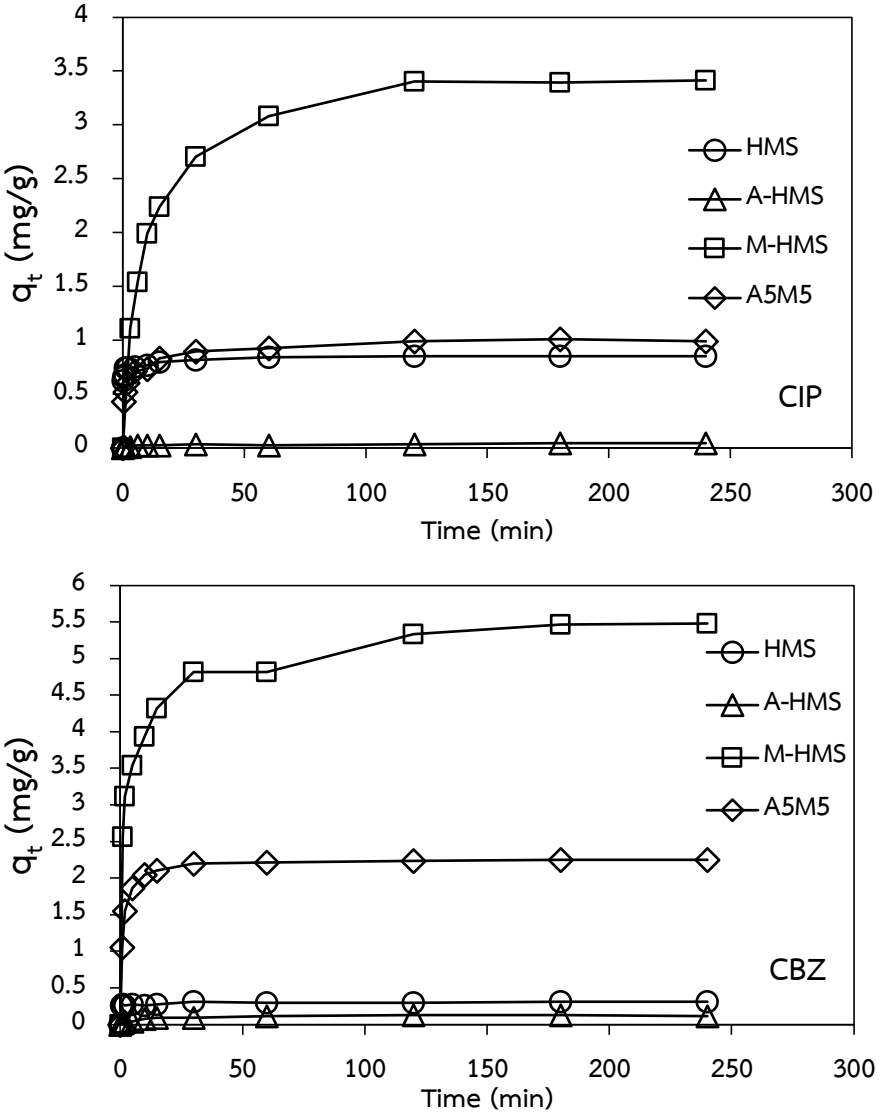

Figure 24 Adsorption kinetics of CIP and CBZ on pristine HMS and grafted HMS

Figure 24 shows adsorption kinetics of CIP and CBZ on pristine HMS and grafted HMS including A-HMS, M-HMS, and A5M5, which provided different surface functional group. It can be seen that the concentration of both CIP and CBZ decreased in the first 30 minutes and reached equilibrium stage within 4 hours.

In case of GO modified HMS, the concentration of both CIP and CBZ decreased in the first 30 minutes and then achieved the equilibrium stage at approximately 6 hours as shown in Figure 25. The higher equilibrium time of GO-A-HMS and GO-A5M5 could be the results of the presence of GO on the materials. Figure 26 reveals the adsorption kinetic of CIP and CBZ on GO that reached the equilibrium within 24 hours approximately.

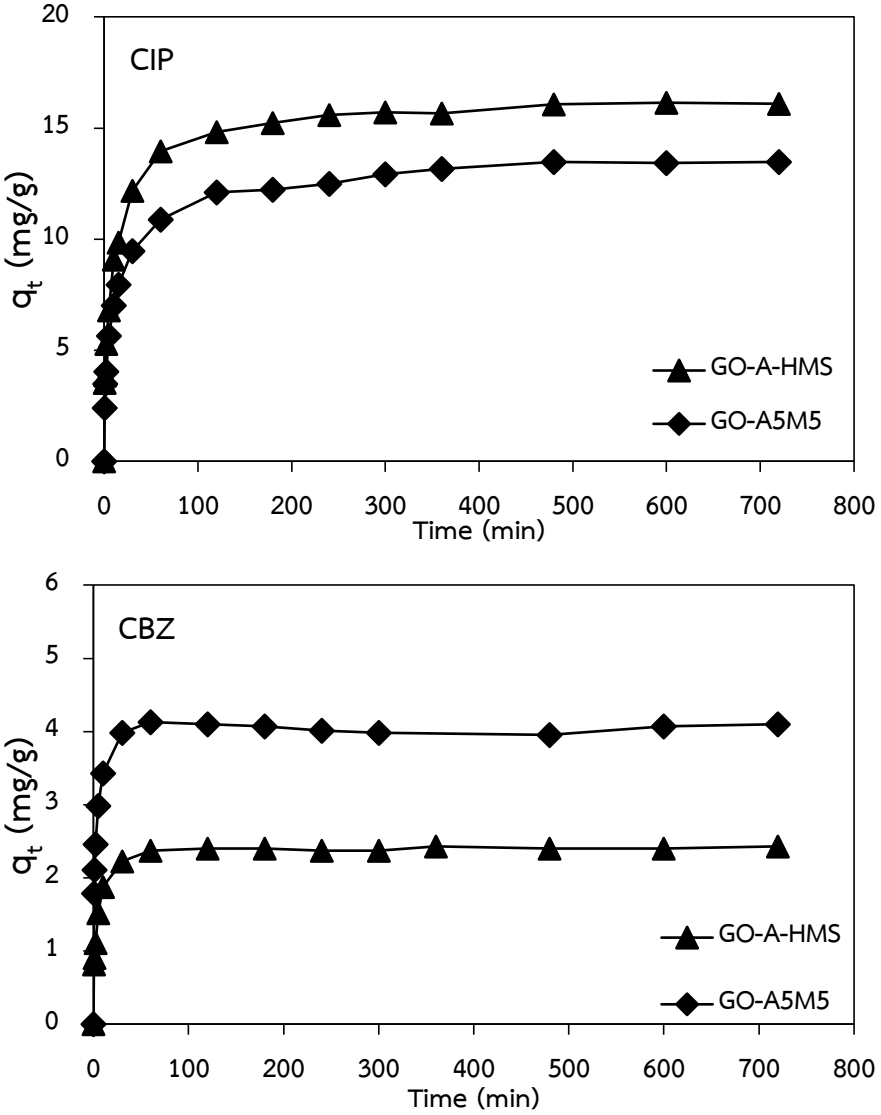

Figure 25 Adsorption kinetics of CIP and CBZ on GO modified HMS

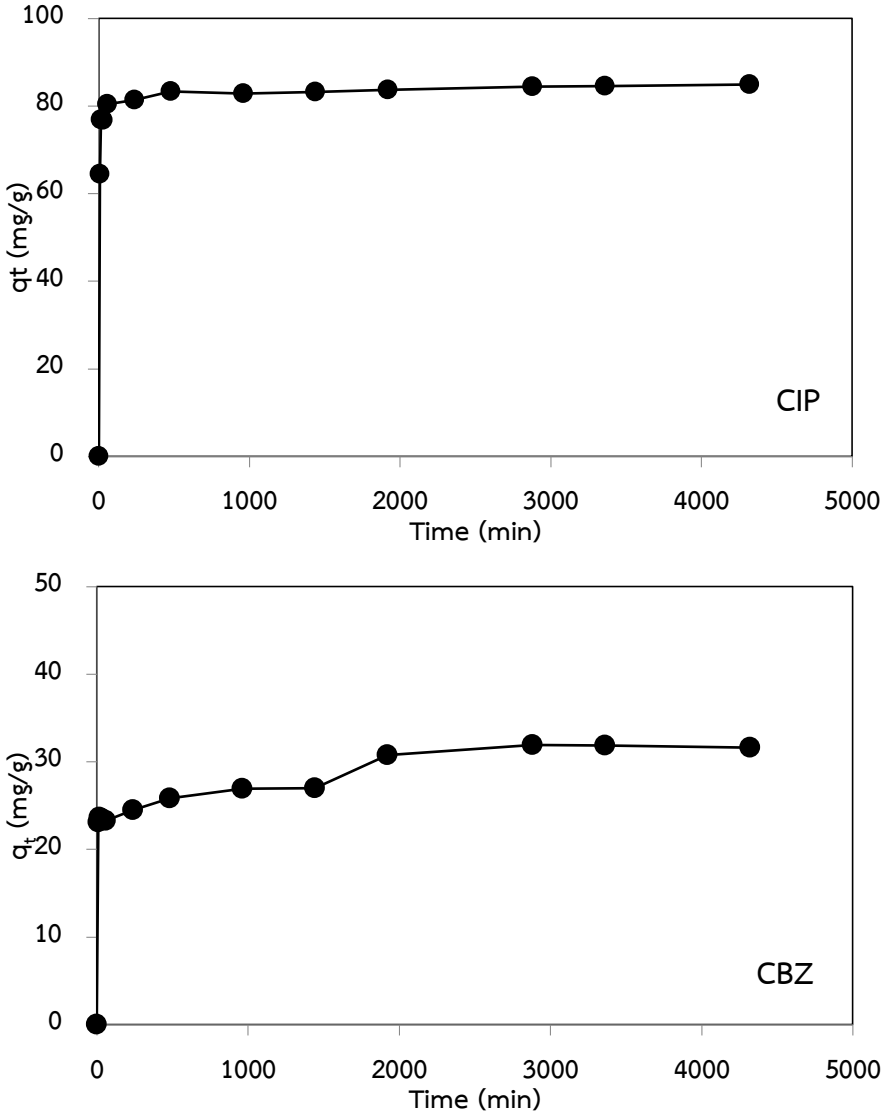

Figure 26 Adsorption kinetics of CIP and CBZ on GO

In order to analyze the adsorption rate of CIP and CBZ on the synthesized adsorbents, the pseudo-second-order and Ritchie's-second-order adsorption kinetic model were used for analyze the experimental data. Then, the pseudo-second-order adsorption kinetic model could be described the adsorption kinetic study.

The pseudo-second-order and Ritchie's-second-order are expressed as in the Equation 4.1.2. and 4.2.2, respectively.

$$\frac{t}{q_t} = \frac{1}{2k_2 q_e^2} + \frac{t}{q_e} \quad (4.2.1)$$

$$\frac{1}{q_t} = \frac{1}{k_R q_e t} + \frac{1}{q_e} \quad (4.2.2)$$

Where k_2 is the pseudo-second-order rate constant ($g \cdot mg^{-1} \cdot min^{-1}$)

k_R is the Ritchie's-second-order rate constant ($1 \cdot min^{-1}$)

q_e is the amount of pharmaceutical adsorbed ($mg \cdot g^{-1}$) at equilibrium

q_t is the amount of pharmaceutical adsorbed ($mg \cdot g^{-1}$) at time t (min)

Moreover, the initial adsorption rate (h) can be calculated as in the Equation 4.2.3

$$h = k_2 q_e^2 \quad (4.2.3)$$

Where h is the initial sorption rate ($mg \cdot (g \cdot min)^{-1}$)

The experimental data were plotted between t/q_t versus time for pseudo-second-order rate and $1/q_t$ versus $1/t$ for Ritchie's-second-order rate as shown in Figure 27 and 28 for CIP and CBZ kinetic adsorption, respectively. The calculated kinetic parameters (experimental q_e, calculated qe, rate constant, initial sorption rate, and R^2 values) of CIP and CBZ on all adsorbents were summarized in Table 12.

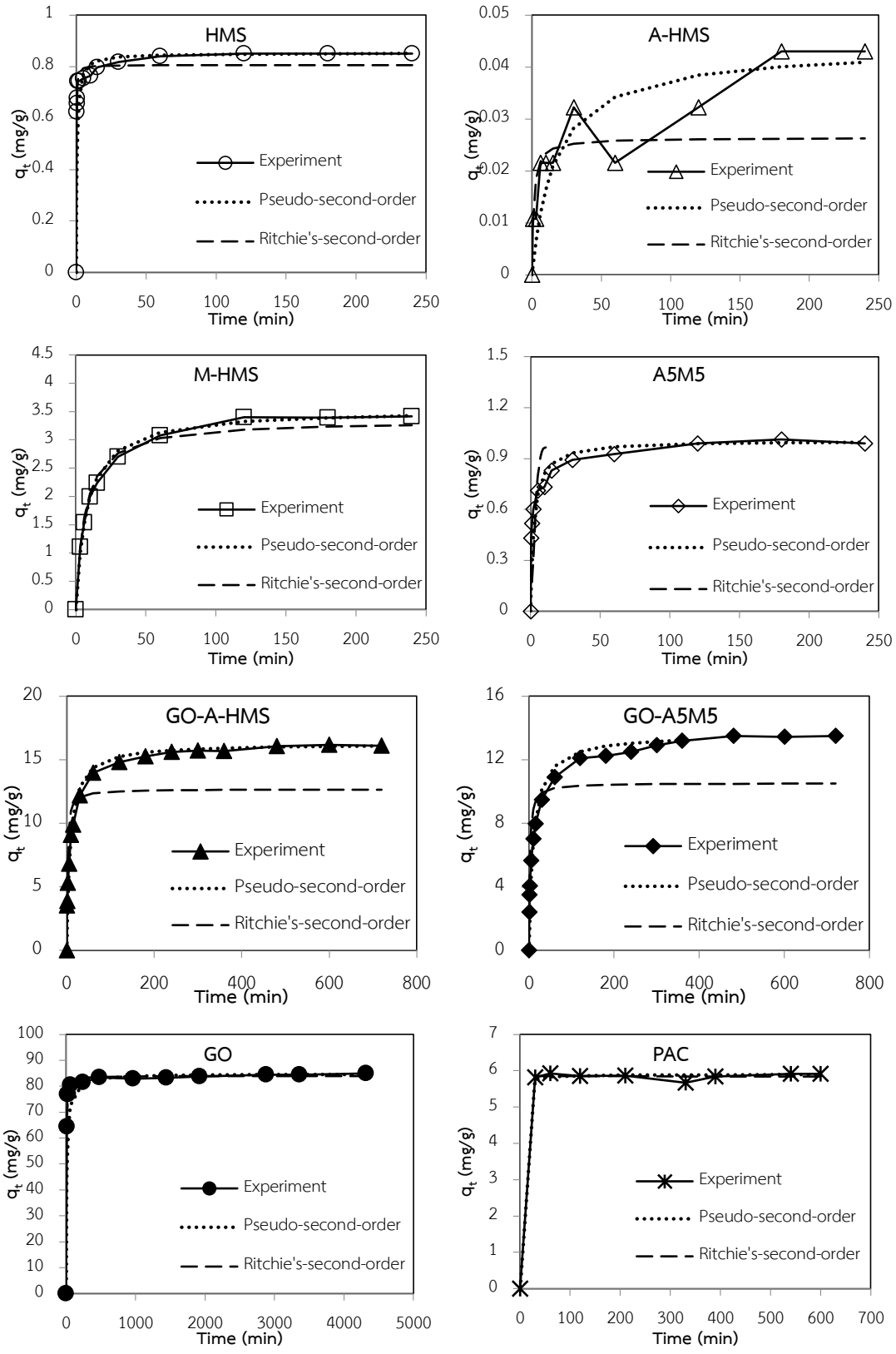

Figure 27 Adsorption kinetics of CIP on the synthesized adsorbents and PAC

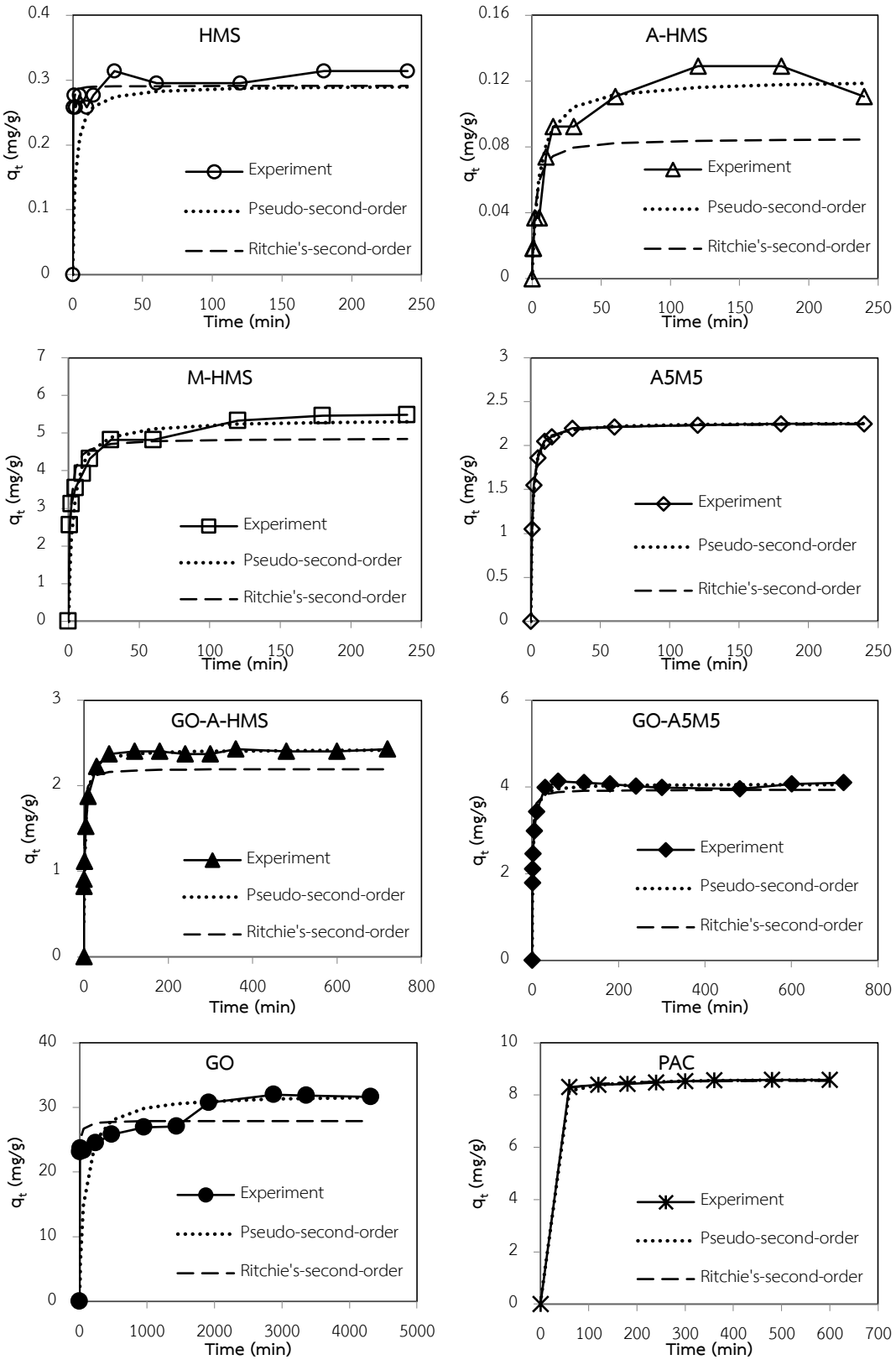

Figure 28 Adsorption kinetics of CBZ on the synthesized adsorbents and PAC

Table 12 Kinetic parameters of CIP and CBZ adsorption on the synthesized adsorbents and PAC at 6 mg/L and 9 mg/L, respectively. (pH 7 and IS 0.01 M)

Adsorbents	$q_{e,exp}$[a]	Pseudo-second-order				Ritchie's-second-order		
		q_e[a]	k_2[b]	h[d]	R^2	q_e[a]	k_R[c]	R^2
CIP								
HMS	0.850	0.852	1.066	0.775	1	0.81	11.39	0.817
A-HMS	0.043	0.044	0.691	0.001	0.949	0.026	0.778	0.611
M-HMS	3.412	3.539	0.018	0.225	0.999	3.346	0.158	0.990
A5M5	0.990	1.007	0.208	0.211	0.999	0.974	0.456	0.873
GO	84.947	84.746	0.001	4.198	0.999	84.034	0.391	0.891
GO-A-HMS	16.103	16.260	0.004	1.024	0.999	12.674	0.634	0.852
GO-A5M5	13.477	13.605	0.003	0.646	0.999	10.526	0.542	0.920
PAC	5.910	5.896	0.040	1.394	0.999	5.845	34.918	0.001
CBZ								
HMS	0.314	0.292	0.912	0.078	0.999	0.291	13.560	0.329
A-HMS	0.110	0.121	0.845	0.012	0.989	0.085	0.500	0.832
M-HMS	5.480	5.365	0.032	0.916	0.998	0.4861	1.020	0.897
A5M5	2.251	2.261	0.197	1.009	1	2.250	1.061	0.999
GO	31.164	32.051	0.000	0.230	0.997	27.933	0.365	0.431
GO-A-HMS	2.430	2.424	0.085	0.498	0.999	2.198	0.987	0.873
GO-A5M5	4.100	4.065	0.080	1.322	0.999	3.937	1.160	0.965
PAC	8.58	8.628	0.017	1.238	1	8.584	0.451	0.862

[a] Unit of the equilibrium adsorption capacity (q_e) is mg·g^{-1}

[b] Unit of the pseudo-second-order rate constant (k_2) is g·mg^{-1}·min^{-1}

[c] Unit of the Ritchie's-second-order rate constant (k_R) is 1·min^{-1}

[d] Unit of the initial sorption rate (h) is mg·(g·min)$^{-1}$

The kinetic parameters could be suggested the adsorption rate of the adsorbents. The pseudo-second-order rate constant (k_2) illustrated that the adsorbents with high k_2 required higher quantity of adsorbate than the low k_2 adsorbents. Considering the pseudo-second-order kinetic parameters by comparison on the initial adsorption rate (h), the initial adsorption rate of CIP decreased followed the order of GO < GO-A-HMS < GO-A5M5 < M-HMS < A5M5 < HMS < A-HMS as showed in Table 12. The initial adsorption rate showed the rate of adsorption at the initial period, which can be implied to the drastically decrease of CP and CBZ concentration in the first 30 minutes. The initial adsorption rate of CBZ was similar to CIP, except GO-A5M5 had higher rate than GO-A-HMS.

4.2.2 Intraparticle diffusion mechanism

The intraparticle diffusion model was also applied to analyze the diffusion mechanism inside the adsorbent particles. The adsorption process can be described in three step; (i) film or external diffusion, (ii) pore or intraparticle diffusion, and (iii) interaction at a site on the surface of the adsorbent. Among these three steps, the rate-limiting step in the adsorption process can be found by the slowest one. The third step is not considered to be the rate-limiting step because it is relatively fast comparing with the others. Thus, the rate of the adsorption is controlled by film diffusion or intraparticle diffusion.

The intraparticle diffusion model can be defined as in the Equation 4.3.4.

$$q_t = k_{ip} \cdot t^{0.5} + C_i \quad (4.3.4)$$

Where k_{ip} is the intraparticle diffusion rate constant ($mg \cdot g^{-1} \cdot min^{-0.5}$).

q_t is the amount of pharmaceutical adsorbed ($mg \cdot g^{-1}$) at time (t).

C_i is the constant relating to the thickness of the boundary layer ($mg\ g^{-1}$), which is determined from the intercept of the plot.

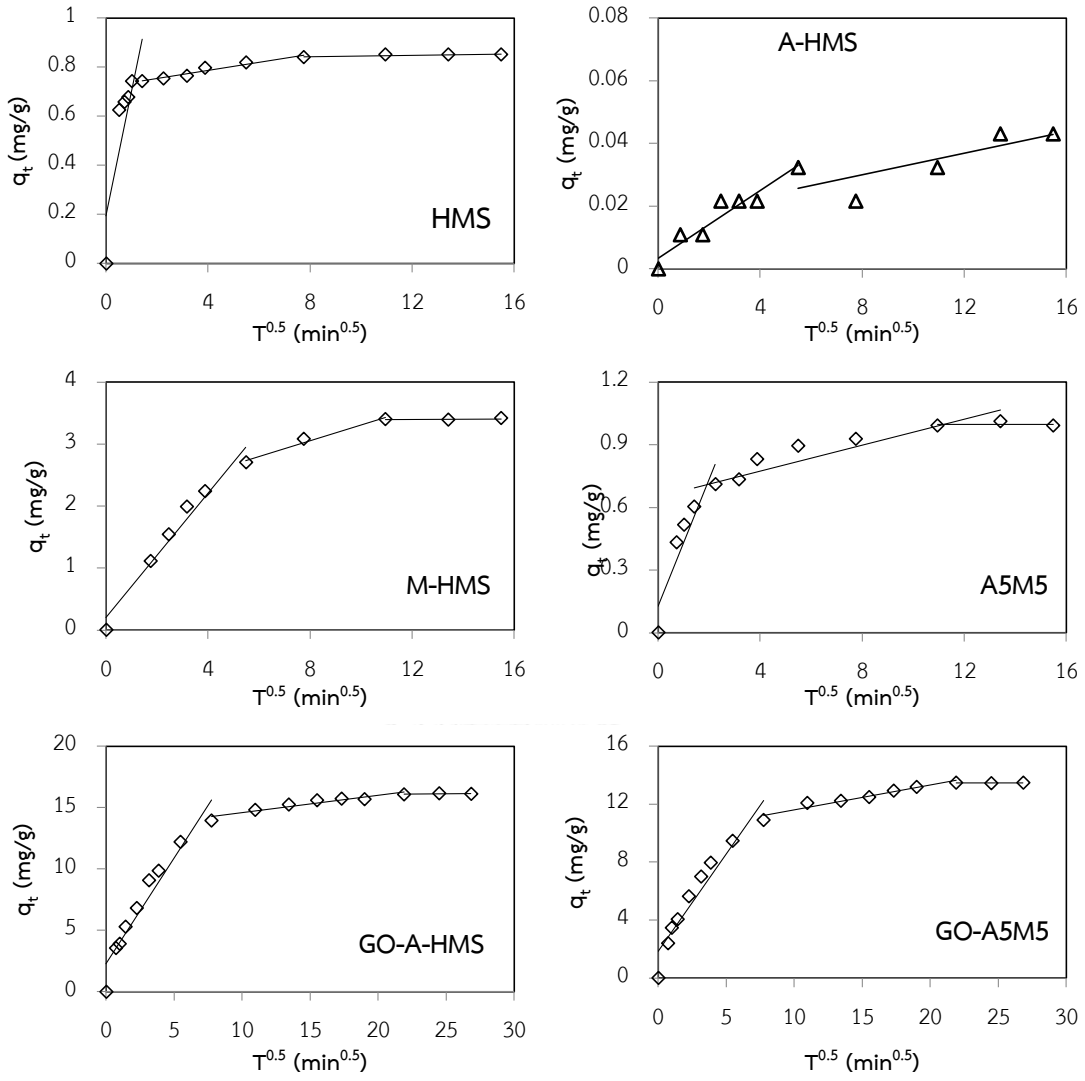

Figure 29 Intraparticle diffusion plot of CIP onto the adsorbents

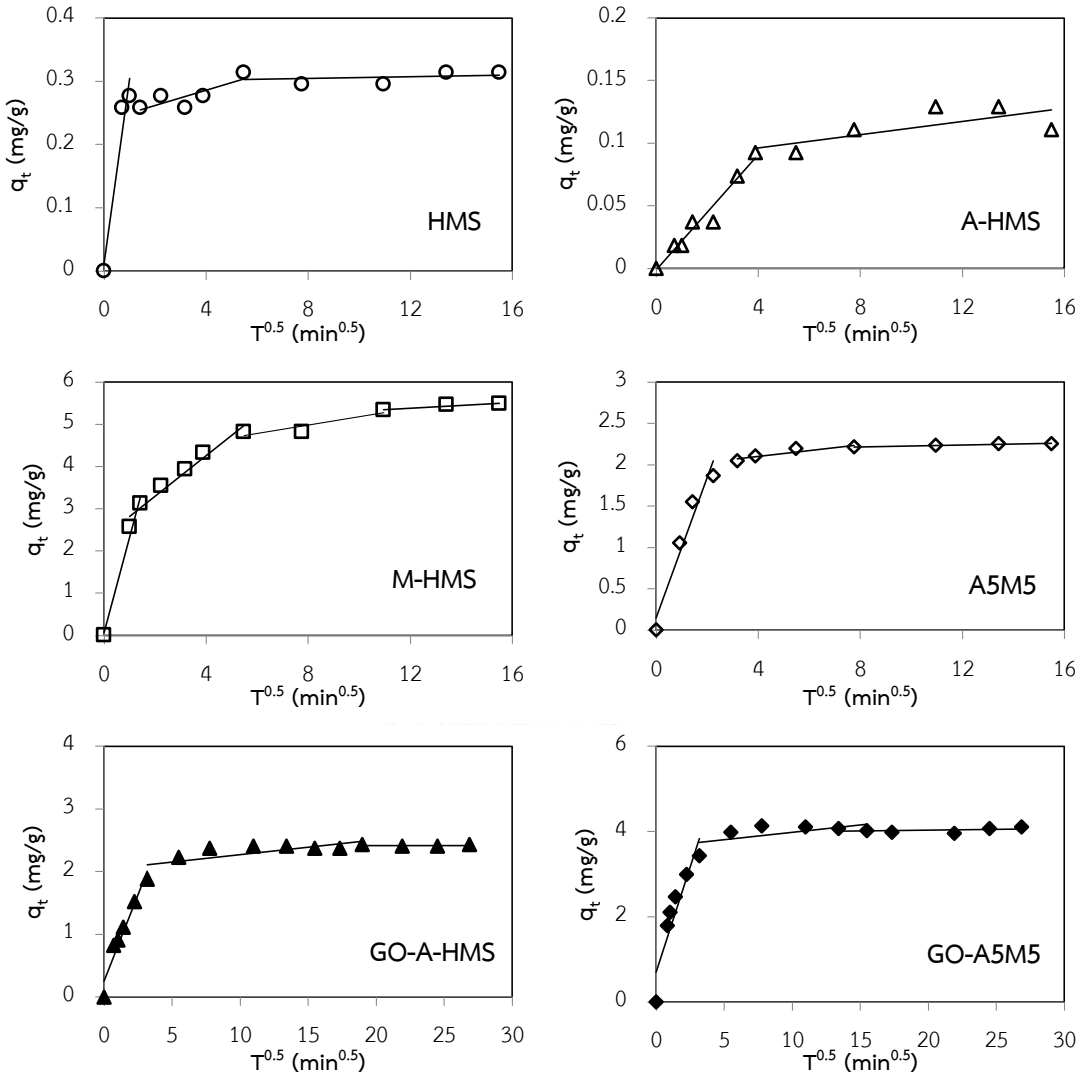

Figure 30 Intraparticle diffusion plot of CBZ onto the adsorbents

As shown in Figure 29 and 30, the experimental data were plotted between q_t versus $t^{0.5}$. The intraparticle plot could be exhibit a multi-linearity pattern of three steps in the adsorption process. The slope did not pass through the origin for all adsorbents that implied to it was not only the intraparticle diffusion occur in the adsorption, but film diffusion could be affected the interaction. For the multi-linear stage, the first linear refer to the adsorption is controlled by film diffusion and the second linear stage is indicated the intraparticle diffusion. The rate of both stages were show in Table 13 as k_{ip1} and k_{ip2} were the rate of film and intraparticle diffusion, respectively. The obtained results showed two or three linear diffusion stage of all adsorbents. The less value of k_{ip} indicated the lower rate constant as it could be the rate limiting step of the adsorption. From the results of all the adsorbents, the intraparticle diffusion rate constant (k_{ip2}) were lower than film diffusion rate constant (k_{ip1}), except A-HMS. The calculated k_{ip2} values follow the order M-HMS > A5M5 > HMS > A-HMS implied that pore size of adsorbents might influence the adsorption rate for both CIP and CBZ adsorption. In case of GO-AHMS and GO-A5M5 the result were similar to HMS adsorption due to their pore size that GO-A-HMS provided higher than GO-A5M5. Therefore, the rate limiting step for CIP and CBZ adsorption on all adsorbents were controlled by intraparticle diffusion, and also related to low porosity of the adsorbents. In case of A-HMS, the film diffusion was limited by a high hydrophilic surface of A-HMS.

Table 13 Intraparticle diffusion model parameters of CIP and CBZ adsorption on the synthesized adsorbents

Adsorbents	Film diffusion	Intraparticle diffusion		
	k_{iP1}[a]	k_{ip2}[b]	Intercept *(C1)*	R^2
CIP				
HMS	0.508	0.016	0.721	0.9515
A-HMS	0.005	-	-	-
M-HMS	0.052	0.126	2.046	0.9797
A5M5	0.304	0.031	0.650	0.8525
GO-A-HMS	1.719	0.140	13.172	0.9102
GO-A5M5	1.341	0.172	9.873	0.9427
CBZ				
HMS	0.293	0.012	0.238	0.6951
A-HMS	0.023	-	-	-
M-HMS	2.271	0.099	4.192	0.8301
A5M5	0.847	0.036	1.960	0.8502
GO-A-HMS	0.552	0.024	2.026	0.5592
GO-A5M5	0.991	0.035	3.626	0.3951

[a] Unit of the rate of film diffusion (k_{iP1}) is $mg \cdot g^{-1} \cdot min^{-0.5}$

[b] Unit of the rate of intraparticle diffusion (k_{ip2}) is $mg \cdot g^{-1} \cdot min^{-0.5}$

4.3 ADSORTION ISOTHERM

The adsorption isotherm study can be used to describe the adsorption phenomena of the process by equilibrium experimental data. The results from adsorption isotherm were applied with physicochemical characteristic of the synthesized adsorbents to describe the adsorption mechanisms and capacities. The parameters from isotherm models (i.e. Langmuir and Freundlich model) were also used to determine the adsorption mechanism. The adsorption isotherm of selected pharmaceuticals including ciprofloxacin (CIP) and carbamazepine CBZ) on pristine HMS, grafted HMS, GO, and GO modified HMS were conducted to investigate the effects of surface functional group, compared with powdered activated carbon (PAC). The batch experiment were performed in single solute solution at pH around 7±0.2 with ionic strength of 0.01 M controlled by phosphate buffer.

4.3.1 Effect of surface functional group

The effect of different surface functional group including silanol, amino, and mercapto on HMS can be determined the main adsorption interaction. The adsorption capacities of CIP and CBZ on the synthesized adsorbents and PAC at pH 7 with 0.01 M ionic strength controlled by phosphate buffer are shown in Figure 31 and 32, respectively. CIP has pK_a at 6.10 (carboxyl group) and 8.70 (amine group), and CBZ has pK_a at 2.30 (ketone group) and 13.90 (amine group). These pharmaceuticals have two pK_a values that mean they can be ionized depend on pH of the solution. Thus, CIP and CBZ are neutral charge species at pH 7. The molecule dimensions of CIP (0.57 nm in width and 0.95 nm in length) and CBZ (0.72 nm in width and 1.35 nm in length) are smaller than pore size of all adsorbents; therefore, the effect of adsorbents' pore size can be neglected.

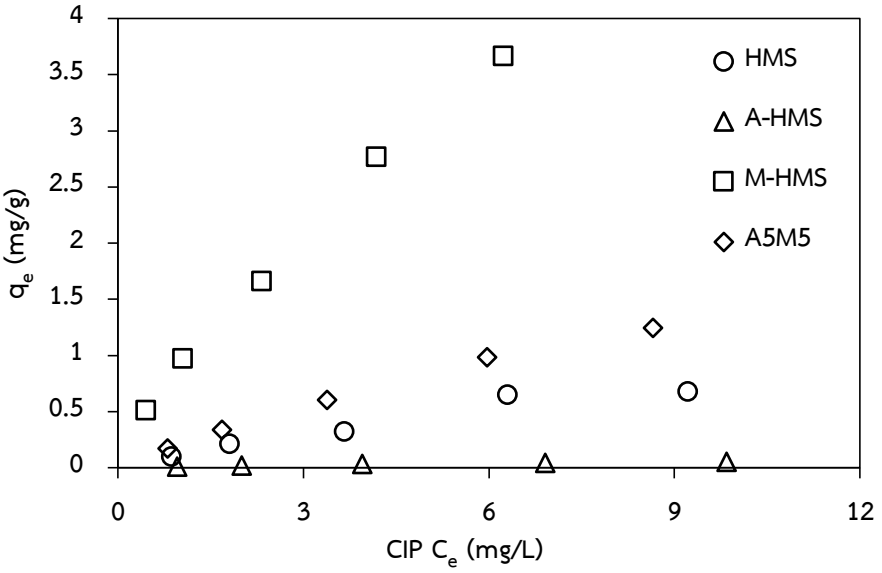

Figure 31 Adsorption capacities of CIP on pristine HMS and grafted HMS

Figure 31 shows adsorption isotherms of CIP on pristine HMS and grafted HMS. The hydrophobic adsorbents (M-HMS > A5M5) provided higher adsorption capacities than the hydrophilic adsorbents (HMS > A-HMS). The adsorption mechanism of CIP on the adsorbents surface tend to be the results of water affinity of adsorbents due to hydrogen bonding. In case of M-HMS, which had the highest efficiency, hydrogen bonding caused by mercapto functional group can be enhanced the adsorption capacity. The adsorption capacity of A5M5 had lower than M-HMS caused by the presence of mecapto functional group on the surface, which M-HMS (7.98%) had sulfur content more than A5M5 (3.80%) as shown in Table 14. The hydrogen bonding between silanol group on HMS surface and CIP molecule might be stronger than interaction of amino functional group on A-HMS surface.

Table 14 Quantity of amino- and mercapto- functional group

Adsorbents	Percent (% w/w)	
	S	N
A-HMS	-	3.27
A5M5	3.80	1.77
M-HMS	7.98	-

In order to neglect the effect of the surface area of the synthesized adsorbents, the adsorption capacities of the adsorbents per square meter was shown in Figure 32. It reveals CIP adsorption isotherms of the hydrophobic adsorbents (M-HMS > A5M5) had higher adsorption capacities per square meter than the hydrophilic adsorbents (A-HMS ~ HMS). It can be concluded that the hydrophobicity via van der Waals interaction were the main CIP adsorption interaction.

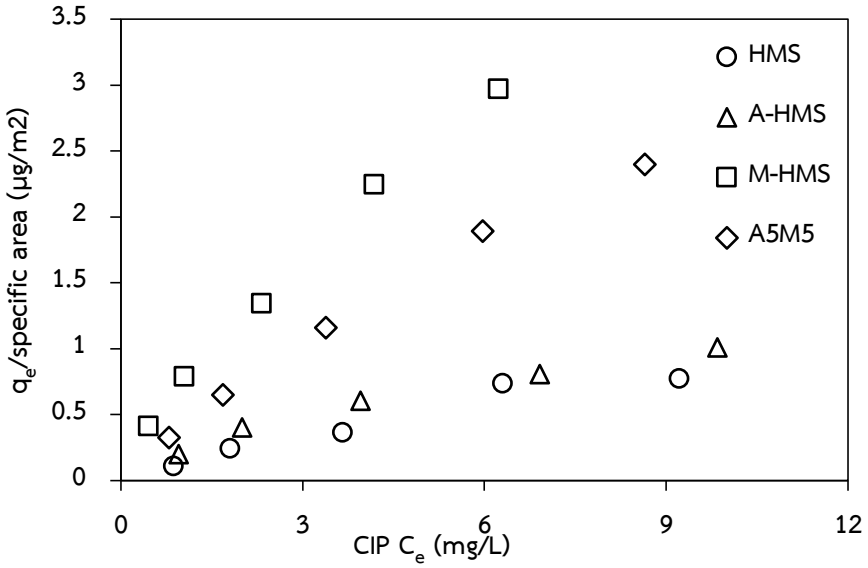

Figure 32 Adsorption capacities per specific surface area of CIP on HMS and grafted HMS

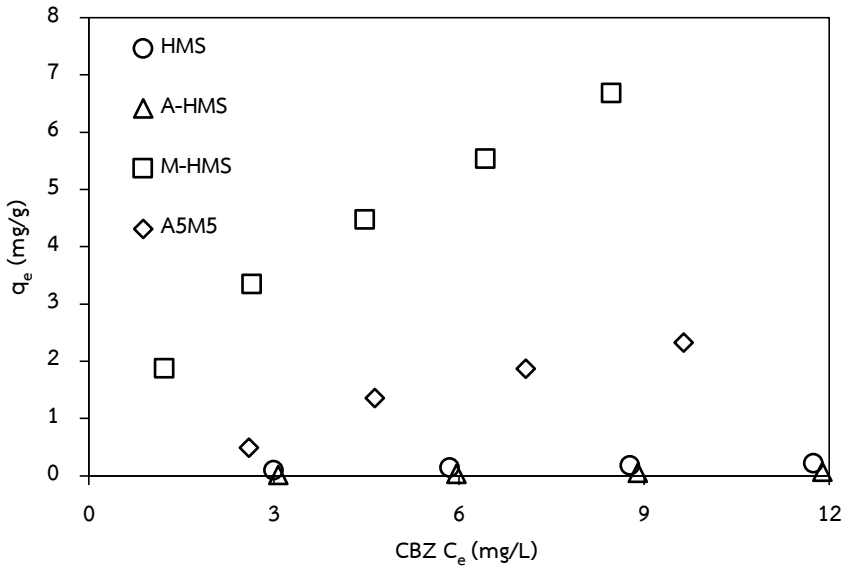

Figure 33 Adsorption capacities of CBZ on HMS and grafted HMS

Figure 33 shows adsorption isotherms of CBZ on pristine HMS and grafted HMS. The adsorption capacity of CBZ had a similar trend with CIP adsorption. As same as CIP adsorption, Figure 34 illustrates CBZ adsorption isotherms of the hydrophobic adsorbents (M-HMS > A5M5) had higher adsorption capacities per square meter than the hydrophilic adsorbents (A-HMS > HMS). It can be concluded that the hydrophobicity might cause the main CBZ adsorption interaction.

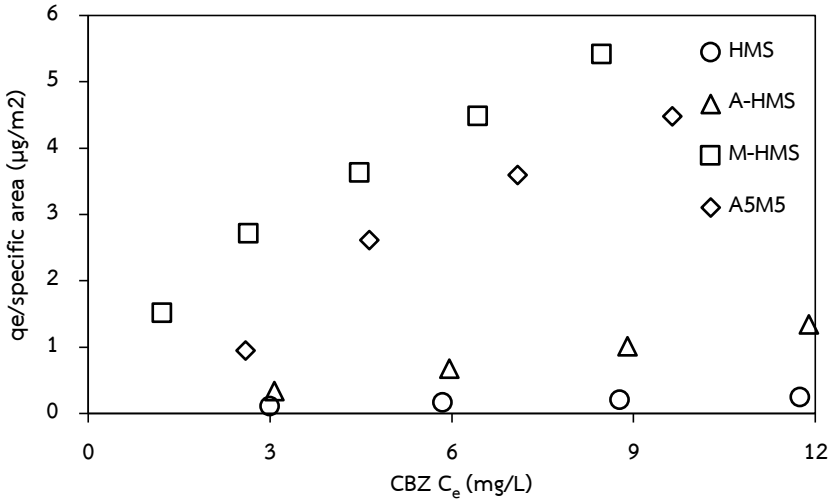

Figure 34 Adsorption capacities per specific surface area of CBZ on HMS and grafted HMS

4.3.2 Effect of graphene oxide

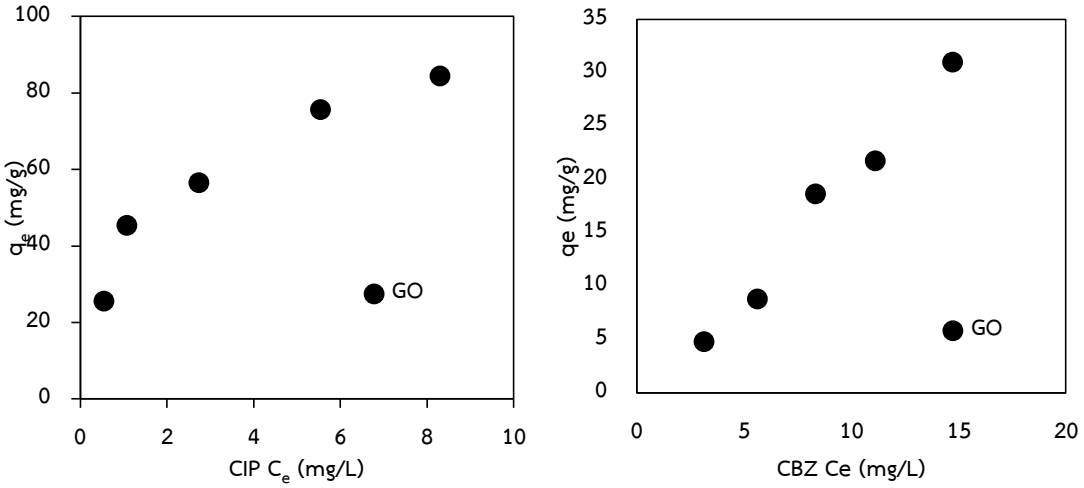

Figure 35 Adsorption capacities of CIP and CBZ on GO

From Figure 35, graphene oxide (GO) showed extremely high adsorption capacity of CIP and slightly lower for CBZ. The effect of GO that modified on mesoporous silica could be suggest to determine the main interaction of both CIP and CBZ adsorption via π-π interaction. The adsorption capacities of CIP and CBZ on GO and GO modified HMS at pH 7 with 0.01 M ionic strength controlled by phosphate buffer are showed in Figure 36 and 38, respectively.

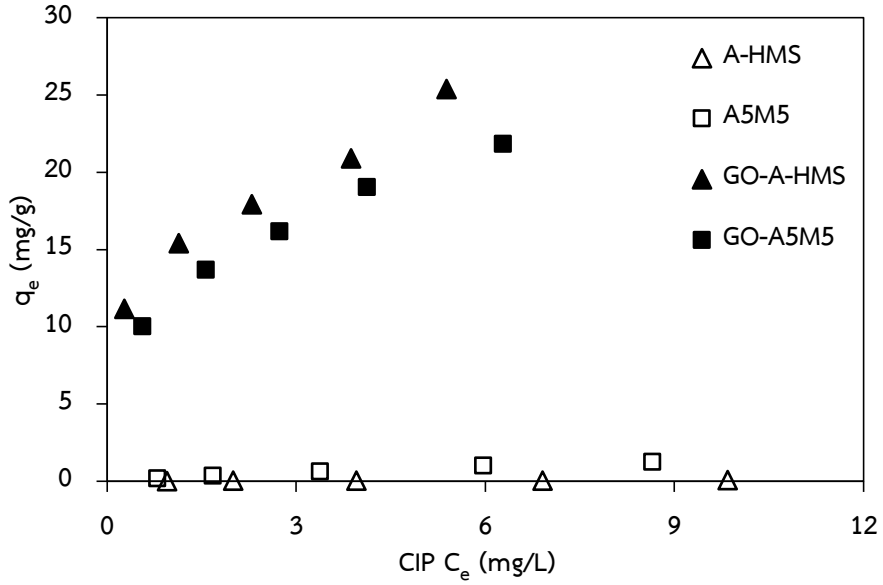

Figure 36 Adsorption capacities of CIP on grafted HMS and GO modified HMS

Figure 36 displays the comparison between the adsorption capacities of CIP on grafted HMS and GO modified HMS. Firstly, it can be seen the modification of GO on HMS could be enhanced the adsorption capacity even for A-HMS, which had less CIP adsorption capacity. Among GO modified HMS, GO-A-HMS provided slightly higher adsorption capacity than GO-A5M5. Although GO-A5M5 had mercapto functional group on the surface which could be enhanced the adsorption capacity more than silanol group on the surface of GO-A-HMS; therefore, the effect of surface functional group can be neglected. In addition, the presence of GO on each adsorbents was recommended to describe the main interaction. Table 15 illustrated the approximate quantity of GO, GO-A-HMS (22.35%) had higher than GO-A5M5 (18.39%). Thereby, the adsorption mechanism of CIP on GO-A-HMS tend to be the results of cationic CIP species and carboxyl or phenyl groups on GO and hydrogen bonding via silanol group (non-grafted silanol) on A-HMS surface. As same as GO-A-HMS, electrostatic could occur between CIP and GO on GO-A5M5. Moreover, it had mercapto functional group on A5M5 surface that could increase the adsorption capacity by hydrophobic interaction. The comparison of CIP adsorption on GO-A-HMS and GO-A5M5 was showed in Figure 37.

Table 15 Quantity of GO on the synthesized adsorbents

Adsorbents	Percent (% w/w)
GO-A-HMS	22.85
GO-A5M5	18.39

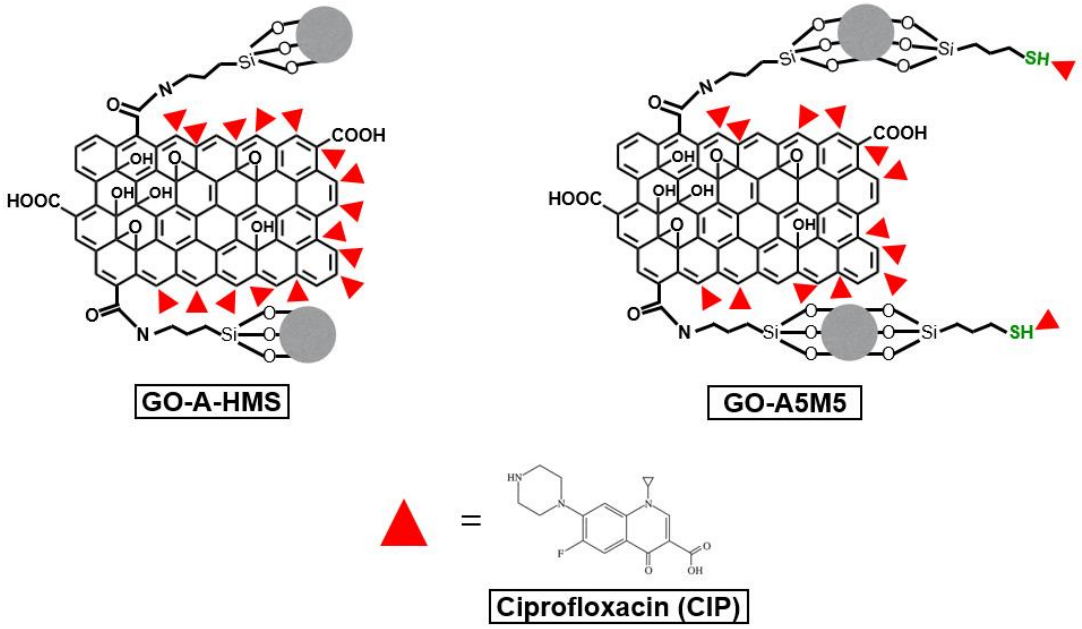

Figure 37 The comparison of CIP adsorption on GO-A-HMS and GO-A5M5

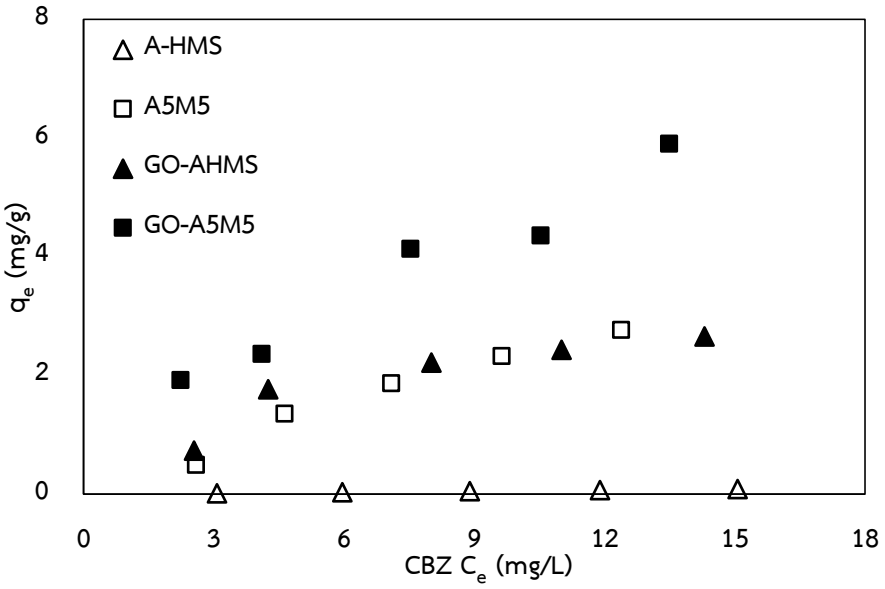

Figure 38 Adsorption capacities of CBZ on grafted HMS and GO modified HMS

In case of CBZ, the modification of GO on HMS could increase the adsorption capacity of grafted HMS as same as CIP. In contrast, GO-A5M5 had higher adsorption

capacity than GO-A-HMS as shown in Figure 38. The main interaction might not cause by GO because GO-A5M5 had less GO than GO-A-HMS as shown in Table 15, and individual GO adsorption did not show the good result comparing with CIP adsorption. The effect of surface functional group that mentioned before was expected to be the key role in the adsorption mechanism. The mercapto functional group on the surface of A5M5 could be improved the adsorption capacity of GO-A5M5 via hydrophobicity. However, GO could enhance the adsorption capacity of A-HMS even it did not provide the good result as A5M5. The comparison of CBZ adsorption on GO-A-HMS and GO-A5M5 was showed in Figure 39.

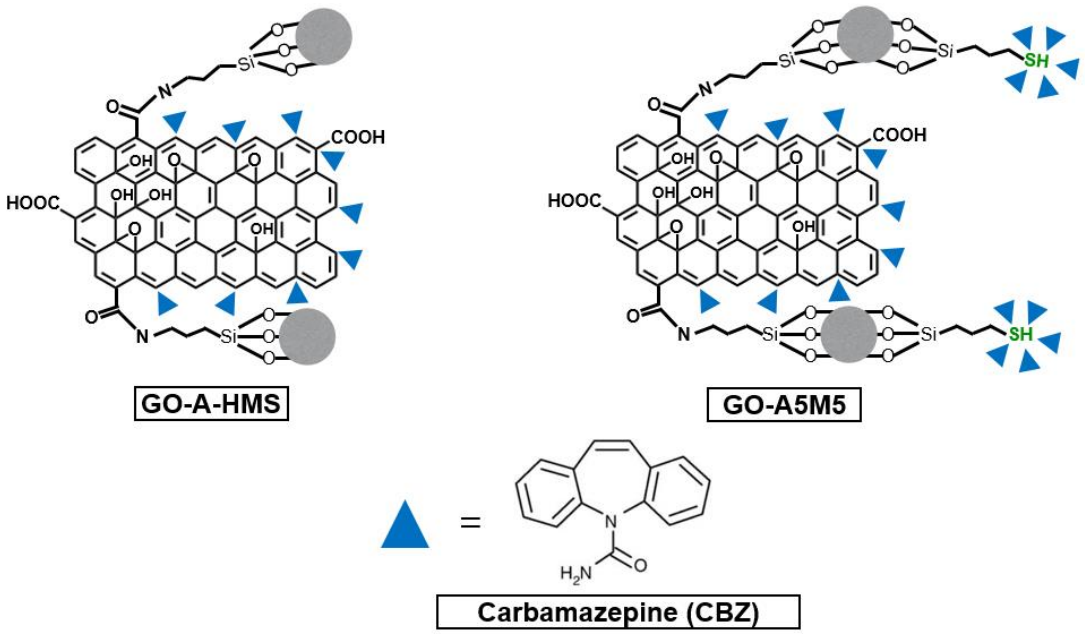

Figure 39 The comparison of CBZ adsorption on GO-A-HMS and GO-A5M5

4.3.3 Adsorption isotherm models

In order to describe the adsorption interaction of CIP and CBZ on the synthesized adsorbents, Langmuir and Freundlich isotherm model were used for analyze the equilibrium experimental data. The Langmuir isotherm model can be assumed as monolayer adsorption on the homogeneous active site of the adsorbent. In contrast, multilayer adsorption and heterogeneous surface is based on the Freundlich isotherm model.

The Langmuir and Freundlich isotherm equation can be defined as in the Equation 4.3.1 and 4.3.2, respectively.

$$q_e = \frac{K_L q_m C_e}{1+K_L C_e} \quad (4.3.1)$$

$$q_e = K_F C_e^{\frac{1}{n}} \quad (4.3.2)$$

Where q_e is the equilibrium adsorption capacity ($mg \cdot g^{-1}$)

q_m is the maximum adsorption capacity ($mg \cdot g^{-1}$)

C_e is the equilibrium concentration ($mg \cdot L^{-1}$)

k_L is the Langmuir constant.

k_F is the Freundlich constant

n is the adsorption intensity

Figure 40 and 41 displays the adsorption isotherm of CIP and CBZ on the synthesized adsorbents and PAC, respectively. The adsorption capacity were fitted with the Langmuir and Freundlich isotherm model and the Freundlich were the best-fitted isotherm model base on the correlation coefficients ($R^2 > 0.90$) for both CIP and CBZ adsorption as shown in Table 16. It revealed that a multilayer adsorption and heterogeneous was occurred on the surface sites within the adsorbent.

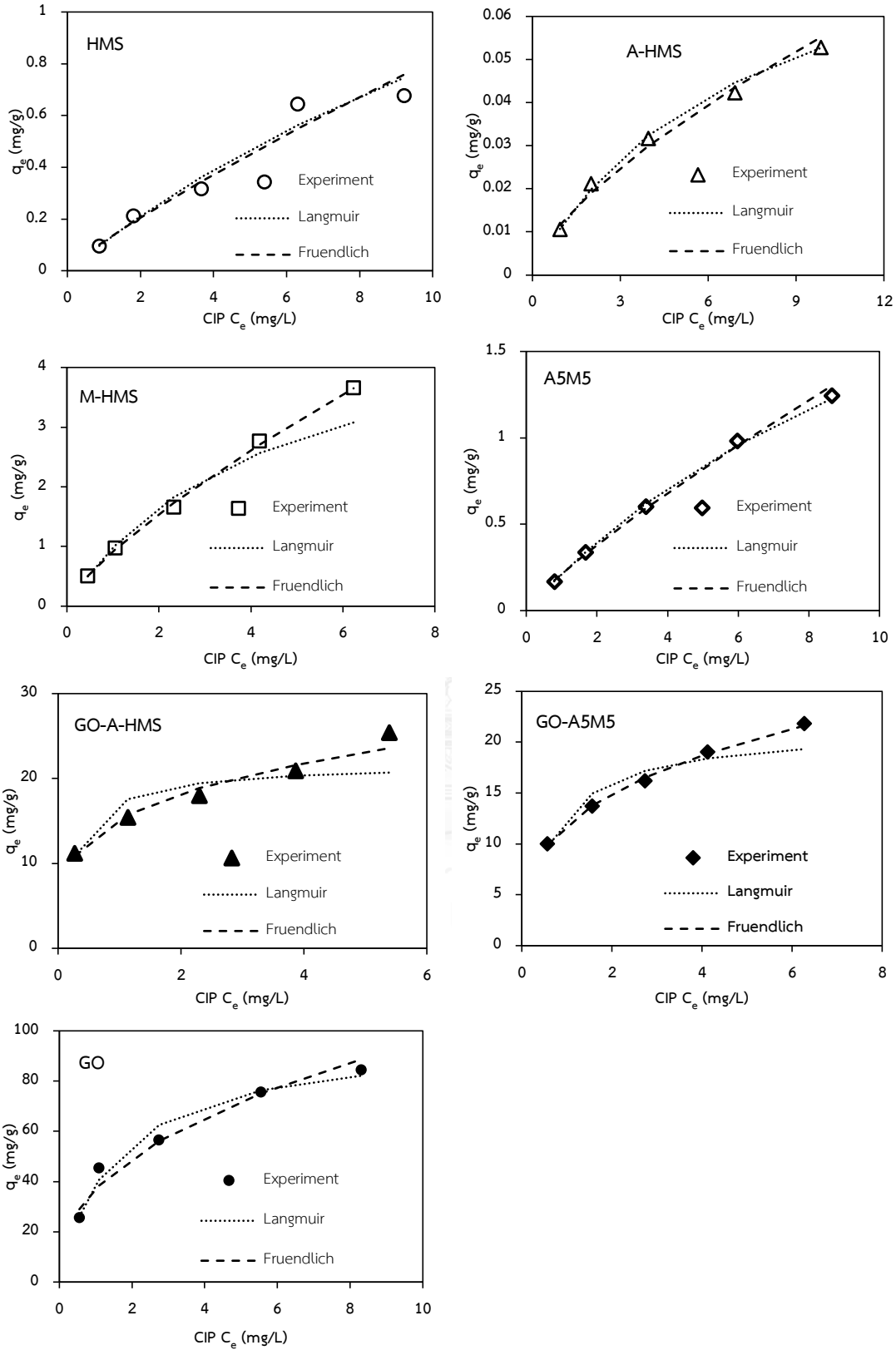

Figure 40 Adsorption isotherms of CIP on the synthesized adsorbents

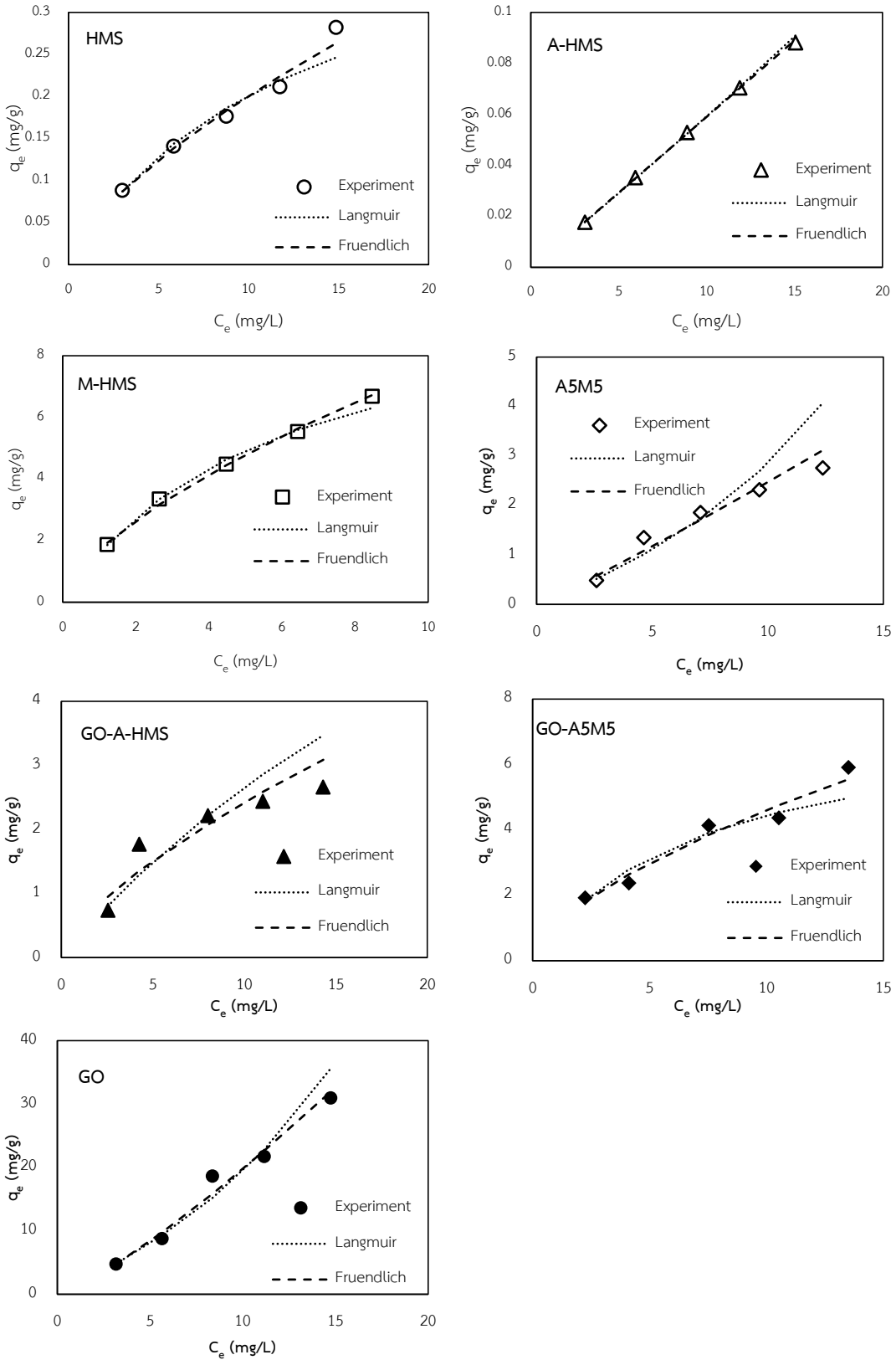

Figure 41 Adsorption isotherms of CBZ on the synthesized adsorbents

Table 16 Isotherm parameters of CIP and CBZ adsorption on the synthesized adsorbents at pH 7

Adsorbents	Langmuir			Freundlich		
	q_m [a]	K_L [b]	R^2	K_F [b]	*1/n*	R^2
CIP						
HMS	2.50	0.05	0.992	0.11	0.85	0.977
A-HMS	0.09	0.14	0.997	0.012	0.67	0.984
M-HMS	5.19	0.23	0.995	0.92	0.76	0.999
A5M5	3.37	0.07	0.999	0.21	0.84	0.998
GO	97.09	0.66	0.979	36.94	0.41	0.948
GO-A-HMS	21.74	3.71	0.888	15.20	0.26	0.973
GO-A5M5	21.37	1.50	0.947	11.92	0.32	0.998
CBZ						
HMS	0.46	0.08	0.988	0.04	0.69	0.987
A-HMS	1.52	0.00	0.999	0.21	1.01	0.999
M-HMS	10.54	0.18	0.998	1.69	0.64	0.996
A5M5	5.07	0.04	0.951	0.01	1.07	0.947
GO	46.95	0.03	0.990	1.14	1.24	0.983
GO-A-HMS	9.94	0.03	0.900	0.50	0.68	0.849
GO-A5M5	7.58	0.14	0.930	1.09	0.63	0.963

[a] Unit of the maximum adsorption capacity (q_m) is mg•g^{-1}

[b] Unit of the equilibrium adsorption constant (k_L, k_F) is L•mg^{-1}

4.3.4 Effect of pH on selected adsorbents

In order to investigate the effect of pH on the adsorption mechanism, the adsorption of CIP on GO-A-HMS and CBZ on GO-A5M5, which had the highest adsorption capacities, were performed by varying pH at pH 5, 7, and 9 as shown in Figure 42 and 43, respectively. Generally, CIP has pK_a at 6.10 (carboxyl group) and 8.70 (amine group), and CBZ has pK_a at 2.30 (ketone group) and 13.90 (amine group). These pharmaceuticals have two pK_a values that mean they can be ionized depend on pH of the solution. A pH varying also depended on different charge type in adsorbents due to pH_{pzc} of each adsorbent.

Figure 42 shows the different adsorption capacity of CIP on GO-A-HMS on the varying pH. At pH 5, the surface of GO-A-HMS had a net positive charge caused by pH lower than pH_{pzc}. The electrostatic repulsion might occur between positive charges as same as at pH 9, where both CIP and GO-A-HMS were negative charge. At pH 7, GO-A-HMS provided weak positive charge, while CIP was in neutral charge. In contrast, the highest adsorption capacity was occur at pH 5 following by pH 7 and 9. To consider pH_{pzc} of single GO, it can be a negative charge due to the pH more than pH_{pzc} (3.2). Then, it can be concluded that the electrostatic might be occur between GO on the surface of GO modified HMS and CIP. The possible interaction might be a combination between hydrogen bonding with the silanol group (non-grafted silanol) and functional group of GO on the surface of GO-A-HMS.

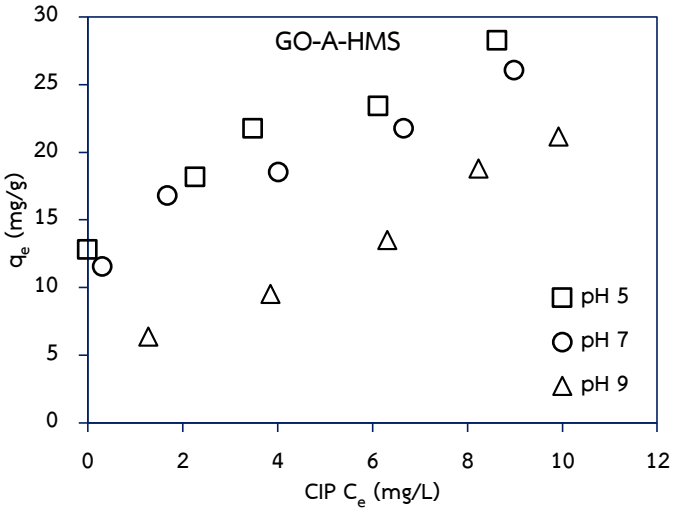

Figure 42 Effect of pH on the adsorption on CIP on GO-A-HMS at pH 5, 7, and 9

Figure 43 shows the different adsorption capacity of CBZ on GO-A5M5 on the varying pH. At pH 5, the surface of GO-A5M5 had a net positive charge caused by pH lower than pH_{pzc}. The electrostatic repulsion might occur between positive charges as same as at pH 9, where both CIP and GO-A5M5 were negative charge. At pH 7, GO-A5M5 provided positive charge, while CBZ was in neutral charge. In contrast, the highest adsorption capacity was occur at pH 5 following by pH 7 and 9 as same as CIP adsorption. Therefore, the electrostatic interaction might be influenced the adsorption capacity of CBZ on GO-A5M5.

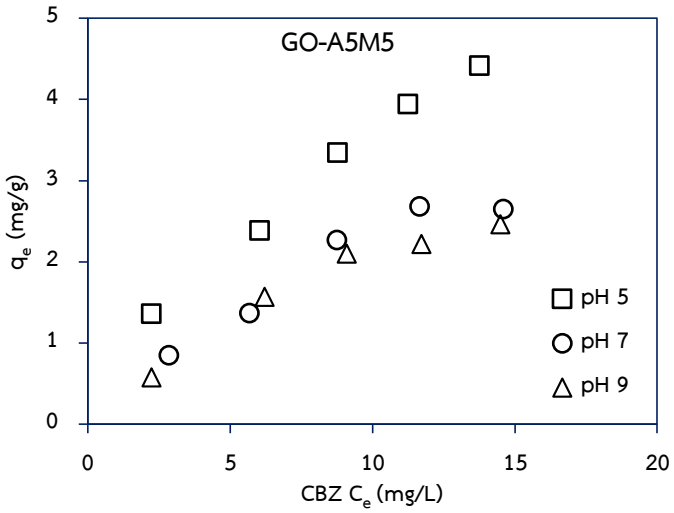

Figure 43 Effect of pH on the adsorption on CBZ on GO-A5M5 at pH 5, 7, and 9

4.3.5 Low concentration adsorption

The adsorption at low concentration was performed by the initial concentration of pharmaceuticals in ppb level adsorbed on GO-A-HMS and GO-A5M5, which had the highest adsorption capacities at high concentration. In order to describe the adsorption interaction of CIP on GO-A-HMS and CBZ on GO-A5M5 in low concentration, the Linear, Langmuir and Freundlich isotherm model were used to describe the equilibrium experimental data.

The Linear isotherm equation can be defined as in the Equation 4.3.4.

$$q_e = K_p C_e \tag{4.3.4}$$

Where *Kp* is linear partition coefficient

The adsorption capacity were fitted with the isotherm models and the Linear was the best-fitted isotherm model base on the correlation coefficients ($R^2 > 0.93$) for both CIP and CBZ low concentration adsorption as shown in Table 17 and 18, respectively.

Table 17 Isotherm parameters of CIP and CBZ low concentration adsorption on the selected adsorbents

Pharmaceutical	Adsorbents	Linear		Langmuir			Freundlich		
		K_p	R^2	q_m [a]	K_L [b]	R^2	K_F [b]	1/n	R^2
CIP	GO-A-HMS	52.50	0.937	-	-	-	0.07	2.29	0.916
CBZ	GO-A5M5	1.86	0.945	-	-	-	0.85	1.20	0.907

Figure 44 shows the adsorption isotherm of CIP on GO-A-HMS and CBZ on GO-A5M5, respectively. It was found that the data were well-fitted with the Linear isotherm model. Therefore, the adsorption interaction of both CIP and CBZ at low concentration was suggested to determine by the Linear isotherm model rather than the Langmuir and Freundlich. It can be described that the adsorption was the initial part of practical isotherm.

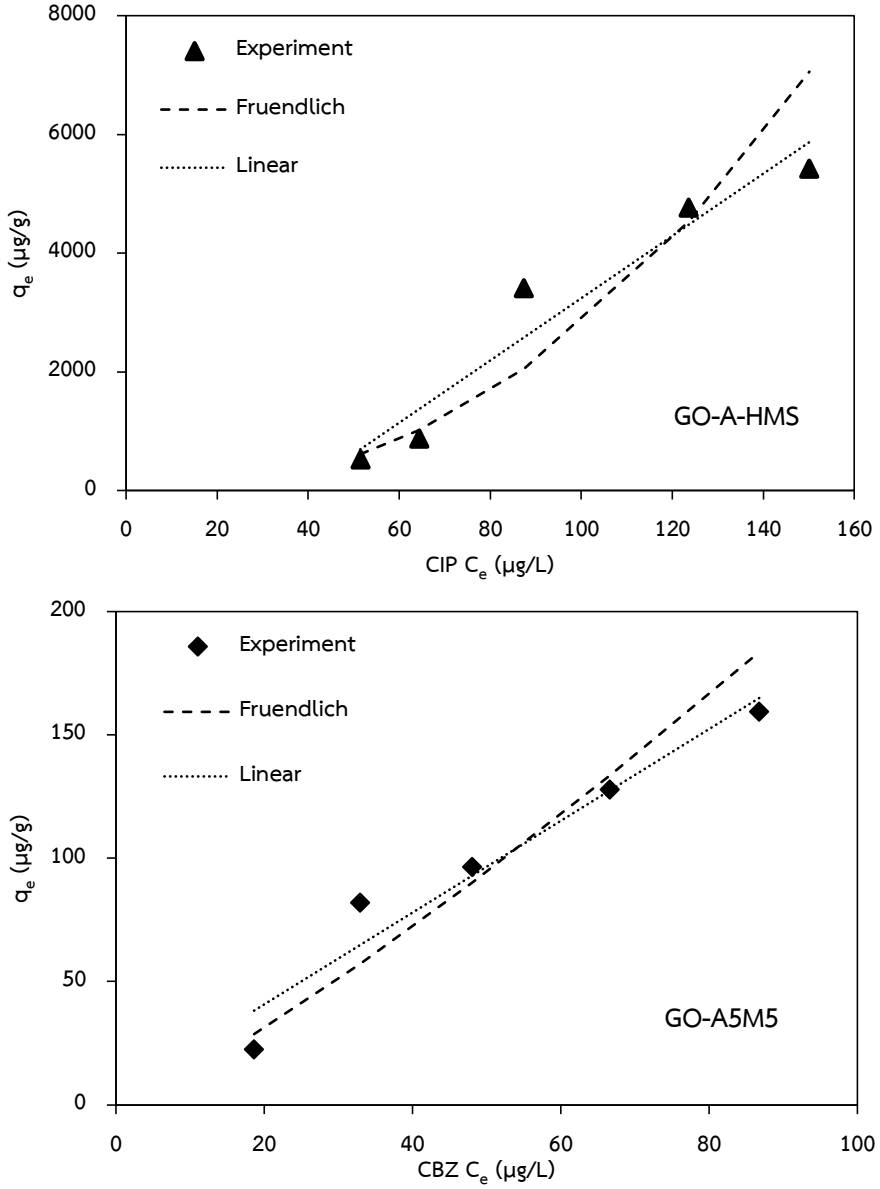

Figure 44 Adsorption isotherms of CIP on GO-A-HMS and CBZ on GO-A5M5 at low concentration

4.3.6 Selective adsorption

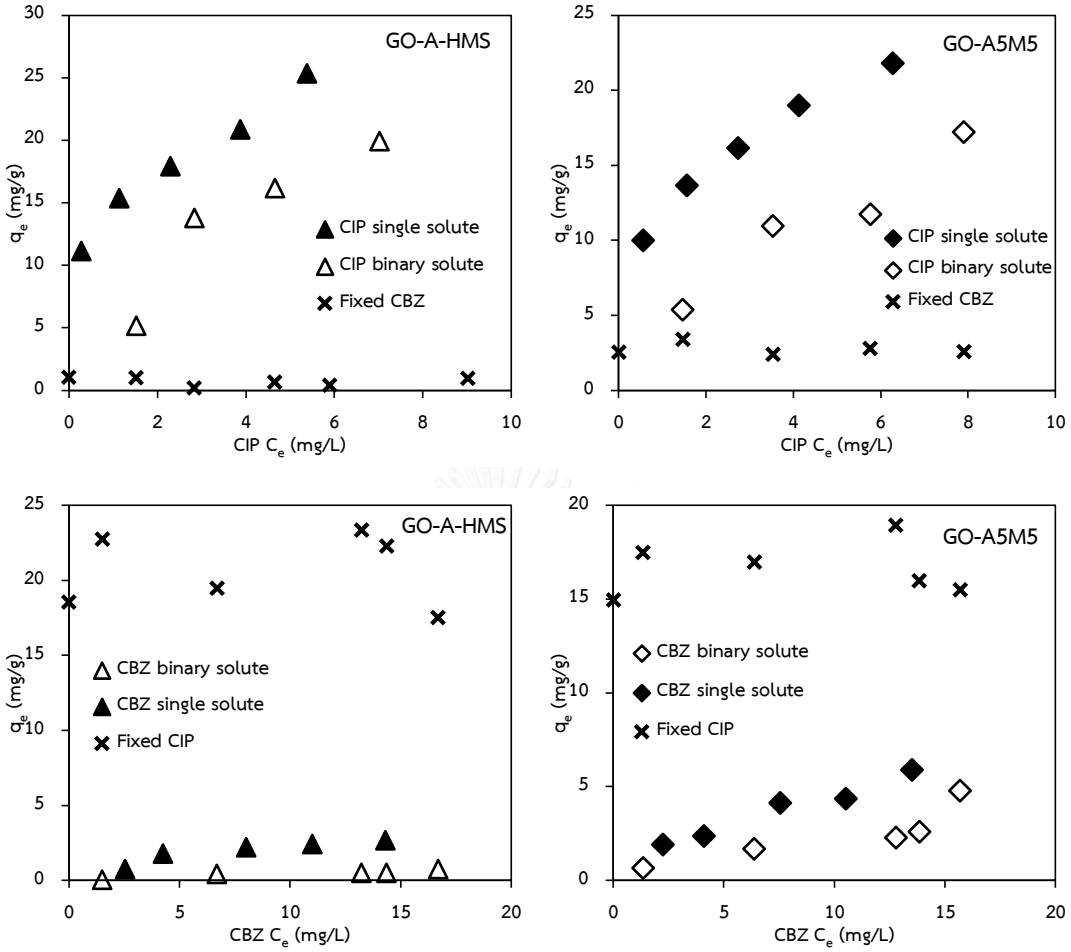

Figure 45 Selective adsorption isotherms of CIP on GO-A-HMS and GO-A5M5

The competitive adsorption of binary solute solution of CIP and CBZ was performed by fixing one pharmaceutical as the same concentration and varying initial concentration another one to investigate the selective adsorption of GO-A-HMS and GO-A5M5 as shown in Figure 45 GO-A-HMS had a higher adsorption capacity for CIP than for CBZ in both single and binary solute solution. It can be observed the adsorption capacity of CIP in binary solute solution was extremely lower than in single solute solution. In case of GO-A5M5, it shows the similar result as GO-A-HMS, but the adsorption capacity of CBZ in binary solute solution was slightly lower than in single solute solution. These results could be explained the competition between CIP and CBZ adsorb on the adsorbents. Firstly, the higher adsorption capacity of CIP on GO-A-

HMS and GO-A5M5 in both single and binary solute solution might be related to the molecular size of pharmaceuticals. CIP has a lower molecular size than CBZ that could enhance the movement to the inner surface of the adsorbents. Moreover, the adsorption mechanism of CIP and both GO modified HMS tend to be the results of π-π interaction between CIP molecule and surface of GO. In case of CBZ, the lower adsorption capacities of both adsorbents in binary-solute solution were observed. However, the adsorption capacity of CBZ on GO-A5M5 was not extremely reduce that might be the result of hydrophobicity of mercapto functional group on the surface of GO-A5M5.

4.3.7 Adsorption mechanism evaluation from XPS Analysis

Adsorption mechanism between pharmaceutical molecule and graphene oxide could be proved by XPS analysis. The XPS spectra were analyze to identified the surface chemical composition of pristine GO and adsorbed GO with CIP and CBZ, which GO was dispersed in DI water, as shown in Figure 46. In case of pristine GO, the components included C-C in aromatic ring (284.6 eV), C-O (286.8 eV), and C-O-C (288.0 eV), respectively. After adsorption of CIP and CBZ on pristine GO in DI water, the obtained results showed the similar bond as pristine GO. In contrast, the peaks of C-O component of CIP and CBZ were lower than pristine GO. It might be conclude that CIP and CBZ adsorbed on the hydroxyl group of GO due to the decreasing of C-O component.

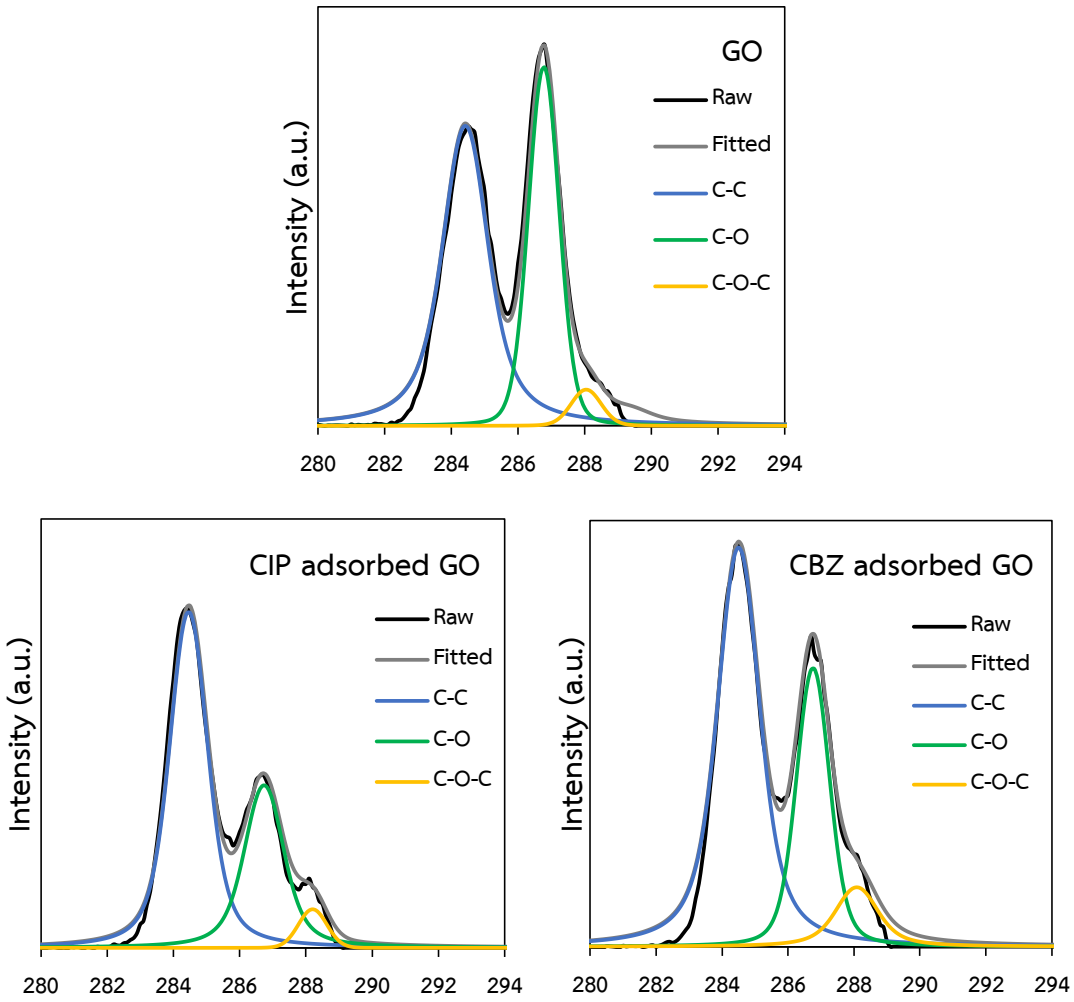

Figure 46 Representative XPS spectra C 1s of GO dispersion in DI water and CIP and CBZ adsorbed GO

Figure 47 shows XPS spectra of pristine GO dispersion in phosphate buffer and adsorbed GO with CIP and CBZ. In case of pristine GO, the components included C-C in aromatic ring (284.6 eV), C-O (286.8 eV), and C-O-C (288.0 eV) respectively. After adsorption of CIP and CBZ on pristine GO in phosphate buffer, the obtained results showed the similar bond as pristine GO. Similar to GO dispersion in DI, the peaks of C-O bond of both CIP and CBZ were lower than pristine GO. It might be conclude that CIP and CBZ adsorbed on the hydroxyl group of GO due to the decreasing of C-O component. Moreover, the peak at 293 eV was observe in GO and CIP and CBZ adsorbed GO. It might be π-π^* signal, which indicated that π-electrons were delocalized

at the aromatic network in GO. (Teng, Ma et al. 2011).The shake-up peak was not found in GO dispersion in DI water because of increasing oxidation. The disappearance of shake-up was possible to established evidence for **π-π** interaction. (Yang, Rochette et al. 2005). It tend to be the result of **π-π** interaction that corresponding to the hypothesis. However, these evidences of CIP and CBZ adsorbed GO was unclear.

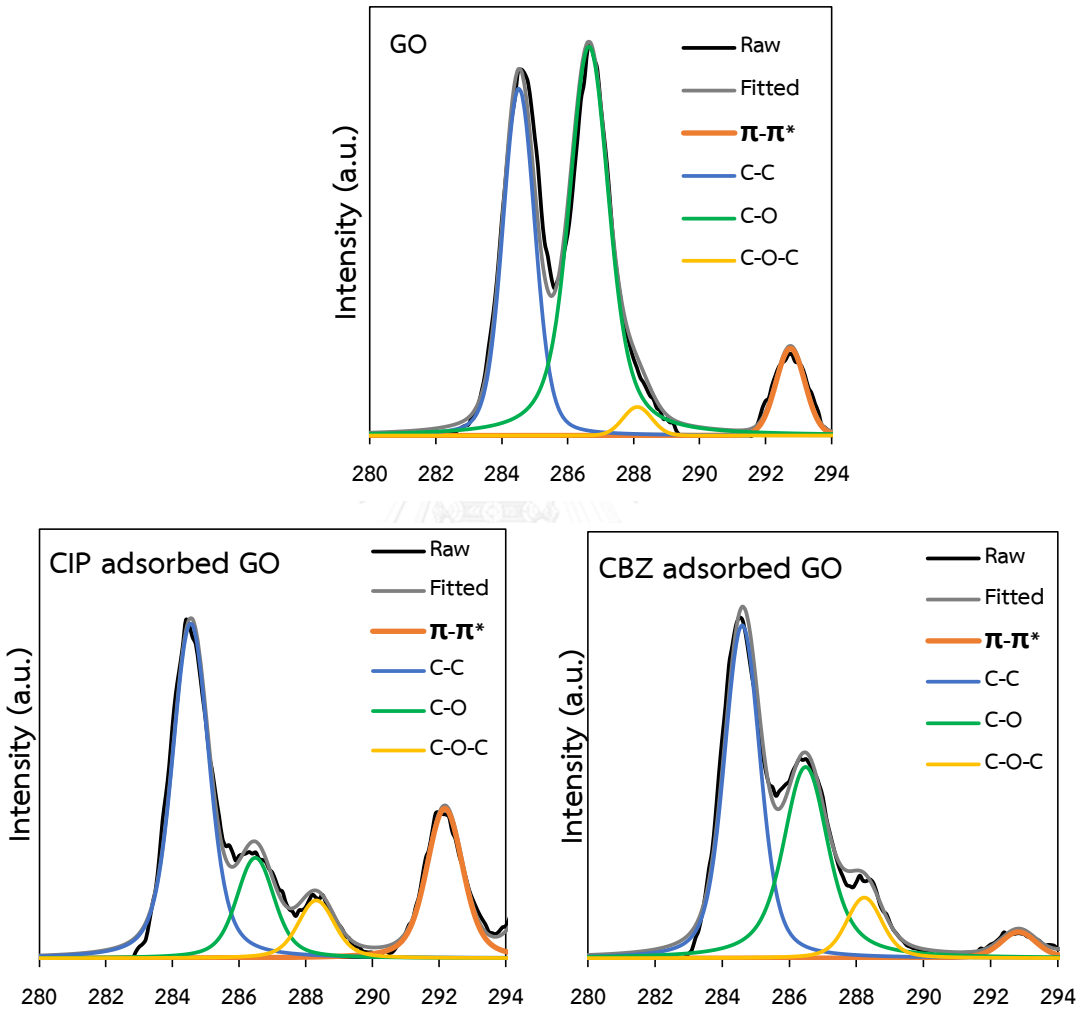

Figure 47 Representative XPS spectra C 1s of GO dispersion in phosphate buffer and CIP and CBZ adsorbed GO

CHAPTER 5
CONCLUSIONS AND RECOMMENDATION

5.1 CONCLUSIONS

The overall purpose of this study was to determine the comparative removal of pharmaceutical residues including ciprofloxacin (CIP) and carbamazepine (CBZ) by adsorption on various types of adsorbent such as HMS, grafted HMS, GO and GO modified HMS. The physicochemical properties of synthesized adsorbents were characterized using various instruments and methods. Adsorption kinetic and adsorption isotherm were conducted under batch experiments by controlling ionic strength. The results were interpreted as kinetic parameters and adsorption isotherm model to understand the adsorption mechanism including hydrophobic interaction, electrostatic interaction and hydrogen bonding. In addition, the effects of pH on adsorption and mechanism were studied. Moreover, selective adsorption in binary-solute solution of pharmaceuticals on the synthesized adsorbents was investigated.

The synthesized adsorbents can be classified into three categories: (i) hexagonal mesoporous silica (HMS), (ii) graphene oxide (GO), and (iii) GO modified HMS. According to the physico-chemical properties of pristine HMS and grafted HMS, the synthesized adsorbents can be sorted into two types: (i) hydrophobic adsorbent surface (M-HMS and A5M5) and (ii) hydrophilic adsorbent surface (A-HMS and HMS). Graphene oxide (GO) was also synthesized and the modification of GO was performed as GO-modified HMS (GO-A-HMS and GO-A5M5. The porous structure was evaluated by N_2 adsorption-desorption isotherm. The presence of organo-functional group on the surface can be identified by the FT-IR spectra. XRD pattern was investigated to confirm the modification of GO and HMS.

From adsorption kinetic studies, the experimental data was well-fitted with the pseudo-second order kinetic model. The adsorption of CIP and CBZ on pristine HMS and grafted HMS reached equilibrium stage within 4 hours, and 6 hours for GO modified

HMS. In case of GO, the equilibrium adsorption stage was occur within 24 hours. The adsorption of CIP and CBZ was controlled by intraparticle diffusion.

According to adsorption isotherm studies, the adsorption isotherm were well-fitted with Freundlich isotherm model as multilayer adsorption. The main adsorption mechanism of CIP and CBZ might be governed by hydrophobic interaction via hydrogen bonding. Nevertheless, it cannot be clearly proved **π-π** interaction between pharmaceutical molecule and graphene oxide. However, **π-π** interaction was possible to play a key role on CIP and CBZ adsorption corresponding to the hypothesis.

For CIP and CBZ adsorption on pristine HMS and grafted HMS, the main mechanism can be described from the effect of surface functional group. The higher adsorption capacities of M-HMS and A5M5, which had hydrophobic surface functional group were cause by hydrophobic interaction via hydrogen bonding. While silanol group on HMS and amino group on A-HMS provided less adsorption capacities via weaker hydrogen bonding.

In case of GO-A-HMS and GO-A5M5, the results were different. CIP can be adsorbed on GO-A-HMS more than GO-A5M5 due to **π-π** interaction and electrostatic interaction between GO and CIP, which GO-A-HMS had higher GO on the surface. In contrast, GO-A5M5 provided higher adsorption capacity than GO-A-HMS for CBZ due to the presence of mercapto functional group on GO-A5M5's surface.

The adsorption interaction of both CIP and CBZ at low concentration (ppb level) were suggested to determine by the Linear isotherm model. It can be described that the adsorption was the initial part of practical isotherm.

For selective adsorption study, the lower adsorption capacities of CIP and CBZ on GO modified HMS in binary-solute solution than single-solute solution was caused by the competition among CIP and CBZ. CIP can be adsorbed on GO-A-HMS and GO-A5M5 more than CBZ due to **π-π** interaction, electrostatic, and smaller molecular size. Although the less adsorption capacity of CBZ on GO-A5M5, it was slightly reduce comparing with single-solute solution. Then, hydrophobicity of mercapto functional group on surface of GO-A5M5 also affected the adsorption capacity in the selective adsorption.

5.2 RECOMMENDATIONS

5.2.1 The ratio of surface functional group on HMS should be optimized to modify with graphene oxide for higher efficiency.

5.2.2 The dispersion of graphene oxide should be developed.

5.2.3 The total organic carbon (TOC) which occur during the adsorption process should be investigated.

5.2.4 Separation technique for removal of the synthesized adsorbents from water treatment system should be developed.

5.2.5 Regeneration processes and their effects on reused efficiency of the synthesized adsorbents should be investigated.

REFERENCES

Adams, C., et al. (2002). "Removal of antibiotics from surface and distilled water in conventional water treatment processes." Journal of environmental engineering **128**(3): 253-260.

Bryan, L., et al. (1989). "Quinolone antimicrobial agents: mechanism of action and resistance development." Clinical and investigative medicine. Medecine clinique et experimentale **12**(1): 14-19.

Bui, T. X. and H. Choi (2009). "Adsorptive removal of selected pharmaceuticals by mesoporous silica SBA-15." Journal of Hazardous Materials **168**(2): 602-608.

Chen, H., et al. (2015). "Removal of sulfamethoxazole and ciprofloxacin from aqueous solutions by graphene oxide." Journal of Hazardous Materials **282**: 201-207.

Cordova-Kreylos, A. L. and K. M. Scow (2007). "Effects of ciprofloxacin on salt marsh sediment microbial communities." The ISME journal **1**(7): 585-595.

Duong, H. A., et al. (2008). "Occurrence, fate and antibiotic resistance of fluoroquinolone antibacterials in hospital wastewaters in Hanoi, Vietnam." Chemosphere **72**(6): 968-973.

Gibs, J., et al. (2007). "Persistence of pharmaceuticals and other organic compounds in chlorinated drinking water as a function of time." Science of the Total Environment **373**(1): 240-249.

Halling-Sørensen, B., et al. (2000). "Environmental risk assessment of antibiotics: comparison of mecillinam, trimethoprim and ciprofloxacin." Journal of antimicrobial chemotherapy **46**(suppl 1): 53-58.

Heberer, T., et al. (2002). "From municipal sewage to drinking water: fate and removal of pharmaceutical residues in the aquatic environment in urban areas." Water Science and Technology **46**(3): 81-88.

Hoffmann, F., et al. (2006). "Silica-based mesoporous organic–inorganic hybrid materials." Angewandte Chemie International Edition **45**(20): 3216-3251.

Homem, V. and L. Santos (2011). "Degradation and removal methods of antibiotics from aqueous matrices–a review." Journal of environmental management **92**(10): 2304-2347.

Hongsawat, P., et al. (2014). "Adsorption of ciprofloxacin on surface functionalized superparamagnetic porous silicas." Desalination and Water Treatment **52**(22-24): 4430-4443.

Kim, Y., et al. (2007). "Aquatic toxicity of acetaminophen, carbamazepine, cimetidine, diltiazem and six major sulfonamides, and their potential ecological risks in Korea." Environment International **33**(3): 370-375.

Kümmerer, K. (2009). "Antibiotics in the aquatic environment–a review–part I." Chemosphere **75**(4): 417-434.

Larsson, D. J., et al. (2007). "Effluent from drug manufactures contains extremely high levels of pharmaceuticals." Journal of Hazardous Materials **148**(3): 751-755.

Lee, B., et al. (2001). "Synthesis of functionalized porous silicas via templating method as heavy metal ion adsorbents: the introduction of surface hydrophilicity onto the surface of adsorbents." Microporous and Mesoporous materials **50**(1): 77-90.

Lester, Y., et al. (2010). "Photodegradation of the antibiotic sulphamethoxazole in water with UV/H2O2 advanced oxidation process." Environmental technology **31**(2): 175-183.

Li, S.-z., et al. (2004). "Membrane (RO-UF) filtration for antibiotic wastewater treatment and recovery of antibiotics." Separation and Purification Technology **34**(1): 109-114.

Li, X., et al. (2015). "Preparation, characterization, and application of mesoporous silica-grafted graphene oxide for highly selective lead adsorption." Chemical Engineering Journal **273**: 630-637.

Mompelat, S., et al. (2009). "Occurrence and fate of pharmaceutical products and by-products, from resource to drinking water." Environment International **35**(5): 803-814.

Nakata, H., et al. (2005). "Determination of fluoroquinolone antibiotics in wastewater effluents by liquid chromatography–mass spectrometry and fluorescence detection." Chemosphere **58**(6): 759-766.

Punyapalakul, P. and T. Sitthisorn (2010). "Removal of ciprofloxazin and carbamazepine by adsorption on functionalized mesoporous silicates." World Academy of Science, Engineering and Technology **69**: 546-550.

Renew, J. E. and C.-H. Huang (2004). "Simultaneous determination of fluoroquinolone, sulfonamide, and trimethoprim antibiotics in wastewater using tandem solid phase extraction and liquid chromatography–electrospray mass spectrometry." Journal of Chromatography A **1042**(1): 113-121.

Scheytt, T. J., et al. (2006). "Mobility of pharmaceuticals carbamazepine, diclofenac, ibuprofen, and propyphenazone in miscible-displacement experiments." Journal of Contaminant Hydrology **83**(1): 53-69.

Sim, W.-J., et al. (2011). "Occurrence and distribution of pharmaceuticals in wastewater from households, livestock farms, hospitals and pharmaceutical manufactures." Chemosphere **82**(2): 179-186.

Tanev, P. T. and T. J. Pinnavaia (1996). "Mesoporous silica molecular sieves prepared by ionic and neutral surfactant templating: a comparison of physical properties." Chemistry of materials **8**(8): 2068-2079.

Wang, C., et al. (2013). "Coadsorption, desorption hysteresis and sorption thermodynamics of sulfamethoxazole and carbamazepine on graphene oxide and graphite." Carbon **65**: 243-251.

Xu, W.-h., et al. (2007). "Determination of selected antibiotics in the Victoria Harbour and the Pearl River, South China using high-performance liquid chromatography-electrospray ionization tandem mass spectrometry." Environmental Pollution **145**(3): 672-679.

Xu, Y., et al. (2008). "Flexible graphene films via the filtration of water-soluble noncovalent functionalized graphene sheets." Journal of the American Chemical Society **130**(18): 5856-5857.

APPENDICES

APPENDIX A

Standard curve

Standard curve

The concentration of standard solution of CIP and CBZ were analyzed by UV-Vis spectroscopy. Standard curve was plotted between adsorbance and concentration of standard solution of CIP and CBZ

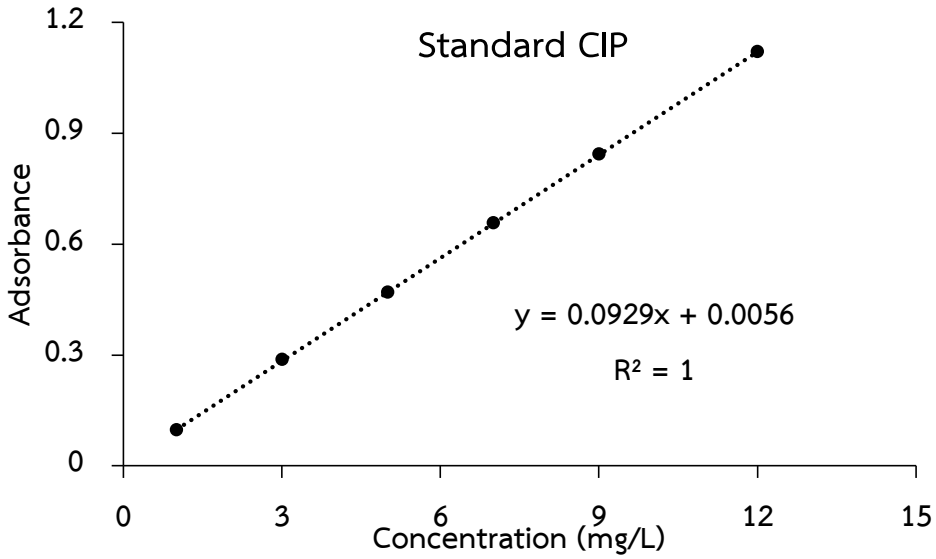

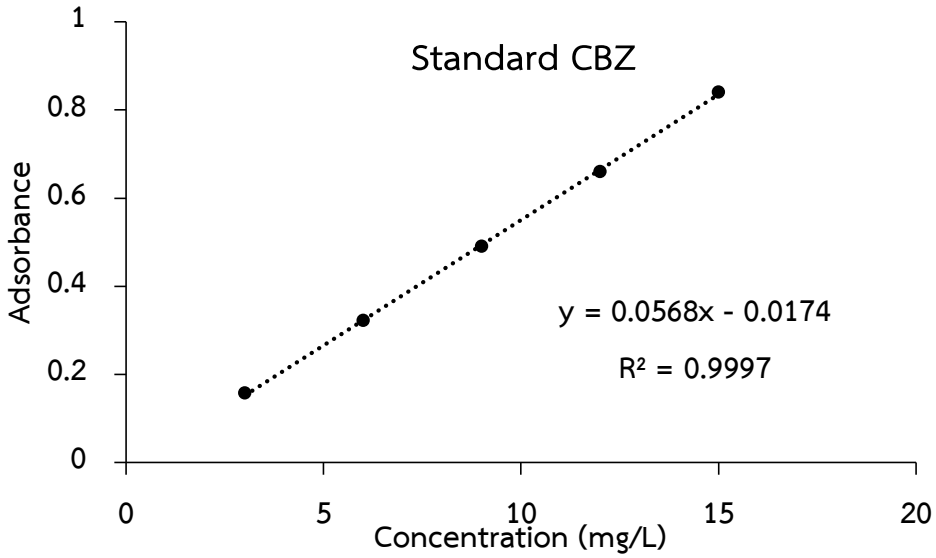

Standard curve

The concentration of standard solution of CIP and CBZ were analyzed by HPLC-DAD. Standard curve was plotted between peak area and concentration of standard solution of CIP and CBZ

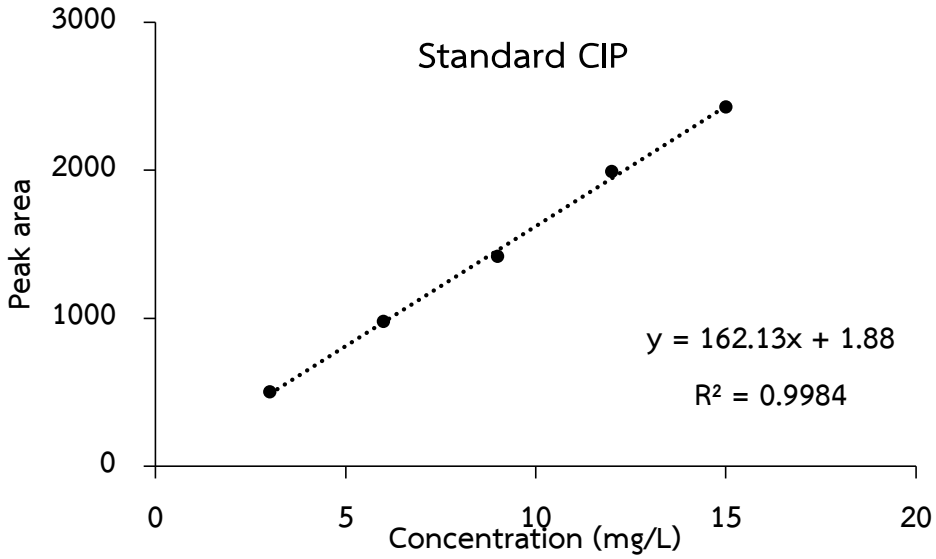

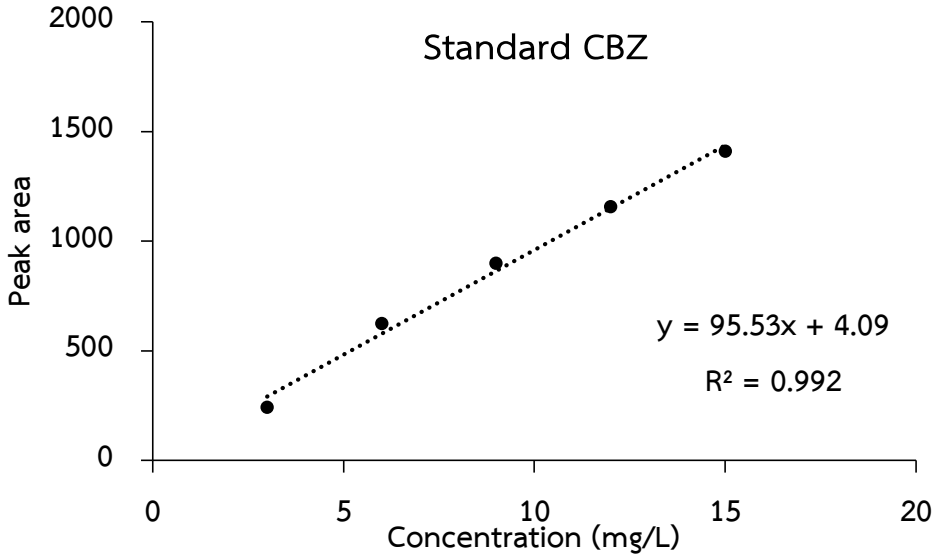

APPENDIX B

Data of Physicochemical Characterization of Adsorbents

1. Surface charge determination by Acid-Base Titration Method

Table B-1 Data from surface charge of HMS

Sample	Initial pH	Equilibrium pH
1	3.01	3.04
2	3.01	3.04
3	4.8	4.93
4	6.21	5.8
5	10.75	9.08
6	11.97	11.69

Table B-2 Data from surface charge of A-HMS

Sample	Initial pH	Equilibrium pH
1	3.13	3.31
2	5.93	7.63
3	6.63	7.90
4	6.8	7.95
5	10.95	9.64
6	12.03	11.26

Table B-3 Data from surface charge of M-HMS

Sample	Initial pH	Equilibrium pH
1	3.02	3.03
2	5.08	5.17
3	6.23	5.55
4	6.41	6.04
5	10.89	9.36
6	12.00	11.80

Table B-4 Data from surface charge of A5M5

Sample	Initial pH	Equilibrium pH
1	3.09	3.18
2	5.57	6.83
3	6.43	7.26
4	6.83	7.68
5	11.03	9.71
6	12.03	11.79

Table B-5 Data from surface charge of GO

Sample	Initial pH	Equilibrium pH
1	2.80	2.81
2	3.06	3.03
3	3.08	3.10
4	3.12	3.15
5	4.07	3.73
6	11.74	11.64

Table B-6 Data from surface charge of GO-A-HMS

Sample	Initial pH	Equilibrium pH
1	3.13	3.31
2	5.93	7.63
3	6.63	7.90
4	6.80	7.95
5	10.95	9.64
6	12.03	11.26

Table B-7 Data from surface charge of GO-A5M5

Sample	Initial pH	Equilibrium pH
1	3.07	3.12
2	5.38	5.73
3	6.30	6.09
4	6.46	6.55
5	10.96	9.58
6	12.01	11.82

APPENDIX C

Data of Adsorption Kinetics

Table C-1 Data from adsorption kinetic of HMS, A-HMS, M-HMS, and A5M5 at initial concentration of CIP at 6 mg/L (pH 7 with IS 0.01 M)

HMS		A-HMS		M-HMS		A5M5	
t (min)	q_t	t (min)	q_t	t (min)	q_t	t (min)	q_t
0	0	0	0	0	0	0	0
0.5	0.65	0.75	0.01	3	1.11	0.5	0.43
1	0.74	3	0.01	6	1.54	1	0.52
2	0.74	6	0.02	10	1.99	2	0.60
5	0.75	10	0.02	15	2.24	5	0.71
10	0.76	15	0.02	30	2.70	10	0.73
15	0.79	30	0.03	60	3.08	15	0.83
30	0.81	60	0.02	120	3.40	30	0.89
60	0.83	120	0.03	180	3.39	60	0.92
120	0.85	180	0.04	240	3.41	120	0.99
180	0.85	240	0.04			180	1.01
240	0.85					240	0.99

Table C-2 Data from adsorption kinetic of GO, GO-A-HMS, GO-A5M5 and PAC at initial concentration of CIP at 6 mg/L (pH 7 with IS 0.01 M)

GO		GO-A-HMS		GO-A5M5		PAC	
t (min)	q_t	t (min)	q_t	t (min)	q_t	t (min)	q_t
0	0	0	0	0	0	0	0
10	64.44	0.5	3.53	0.5	2.41	30	5.82
15	76.88	1	3.88	1	3.49	60	5.93
30	76.81	2	5.30	2	4.05	120	5.85
60	80.46	5	6.80	5	5.64	210	5.86
240	81.43	10	9.08	10	7.02	330	5.67
480	83.32	15	9.86	15	7.96	390	5.84
960	82.86	30	12.18	30	9.47	540	5.91
1440	83.19	60	13.95	60	10.89	600	5.91
1920	83.71	120	14.81	120	12.10		
2880	84.36	180	15.24	180	12.23		
3360	84.49	240	15.59	240	12.49		
4320	84.95	300	15.72	300	12.92		
		360	15.67	360	13.18		
		480	16.06	480	13.48		
		600	16.15	600	13.43		
		720	16.10	720	13.48		

Table C-3 Data from adsorption kinetic of HMS, A-HMS, M-HMS, and A5M5 at initial concentration of CBZ at 9 mg/L (pH 7 with IS 0.01 M)

HMS		A-HMS		M-HMS		A5M5	
t (min)	q_t	t (min)	q_t	t (min)	q_t	t (min)	q_t
0	0	0	0	0	0	0	0
0.5	0.26	0.5	0.02	1	2.56	0.83	1.05
1	0.28	1	0.02	2	3.12	2	1.55
2	0.26	2	0.04	5	3.54	5	1.86
5	0.28	5	0.04	10	3.93	10	2.05
10	0.26	10	0.07	15	4.32	15	2.10
15	0.28	15	0.09	30	4.82	30	2.20
30	0.31	30	0.09	60	4.82	60	2.21
60	0.30	60	0.11	120	5.33	120	2.23
120	0.30	120	0.13	180	5.46	180	2.25
180	0.31	180	0.13	240	5.48	240	2.25
240	0.31	240	0.11				

Table C-4 Data from adsorption kinetic of GO, GO-A-HMS, GO-A5M5 and PAC at initial concentration of CBZ at 9 mg/L (pH 7 with IS 0.01 M)

GO		GO-A-HMS		GO-A5M5		PAC	
t (min)	q_t	t (min)	q_t	t (min)	q_t	t (min)	q_t
0	0	0	0	0	0	0	0
10	23.08	0.5	0.82	0.67	1.79	60	8.31
15	23.63	1	0.91	1	2.11	120	8.39
30	23.52	2	1.11	2	2.46	180	8.42
60	23.30	5	1.52	5	2.99	240	8.48
240	24.50	10	1.87	10	3.43	300	8.52
480	25.82	30	2.22	30	3.98	360	8.56
960	26.91	60	2.37	60	4.13	480	8.58
1440	27.02	120	2.40	120	4.10	600	8.58
1920	30.74	180	2.40	180	4.07		
2880	31.94	240	2.37	240	4.01		
3360	31.83	300	2.37	300	3.98		
4320	31.61	360	2.43	480	3.95		
		480	2.40	600	4.07		
		600	2.40	720	4.10		
		720	2.43				

APPENDIX D

Data of Adsorption Isotherm

1. Adsorption isotherm

Table D-1 Data from adsorption isotherm of CIP and CBZ in single solute solution on HMS in phosphate buffer pH 7 with IS 0.01 M

CIP			CBZ		
C_0 (mg/L)	C_e (mg/L)	q_t (mg/g)	C_0 (mg/L)	C_e (mg/L)	q_t (mg/g)
0.96	0.87	0.10	3.09	3.00	0.09
2.02	1.81	0.21	5.99	5.85	0.14
3.98	3.67	0.32	8.95	8.77	0.18
6.95	6.31	0.64	11.96	11.75	0.21
9.90	9.22	0.68	15.15	14.87	0.28

Table D-2 Data from adsorption isotherm of CIP and CBZ in single solute solution on A-HMS in phosphate buffer pH 7 with IS 0.01 M

CIP			CBZ		
C_0 (mg/L)	C_e (mg/L)	q_t (mg/g)	C_0 (mg/L)	C_e (mg/L)	q_t (mg/g)
0.96	0.95	0.01	3.09	3.07	0.02
2.02	2.00	0.02	5.99	5.96	0.04
3.98	3.95	0.03	8.95	8.90	0.05
6.95	6.91	0.04	11.96	11.89	0.07
9.90	9.84	0.05	15.15	15.06	0.09

Table D-3 Data from adsorption isotherm of CIP and CBZ in single solute solution on M-HMS in phosphate buffer pH 7 with IS 0.01 M

CIP			CBZ		
C_0 (mg/L)	C_e (mg/L)	q_t (mg/g)	C_0 (mg/L)	C_e (mg/L)	q_t (mg/g)
0.96	0.46	0.51	3.09	1.22	1.87
2.02	1.05	0.97	5.99	2.65	3.35
3.98	2.33	1.66	8.95	4.48	4.47
6.95	4.18	2.77	11.96	6.43	5.53
9.90	6.23	3.66	15.15	8.48	6.67

Table D-4 Data from adsorption isotherm of CIP and CBZ in single solute solution on A5M5 in phosphate buffer pH 7 with IS 0.01 M

CIP			CBZ		
C_0 (mg/L)	C_e (mg/L)	q_t (mg/g)	C_0 (mg/L)	C_e (mg/L)	q_t (mg/g)
0.96	0.79	0.17	3.09	2.60	0.49
2.02	1.68	0.34	5.99	4.64	1.36
3.98	3.38	0.60	8.95	7.08	1.87
6.95	5.97	0.98	11.96	9.64	2.32
9.90	8.65	1.25	15.15	12.38	2.76

Table D-5 Data from adsorption isotherm of CIP and CBZ in single solute solution on GO in phosphate buffer pH 7 with IS 0.01 M

CIP			CBZ		
C_0 (mg/L)	C_e (mg/L)	q_t (mg/g)	C_0 (mg/L)	C_e (mg/L)	q_t (mg/g)
1.07	0.56	25.48	3.25	3.15	4.78
2.00	1.09	45.29	5.81	5.64	8.76
3.87	2.75	56.38	8.74	8.37	18.61
7.06	5.55	75.45	11.59	11.15	21.70
10.00	8.31	84.36	15.37	14.75	30.96

Table D-6 Data from adsorption isotherm of CIP and CBZ in single solute solution on GO-A-HMS in phosphate buffer pH 7 with IS 0.01 M

CIP			CBZ		
C_0 (mg/L)	C_e (mg/L)	q_t (mg/g)	C_0 (mg/L)	C_e (mg/L)	q_t (mg/g)
3.06	0.27	11.16	2.72	2.54	0.74
4.99	1.13	15.41	4.70	4.25	1.77
6.78	2.30	17.94	8.57	8.02	2.21
9.09	3.87	20.90	11.61	11.01	2.44
11.73	5.39	25.39	14.97	14.31	2.66

Table D-7 Data from adsorption isotherm of CIP and CBZ in single solute solution on GO-A-HMS in phosphate buffer pH 7 with IS 0.01 M

CIP			CBZ		
C_0 (mg/L)	C_e (mg/L)	q_t (mg/g)	C_0 (mg/L)	C_e (mg/L)	q_t (mg/g)
3.06	0.56	10.00	2.72	2.24	1.92
4.99	1.57	13.68	4.70	4.11	2.36
6.78	2.74	16.17	8.57	7.54	4.13
8.88	4.13	19.02	11.61	10.53	4.35
11.73	6.28	21.82	14.97	13.50	5.90

2. Effect of pH solution on adsorption

Table D-8 Data from adsorption isotherm of CIP GO-A-HMS in phosphate buffer pH 7 with IS 0.01 M

pH 5			pH 7			pH 9		
C_0 (mg/L)	C_e (mg/L)	q_t (mg/g)	C_0 (mg/L)	C_e (mg/L)	q_t (mg/g)	C_0 (mg/L)	C_e (mg/L)	q_t (mg/g)
3.20	0.00	12.78	3.19	0.31	11.50	2.86	1.27	6.36
6.80	2.27	18.13	5.87	1.68	16.75	6.24	3.85	9.53
8.91	3.48	21.70	8.65	4.02	18.50	9.69	6.31	13.50
11.98	6.13	23.39	12.10	6.67	21.71	12.93	8.23	18.77
15.69	8.63	28.23	15.50	9.00	26.03	15.21	9.92	21.14

Table D-9 Data from adsorption isotherm of CBZ on GO-A5M5 in phosphate buffer pH 7 with IS 0.01 M

pH 5			pH 7			pH 9		
C_0 (mg/L)	C_e (mg/L)	q_t (mg/g)	C_0 (mg/L)	C_e (mg/L)	q_t (mg/g)	C_0 (mg/L)	C_e (mg/L)	q_t (mg/g)
2.58	2.24	1.35	3.07	2.86	0.84	2.38	2.24	0.58
6.65	6.05	2.38	6.04	5.70	1.36	6.60	6.21	1.57
9.63	8.79	3.34	9.34	8.77	2.26	9.62	9.10	2.10
12.24	11.25	3.94	12.34	11.68	2.67	12.27	11.72	2.22
14.87	13.76	4.41	15.27	14.61	2.64	15.11	14.49	2.46

3. Low concentration adsorption

Table D-10 Data from adsorption isotherm in low concentration of CIP GO-A-HMS in phosphate buffer pH 7 with IS 0.01 M

CIP		
C_0 (µg/L)	C_e (µg/L)	q_t (µg/g)
183.46	51.45	528.04
283.02	64.37	874.61
940.86	87.37	3413.99
1316.41	123.60	4771.27
1507.34	150.06	5429.11

Table D-11 Data from adsorption isotherm in low concentration of CBZ GO-5M5 in phosphate buffer pH 7 with IS 0.01 M

CBZ		
C_0 (µg/L)	C_e (µg/L)	q_t (µg/g)
22.25	18.60	22.45
42.45	32.91	81.93
60.69	48.06	96.52
86.22	66.58	127.95
117.37	86.78	159.37

4. Selective adsorption

Table D-12 Data from selective adsorption isotherm of CIP and CBZ on by fixing CBZ on GO-A-HMS in phosphate buffer pH 7 with IS 0.01 M

CIP			CBZ		
C_0 (mg/L)	C_e (mg/L)	q_t (mg/g)	C_0 (mg/L)	C_e (mg/L)	q_t (mg/g)
-	-	-	9.17	8.90	1.07
2.81	1.52	5.18	9.82	9.57	1.02
6.28	2.83	13.80	9.56	9.51	0.22
8.70	4.65	16.19	13.47	13.29	0.70
12.21	5.89	25.25	9.65	9.54	0.43
15.52	9.02	25.98	10.04	9.80	0.98

Table D-13 Data from selective adsorption isotherm of CIP and CBZ on by fixing CIP on GO-A-HMS in phosphate buffer pH 7 with IS 0.01 M

CIP			CBZ		
C_0 (mg/L)	C_e (mg/L)	q_t (mg/g)	C_0 (mg/L)	C_e (mg/L)	q_t (mg/g)
9.59	4.95	18.56	-	-	-
9.71	4.02	22.75	1.51	1.50	0.05
10.03	5.16	19.48	6.79	6.69	0.42
10.43	4.60	23.35	13.35	13.23	0.51
9.78	4.21	22.29	14.48	14.36	0.50
9.32	4.95	17.50	16.88	16.69	0.76

Table D-14 Data from selective adsorption isotherm of CIP and CBZ on by fixing CBZ on GO-A5M5 in phosphate buffer pH 7 with IS 0.01 M

CIP			CBZ		
C_0 (mg/L)	C_e (mg/L)	q_t (mg/g)	C_0 (mg/L)	C_e (mg/L)	q_t (mg/g)
-	-	-	9.17	8.53	2.56
2.81	1.46	5.40	9.82	8.97	3.41
6.28	3.53	10.99	9.56	8.96	2.41
8.70	5.76	11.77	13.47	12.76	2.83
12.21	7.90	17.22	9.65	9.00	2.59
15.52	10.78	18.95	10.04	9.36	2.71

Table D-15 Data from selective adsorption isotherm of CIP and CBZ on by fixing CIP on GO-A5M5 in phosphate buffer pH 7 with IS 0.01 M

CIP			CBZ		
C_0 (mg/L)	C_e (mg/L)	q_t (mg/g)	C_0 (mg/L)	C_e (mg/L)	q_t (mg/g)
9.59	5.85	14.96	-	-	-
9.71	5.34	17.49	1.51	1.34	0.67
10.03	5.78	16.97	6.79	6.37	1.69
10.43	5.70	18.95	13.35	12.78	2.28
9.78	5.79	15.96	14.48	13.83	2.60
9.32	5.45	15.50	16.88	15.69	4.78

VITA

Miss Jitsupa Suthkota was born on November 15, 1991 in Nakhon Phanom province. She graduated Bachelor's degree of Science from Department of Chemistry, Faculty of Science, Chulalongkorn University in 2013. She pursued her Master's degree in the International Postgraduate Program in Hazardous Substance and Environmental Management, Chulalongkorn University in 2015.